

SHORT TITLE FOR BOUND COPIES OF THESIS

FLOW CHARACTERISTICS IN A

CONFINED VORTEX FLOW

BY

N. BANK

---



MEASUREMENTS OF FLOW CHARACTERISTICS

IN A CONFINED VORTEX FLOW

MEASUREMENTS OF FLOW CHARACTERISTICS

IN A CONFINED VORTEX FLOW

A  
THESIS

by

NADER BANK, B.A.Sc.

Department of Chemical Engineering  
McGill University

Under the Supervision of Dr. W. H. Gauvin

Submitted to the Faculty of Graduate Studies and Research  
of McGill University in partial fulfillment of the  
requirements for the degree of Master of Engineering

McGill University  
Montreal, Canada

March, 1975



Nader Bank

1975

MEASUREMENTS OF FLOW CHARACTERISTICS  
IN A CONFINED VORTEX FLOW

by

Nader Bank

ABSTRACT

A study of air flow patterns by hot-wire anemometry is reported for a vortex chamber consisting of a cylindrical upper section 122 cm in diameter and 61-cm high, with a conical bottom section 183-cm high. Quantitative data are presented for flow angles, profiles of mean tangential and axial velocities, and radial distributions of tangential and axial intensities of turbulence as a function of air entrance velocities (1.6, 2.4 and 3.2 m/s) and axial distance from the top of the chamber. The mean outward radial velocity was found to be very small.

The experimental technique depended on the use of a single inclined hot-wire probe in various azimuthal positions of the inclined wire. Appropriate response equations for the velocity components and turbulence intensities were derived from a theoretical analysis which constitutes an important contribution of the work.

In general, the quantitative results confirm the theoretical predictions and the experimental trends reported in the literature. In particular, they fully support the conclusion that the flow pattern is relatively insensitive to the entrance volumetric flowrate.

M.Eng. (Chemical Engineering)  
March 27, 1975

# ÉTUDE SUR L'ÉCOULEMENT TOURBILLONNAIRE CONFINÉ

par Nader Bank

## RÉSUMÉ

Une étude a été faite de l'écoulement tourbillonnaire de l'air dans une enceinte consistant d'une section cylindrique supérieure d'un diamètre de 122 cm et 61 cm de hauteur, et d'une section conique inférieure de 183 cm de hauteur. Au moyen d'un anémomètre à fil chaud, les variables suivantes ont été mesurées en fonction de la vitesse moyenne de l'air à l'entrée (1.6, 2.4 et 3.2 m/s) et de la position axiale dans l'enceinte: profils des vitesses moyennes tangentielles et axiales, et profils des intensités de turbulence tangentielles et axiales. Les vitesses moyennes radiales mesurées étaient très petites.

La technique expérimentale a été basée sur l'utilisation d'un seul fil chaud incliné, dans des positions azimuthales différentes et pré-déterminées. Les équations de réponse pour les composantes de vitesse et pour les intensités de turbulence ont été dérivées à partir d'une analyse théorique qui constitue une contribution importante de cette thèse.

En général, les résultats confirment les prédictions théoriques et les observations expérimentales rapportées dans la littérature scientifique. Plus particulièrement, ils confirment le fait que l'angle de l'écoulement est très peu affecté par la vitesse d'entrée.

### ACKNOWLEDGEMENTS

The author would like to thank the following individuals and organization as an expression of his appreciation for their contributions toward this investigation.

Dr. S. Katta, a post-doctoral fellow in this Department for many valuable discussions and suggestions.

Dr. D. Bhattacharyya for his help in the computing work.

Mr. W. Phillips for his consultation in derivation of hot-wire response equations.

Mrs. L. Gladwish for her careful typing of this thesis.

The McConnell Foundation for financial support in the form of a Memorial Fellowship held over the period of this study.

And most important Laura, without whose understanding and encouragement this task would have been insurmountable.

TABLE OF CONTENTS

	<u>Page</u>
ABSTRACT	i
ACKNOWLEDGEMENTS	ii
TABLE OF CONTENTS	iii
LIST OF FIGURES	v
LIST OF TABLES	vii
NOMENCLATURE	viii
GENERAL INTRODUCTION	1
LITERATURE REVIEW	
INTRODUCTION	4
SURVEY OF EXPERIMENTAL STUDIES	5
SURVEY OF ANALYTICAL STUDIES	25
SUMMARY	34
METHOD OF MEASUREMENTS IN VORTEX FLOWS	
INTRODUCTION	37
THREE-DIMENSIONAL DIRECTIONAL PRESSURE PROBE	37
FLOW SENSE INDICATOR	38
STATIC PRESSURE MEASUREMENTS	39
THE HOT-WIRE ANEMOMETER	40
EXPERIMENTAL SECTION	
INTRODUCTION	43
EXPERIMENTAL APPARATUS	43

	<u>Page</u>
SPECIFICATIONS OF MEASURING INSTRUMENTS	50
Processing Equipment	50
Probes	52
Traversing Mechanism	52
Measurements of Distances	53
Measurements of Angles	53
OPERATING PROCEDURE	53
Orifice Calibration and Flow Rate Measurements	53
Flow Visualization and Determination of Flow Angles	60
MEASUREMENTS OF VELOCITIES AND TURBULENCE INTENSITIES	61
RESULTS AND DISCUSSION	66
FLOW PATTERNS: VISUALIZATION AND MEASUREMENTS	66
MEAN VELOCITIES	68
TURBULENCE INTENSITIES	79
CONCLUSION	87
BIBLIOGRAPHY	91
APPENDICES	
I: HOT-WIRE ANALYSIS	
Yaw Calibration	A- 1
Analysis	A- 4
Evaluation of Calibration Constants	A-17
Evaluation of Velocity Terms	A-19
Evaluation of Turbulence Intensities	A-19
Evaluation of Reynolds Shear Stresses	A-21
Bibliography	A-23
II: TABULATED EXPERIMENTAL DATA	A-24
Nomenclature	
List of Tables	

## LIST OF FIGURES

<u>Figure</u>		<u>Page</u>
1	Diagram of Spiral Air-Flow Pattern Observed by Thordarson (56) in Lucite Model Dryer When Air Entered Through Four Inlets Set at $30^{\circ}$ to the Circumference of the Tower.	19
2	Diagram of Spiral Air-Flow Pattern in Lucite Model When Air Entered Through Four Inlets Set at $45^{\circ}$ to the Tower Circumference (56).	20
3	Diagram of Spiral Air-Flow Pattern in Lucite Model When Air Entered Through Four Inlets Set at $90^{\circ}$ to the Tower Circumference (56).	21
4	Photograph of the Chamber	44
5	Schematic Diagram of the Chamber	45
6	Photograph of the Motor-Blower Assembly	47
7	Photograph of the Experimental Equipment	48
8	Block Diagram of the Anemometry System	51
9	Typical Linearized Hot-Wire Calibration Curve	54
10	Photograph of the Anemometry System	55
11	Photograph of the Traversing Mechanism	56
12	Close up Photograph of the Traversing Device	57
13	Typical Orifice Calibration Curve	59
14	Flow Angles for Inlet Velocities of 1.6, 2.4 and 3.2 m/s.	67
15	Radial Profiles of Tangential Mean Velocities at Stations 1, 3, 5, 7 and 9.	70
16	Radial Profiles of the Tangential Mean Velocities at Stations 2, 4, 6 and 8.	71
17	Radial Profiles of the Axial Mean Velocities at Stations 7, 8 and 9.	72

<u>Figure</u>		<u>Page</u>
18	Radial Profiles of the Axial Mean Velocities at Stations 1, 3 and 5	73
19	Radial Profiles of the Axial Mean Velocities at Stations 2, 4 and 6	74
20	Radial Distributions of Tangential Velocity at Station 7, for Different Inlet Velocities	77
21	Radial Distributions of Axial Velocity at Station 8, for Different Inlet Velocities	78
22	Radial Distribution of Tangential Intensities of Turbulence at Stations 1, 3, 5, 7 and 9	80
23	Radial Distribution of Tangential Intensities of Turbulence at Stations 2, 4, 6 and 8	81
24	Radial Distribution of R.M.S. Fluctuating Axial Velocity at Stations 1, 3, 5, 7 and 9	83
25	Radial Distribution of R.M.S. Fluctuating Axial Velocity at Stations 2, 4, 6 and 8	84
26	Distribution of Tangential Intensity of Turbulence at Station 7, for Different Inlet Velocities	85
27	Distribution of R.M.S. Turbulent Axial Velocity at Station 7, for Different Inlet Velocities	86
28	Root-Mean-Square Fluctuating Radial Velocity at Station 7, for Inlet Velocity of 3.20 m/s.	88

LIST OF TABLESTablePage

- I Location and Radius of Measuring Station  
List of Tables in Appendix II

65

A-24

NOMENCLATURE

Unless expressly stated otherwise the following notation is applicable.

Roman Symbols

$a_1$ to $a_{13}$	Constants defined in equation A33
A, B, C, D, E, F, G	Constants defined in equation A26
K	Yaw factor
m	Slope of calibration curve, m/s/volts
$m'$	Adjustable constant in linearized response, equation (9)
$q_e$	Effective cooling velocity m/s
$q_i$	Instantaneous resultant velocity vector
$q_x, q_y, q_z$	Components of instantaneous velocity vector in X, Y, Z directions.
$Q_z$	<del>Fictitious dominant mean velocity vector in Z direction</del>
r	Radial position, cm.
$R_0$	Radius, cm.
$\bar{u}, \bar{v}, \bar{w}$	Mean velocities in radial, axial and tangential directions respectively, m/s
$u', w', w'$	Fluctuating velocities in radial, axial and tangential directions respectively, m/s
$V_{in}$	Instantaneous voltage across the wire, input to the linearizer, volts
$V_0$	Adjustable constant in linearizer response, equation (4)
$V_{out}$	Linearizer output, volts
w	Tangential component of velocity in vortex flow, on page 1 and equation (1), m/s

Roman Symbols

$W_0$	Total inlet velocity, m/s
X, Y, Z	Coordinates in radial, axial and tangential directions respectively
X	Also noted as amplification factor in linearizer response, equation (9)

Greek Symbols

$\alpha$	Angle between mean flow direction and normal to the wire axis, degrees
$\alpha'$	Angle between mean flow direction and hot-wire axis, degrees
$\beta$	Angle between instantaneous resultant velocity vector and the normal to the wire axis, degrees
$\beta'$	Angle between the instantaneous resultant velocity and hot-wire axis, degrees
$\theta$	Azimuthal angle of hot-wire, degrees
$\nu$	Kinematic liquid viscosity, equation (5)
$\epsilon$	Kinematic eddy viscosity, equation (5)

## GENERAL INTRODUCTION

## GENERAL INTRODUCTION

Revolving fluid flows in which the tangential velocity distribution is at least crudely described by  $w_r = \text{const.}$  are classed as vortex flows, and are of interest in connection with their natural and induced occurrence.

Vortex flows in which there is large scale rotation of the mean flow occur in many types of fluid motion. In turbo-fluid machinery rotation is imparted directly to the flow by mechanically rotating rotors. Flow in tubes can be made to swirl by passage through stators with vanes angled so as to direct the flow tangentially to the tube walls. Vortex tubes have tangential slots in the tube walls so that flow entering the tube through the slots spirals along the tube. Trailing vortices are formed when the separated flow over wings or blades rolls up into a vortex core. Atmospheric vortices range widely in scale from small dust-devils and whirls to cyclones and hurricanes which may exceed 1 000 miles in diameter.

Interest in vortex flows, and especially intensive study of them, have followed the proposal of their application to various technical uses. Among these are: a method for the separation of gases of different molecular weight, one variation of which is described in (1); a nuclear propulsion scheme based on the above (2); Ranque-Hilsch vortex tube for refrigeration (3,4); magneto-hydrodynamic power generator (5); cyclone separator (6); swirl atomizer (7); gas turbine cyclone combustion chamber (8); vortex-contained nuclear rocket engine (9); rocket engine thrust modulation (10); oil-water separator (11); and spray dryers (12,13), to name only a few. In all, the use of vortex, or swirling flow, is

mainly to enhance the exhaust velocities, to promote mixing and dispersion, and to separate droplets and particles from gases.

Despite the interest created by these applications, the mechanics of swirling flow are not clearly understood, especially with respect to the flow patterns and turbulence profiles. Probably the most important aspect in design and operation of the above-mentioned industrial equipment is the prediction and control of the fluid-flow patterns. However, little is known of the complicated details of vortex flow because the object of most of the past investigations was only the measurement of the gross behavior of the equipment.

Previous analyses have been based on various idealizations of internal flows, which oversimplify its complexities; moreover, they have not considered the significant variations of this flow in equipment of different geometric shapes. Hence, it can be said that the past information is definitely insufficient to provide a clear picture of the spiral flow behavior. The need for more detailed investigations on vortex flow has been pointed out by Gauvin et al. (14), and Katta and Gauvin (15) in their study of the three-dimensional motion of droplets in a spray-drying chamber and its application to the prediction of the thermal efficiency and evaporative capacity of the equipment.

The objectives of the present study were twofold. The first was to analyze a three-dimensional centrifugal flow field and to derive a modified set of response equations from the assumption of cosine law cooling, which would permit the determinations of the components of the mean velocity vectors, turbulence intensities and Reynolds stresses, from

a single inclined hot-wire probe introduced in various orientations in the flow field.

The second objective was to apply this measurement technique to an experimental study of the flow behaviour in a vortex chamber having an upper cylindrical section with a tangential air inlet, and a conical lower part. This geometry combines in a single apparatus the two major forms of vortex flow. It is also typical of many types of industrial equipment, such as spray-drying chamber and cyclone separators.

The purpose of the experimental work was to characterize the spiral motion of air as it swirls through the chamber and to measure velocities and turbulence intensities in the axial, radial and tangential directions, in an attempt to generalize these findings as a function of the flow parameters. Predictions of these characteristics are essential for the sound design of a large number of chemical processing equipment involving the contacting of a dispersed phase of droplets or particles with a conveying gas, such as spray dryers, cyclone evaporators, spray coolers, gas scrubbers and absorbers, pneumatic transport reactors and combustion devices involving fuel sprays.

This thesis is divided into two major parts: the first presents a review of the literature on vortex flows, and contains a description of some of the measuring techniques available, including a brief summary of hot-wire anemometry. The second part consists of a presentation of the experimental work and the interpretation of the obtained experimental data. Detailed theoretical analysis underlying the specialized method of measurement used in this work is presented in Appendix I.

LITERATURE REVIEW

## LITERATURE REVIEW

### INTRODUCTION

Velocity vectors in vortex flows are, as pointed out by Chigier (16), composed of axial, radial and tangential (circumferential) components. A cylindrical co-ordinate system is usually adopted with the origin at the vortex centre, where radial and circumferential velocity components are zero. The established vortex flows are generally axi-symmetric but during formation of the vortex flow the symmetry is often distorted. For the axi-symmetric flows, measurements of velocity fields may be made along any one radial line at a particular axial station. For non axi-symmetric flows, measurements need to be made over many more points in order to map out the flow field.

Vortex flows are generally turbulent in the core regions, with high intensities of turbulence and high turbulent shear stresses in the regions of tangential velocity peaks. Determination of velocity in vortex flows, therefore, requires measurement of three velocity components, detection of direction and reduction of instantaneous velocity measurements into time mean-average values and root mean-square of fluctuating components of velocity.

Experimental work on a vortex chamber, in general, divides itself into two main types. The first consists of parametric studies of the effects of varying the geometry of the vortex chamber components on the overall operating characteristics, mainly pressure drop and temperature differences. The earliest investigation in this category is the one by Hilsch (3). Other major investigations of this type were published by

Dornbrand (17), Martynovskii and Alekseev (18), Westley (19,20) and Suzuki (21).

The second type of experimental investigation concentrates on the flow within the vortex chamber by measuring the pressure, velocity and temperature profiles at various axial stations in the chamber. The earliest of these was by Scheper (22).

The present study places itself in the latter category and deals with the mean flow characteristics and turbulence structure in a spiral gas stream occurring especially in vortex chambers of spray-dryer type.

This literature review is divided into two sections. The first section is devoted to the experimental work done on the vortex flow behavior and begins with consideration of flow in a vortex chamber of simplest geometry, namely the vortex tube. In the second section emphasis will be put on the review of theoretical and analytical studies of the problem, and since spiral flows occur in many engineering works, an attempt is made to present a concise review of the most significant studies dealing with different applications. The reader should be aware that this division is artificial and that there will be some overlap between the two areas.

#### SURVEY OF EXPERIMENTAL STUDIES

In the early 1900's, G.I. Taylor (23) dominated the work in general vortex motion with a series of articles in the proceedings of the Royal Society of London. However, most of Taylor's work did not directly apply

to the confined vortex flow field. The interest in confined vortex studies began in 1931, when a French metallurgist, G. Ranque (24) noticed a temperature decrease in the vortex of a cyclone separator. Ranque constructed a device which attempted to use the vortex temperature effect as a refrigeration process. A typical configuration of this device consisted of a cylindrical tube with tangential injection nozzles around the periphery of one end of the tube. The "cold" stream was ejected through an orifice near the vortex centreline at the injection end of the tube. The "hot" stream was ejected through a back pressure valve at the opposite end of the tube. After patenting the device in 1932, Ranque indicated after further investigation that his device was too inefficient to compete with the conventional refrigeration.

From 1931 to 1946, the vortex tube and, for that matter, the entire field of confined vortex flow lay dormant. In 1946, at the end of World War II, papers were found in R. Hilsch's (3) laboratory that showed the results of a parametric study to determine the effects of tube geometry and operating conditions on the efficiency of the Ranque-Hilsch vortex tube. When these papers were brought back to the United States, they created such interest that by 1954 Westley (19) compiled a list of 116 papers dealing with the Ranque-Hilsch tube and in 1960 Donaldson (25) reviewed an additional 112 papers on the subject. The bulk of the work done during this period was similar to Hilsch's, who gave a qualitative description of the flow in the vortex tube and postulated an outward flow of kinetic energy due to internal friction.

Hartnett and Eckert (26,27) experimentally studied the basic flow characteristics of a cylindrical vortex chamber in 1956. They visualized the flow using wool tufts supported on a fine wire, and reported velocity, pressure, and temperature profiles for a number of inlet conditions and different "hot" stream exit geometries. They also indicated that the radial velocity component was negligible throughout the entire tube. Another significant finding was the fact that the predominant axial velocity was concentrated in an annular region adjacent to the wall, while in the interior of the flow the axial velocities were small. Their inlet velocities were near 150 m/s, and they also showed that the velocity vector (flow pattern) was quite insensitive to changes in the inlet velocity. The two most important findings in this investigation were the areas of reversed axial flow and that the energy separation in a vortex seemed to be independent of the fluid Prandtl Number.

The shapes of the tangential velocity curves obtained by Eckert and Hartnett were confirmed by the work of Schowalter and Johnstone (28), who measured and reported the mean flow patterns and components of the turbulence intensity for two types of spiral flow fields: vortex tube, and cyclone separator. They worked at inlet velocities near 30 m/s, and showed that the mean and turbulent flow structures were not sensitive to change in the flow rate, but were greatly affected by the geometry of the system. This agreed with the results of Eckert and Hartnett (27) as mentioned above.

Schowalter and Johnstone also reported that the flow in the central portion of the vortex tube was one of nearly constant angular velocity (forced vortex), and this confirms the earlier assumptions made by Kassner

and Knoernschild (29), and by Marshall (30). Moreover, they found that the spiral flow patterns were not symmetrical with the centreline axis, and postulated a dynamic centreline with helical shape as explanation for this asymmetrical behavior. However, Soo (31), in his theoretical study of cyclone separators, associated this helical shaped core with the unsymmetrical inlet configuration used, and by solving the basic flow equations, he obtained the radial and axial velocity distributions, and showed that the vorticity is decreased as one goes toward the bottom of the cyclone separator.

Reference (28) contains also a study of longitudinal and radial intensities of turbulence. The longitudinal intensity showed a sharp increase near the centre of the vortex tube, due to the abrupt decrease in mean velocity near the centre. This was found to be similar for radial intensity which decreases near the wall in contrast with the high value observed for longitudinal intensity near the outer wall. Schowalter and Johnstone also attempted to explain the differences between predicted and measured values of confined vortex flows by the phenomenological theories of turbulence. That is, the eddy diffusivity was either assumed constant or a function of an appropriate mixing length.

Lay (32), in the first of a two-part paper, presented an experimental study of compressible flow in a uniform vortex tube. His objective was to provide a better understanding of the separation of a gas stream into regions of high and low stagnation temperatures in a vortex field. The emphasis of his study was directed to a vortex which was generated at the entrance block, and which proceeded in one direction down the tube to

be discharged through the exit at the far end of the tube. This is the so-called uniflow type of vortex tube. He presented the measured values of the velocity, temperature, and pressure profiles at a number of axial stations along a 5.08-cm. diameter vortex tube made of lucite to permit flow visualization studies. Pressure, temperature and velocity traverses were taken by means of hypodermic probes, and velocities were checked by means of a miniature hot-wire anemometer. From these measurements, Lay recognized the three-dimensional character of the flow field and reported that the axial velocities were small when compared to the tangential velocities, and that the predominant axial velocities were concentrated in a small annular region near the wall of the tube, but tangential and total velocity peaks were located more toward the centre of the tube. Actually, the axial velocity fell off sharply toward the centre, and indicated a reverse flow near that region. Another important point made by Lay was revealed when his traverses for flow angle showed that the flow angle was rather independent of changes in inlet pressure, a fact shown by Hartnett and Eckert (27), and Schowalter and Johnstone (28). In part two, the analytical portion of his study, Lay (33) used an inviscid model to describe the flow field in the vortex tube. Solutions for the two-dimensional form of this model were obtained with the use of a hodograph transformation of the inviscid general equations of motion. From the axial momentum equation, Lay then showed that the superposition of a uniform axial flow does not affect the two-dimensional form of the solution. Thus, the solutions obtained were represented by superposition of a potential vortex and a radial sink flow on a uniform axial flow field.

In 1961, Holman and Moore (34) experimentally showed that a relatively simple analysis predicts the functional variation of temperature and pressure in a vortex chamber with radius and inlet velocity. The apparatus used was similar to a Ranque-Hilsch tube except that all the flow passed out one end and no attempt was made to separate the cool gas in the centre from the hotter stream at the outer periphery. The vortex was created in the chamber by injecting air tangentially through two diametrically opposed feeder tubes at the outside edge of the chamber. They solved the energy balance equation for an axially-symmetric flow by assuming a general vortex velocity distribution of the form:

$$wr^n = \text{const.} = c' \quad (1)$$

where  $w$  is the tangential component of velocity in vortex flow,  $r$  is the radius,  $n$  a general vortex exponent and  $c'$  a constant.

Their experimental results showed that it was quite satisfactory to assume that the flow occupied some effective area at the inlet and that this area was essentially independent of flowrate. Thus, they presented the following simple correlations for vortex chamber pressure and temperature, which are useful for engineering purposes:

$$1 - (p/p_1)^{(n_1-n)/n_1} = a[(r_1/r)^{2n} - 1] \quad (2)$$

and

$$1 - T/T_1 = a[(r_1/r)^{2n} - 1] \quad (3)$$

In the above equations  $T$ ,  $p$ , and  $r$  are respectively the temperature, pressure, and the radius; subscript "1" denotes outside edge of chamber, or entrance conditions;  $n$  and  $n_1$  are the general vortex exponent and the polytropic exponent, respectively; and "a" is a defined parameter depending

on the chamber dimensions and the fluid properties at the entrance.

Around 1962, the vortex-contained nuclear rocket engine replaced the Ranque-Hilsch tube as the dominant device initiating confined vortex flow studies. However, because of the similarity of geometries, many studies pertaining to the nuclear rocket engine could also be related to the vortex tube. A large number of experimental investigations in this period (Savino (35), Ragsdale (36)) attempted to explain the differences between predicted and measured values of confined vortex flows.

Ragsdale (36) performed the measurements necessary to evaluate the universal constant for the Prandtl and von Karman mixing-length theories.

The essential weakness of all these studies was brought to light in two separate, very carefully-controlled investigations. The first study by Kendall (37) showed that nearly the entire system of radial mass flow was contained in the boundary layers of the end walls of a cylindrical vortex tube. The second investigation by Donaldson and Williamson (38) experimentally confirmed that the predominance of the radial mass flow was contained in the end wall boundary layers. The latter investigation also measured very low turbulent intensities in the vortex mainstream. Thus, the one and two-dimensional turbulent models used by the previous investigators (discussed in detail in the following section) could not possibly explain the actual flow field in the confined vortex. These two investigations also dramatically demonstrated, for the first time, the important effect of the solid wall boundary layers on the flow of a confined vortex.

Pivirotto (39), working on the gaseous core nuclear rocket engine, observed that even a very small probe inserted radially across a cylindrical vortex drastically disturbed the side wall static pressure profiles. The same physical reason explains the importance of both the wall boundary layers and the disturbance of the probe in vortex flows. The centrifugal forces created by the tangential vortex velocities are counter balanced by a radial static pressure gradient. That is, the static pressure in a vortex is higher in outer regions of the vortex than it is near the vortex centreline. When something such as a probe or the viscous shear of the wall locally destroys the centrifugal force, the radial pressure gradient imposed by the undestroyed portion of the vortex flow pumps fluid radially inward toward the vortex centreline. Thus, it is seen that secondary flows (boundary layer flows) are very important in the determination of the overall flow field in a confined vortex.

Schultz-Jander (40), was another investigator who, in 1963, experimentally studied the flow field in a cylindrical vortex chamber. A vortex flow was created in a cylindrical chamber by tangential injection of a fluid at the outer edge and the subsequent discharge of this fluid through an orifice or nozzle in the centre of one of the end closures. Such a flow had become of interest as a result of its application to the stabilization of electric arcs in plasma jet generators. The merit of this investigation was the effect of wall friction on the velocity and pressure distributions, using water as incompressible fluid with a relatively high viscosity. It was found that for an incompressible medium the flow pattern was mainly determined by the wall friction.

Schulz-Jander's analysis which was based on this fact and which neglected the fluid viscosity was found to agree very well with his experiments.

In 1964, Collins and Stubbs (41) dealt with the similarities existing between the standard vortex tube (upon which most of the past work has been done) and two variations: (a) the tapered vortex tube, and (b) the vortex cooler. As mentioned before, the standard vortex tube consists of a cylindrical tube with a nozzle entering the cross section tangentially at the outer periphery, near one end of the tube's length. The end away from the nozzle has either a valve or a variable annular opening near the tube's outer periphery and is known as the hot side. The end of the tube near the nozzle consists of an orifice plate with a central circular orifice. This is the cold side of the tube. In operation the gas enters the nozzle, creating a vortex due to the nozzle's tangential position. Depending on the orifice size and the hot valve setting, a portion of the gas passes through the hot side and discharges to the surroundings. The remainder passes through the orifice of the cold side to the surroundings. The tapered vortex tube used by Collins and Stubbs was similar to the standard tube except that the tube had a decreasing taper from the inlet nozzle section to the hot-side discharge. The second configuration used in this study was an improved vortex tube called "vortex cooler" by its inventors Blatt and Trusch (42). This was a vortex tube which had been modified by replacing the "hot" valve with a diffuser section and closing the cold orifice completely, making it a no-cold-flow device. The object to be cooled was to be placed inside the tube at the centre of the swirl chamber.

Collins and Stubbs (41) showed that all the three configurations contained no fundamental differences and further, the variation of the tube performance, with respect to the setting of the exit gas "hot" valve, was explained in terms of compressible flow. In their work, mathematical treatments were kept to a minimum, and instead emphasis was placed upon the experimental results obtained from the tests performed on the variations of the standard vortex tube.

A confined vortex flow which contains an annular region of high axial velocity near the peripheral wall was proposed by Travers and Johnson (43,44) in 1965 as one possible flow configuration for use in a gaseous core nuclear rocket engine. For several flow conditions they determined the flow patterns and velocities of water by photographically recording the traces of neutrally-buoyant plastic particles and dye which were injected into the vortex tube as tracer materials. The flow near the peripheral wall of the vortex tube was found to be turbulent for all test conditions, and the vortex-centreline was found to be displaced as much as four percent of the vortex tube radius from the geometric centreline of the tube at some axial test stations.

Also in the same time period, 1965, McFarlin (45) conducted some experiments to investigate the effect of the peripheral-wall injection technique used to derive an air vortex on the level of turbulence in the vortex. Two air vortex tubes with different peripheral-wall injection configurations were used. Both vortex tubes were driven by the injection of air in essentially a tangential direction along the wall.

In one configuration, the vortex tube consisted of a cylindrical metal tube, 25.4-cm in diameter and 76.2-cm in length. Air was injected through a 0.462-cm wide slot extending the entire length of the tube, and withdrawn through ports at the centres of the end closures.

In the second configuration the vortex tube consisted of a cylindrical lucite tube, also with a diameter of 25.4-cm and a length of 76.2-cm. This tube was mounted concentrically inside another lucite tube which was 35.56-cm in inside diameter and 76.2-cm in length, and which served as an injection chamber. A total of 2144 injection ports, 1.524-mm in diameter, were located in 119 staggered circumferential rows 6.4-mm apart. The centreline of each injection port was at an angle of 19-deg. relative to a tangent to the inner wall of the vortex tube. The injected air was withdrawn in the same manner as for the single-slot vortex tube.

Hot-wire anemometer measurements of tangential velocity profiles and root-mean-square velocity fluctuations were made near the peripheral wall of each tube at three different radial distances from the centreline, in a plane normal to the latter, and these results indicated that for the single-slot injection configuration the tangential velocities increased towards the centre of the tube with increasing radial Reynolds Number (Re based on radial velocity), and that the flow in the 2144-port configuration was considerably less turbulent than the flow in the single-slot configuration throughout the region surveyed.

It has been suggested (39,44) that the boundary layers on the end closures of the vortex tube are capable of transporting a large

fraction of the mass flow, which otherwise would have passed through the main vortex flow, thereby weakening the vortex, and the degree of this weakening depends on whether or not the boundary layer flow is returned to the main flow before it leaves the vortex tube. The influence of this boundary layer mass flow on the relation between the mass flowrate and the strength of the vortex (the degree of weakening) was clarified by Nakamura (46) in 1966. He assumed that the fraction of the flow passing through the boundary layer should decrease as the length-to-diameter ratio of the vortex tube becomes larger, so by varying this ratio the effect of the end closure boundary layers should be separated from those of the boundary layers on the cylindrical walls. To this end he constructed a vortex tube with a variable length-to-diameter ratio, and carried out experiments for several radial Reynolds Numbers for a wide range of length-to-diameter ratios. He then concluded that the turbulent eddy viscosity can be reduced by making the vortex tube longer, thereby reducing the boundary layer dissipation.

Perhaps more important than the large number of parametric studies of this particular period was the small number of investigators who studied the basic flow characteristics of the confined vortex flow for different applications. In 1952, Ter Linden (47) considered different types of air cyclones and concluded that, based on economy and size, a cyclone with upper cylindrical and lower conical section with tangential inlet was the most efficient. The same author (48) measured the velocity and pressure distributions in a cyclone dust collector. This investigation gave the first indications of the marked three-dimensional character

of the confined vortex in a cyclone. In particular, in the radial direction, Ter Linden found evidence of flow reversal near the vortex centreline. He also concluded that the tangential component was predominant in the entire chamber, with the exception of the turbulent core in the centre. Unfortunately, the importance of this investigation was to go unnoticed for some time.

The flow pattern in liquid cyclones has been examined experimentally by Kelsall (49), who used an ingenious technique of measuring the trajectories of suspended alumina particles. Also worthy of mention is the experimental study of Yoshioka and Hotta (50) who used a pitot tube to obtain velocity data. Quantitative measurements on the flow pattern have been carried out by Bradley and Pulling (51) by means of dye injection.

Smith reported both an experimental study and an analytical investigation of the vortex flow in cyclone separators with a central exit tube. In his first paper (52) he reported the existence of three flow regimes (laminar, turbulent and periodic) occurring in different parts of a cylindrical cyclone chamber with a flat closed bottom which was constructed from a 100-mm glass tube. The periodic regime was characteristic of the region where the vortex turned and attached to the wall of the inner tube. The point of attachment rotated in a horizontal plane thus producing strong periodic fluctuations in the flow. Smith's apparatus was designed to produce an axially symmetric flow rather than the asymmetric flow normally occurring in cyclones. This symmetric vortex was studied with the aid of smoke, and was probed for the distribution of the velocity; the smoke used was either a fog made by condensing oil vapor or,

on a few occasions, tobacco smoke. In this investigation the changes in the flow pattern with flowrate were not measured because several investigators, First (53), Iinoya (54), Hartnett and Eckert (27), and Schowalter and Johnstone (28), had shown that in the normal operating range of velocity the flow pattern did not vary with flowrate. In his second paper, Smith (55) made a significant contribution to the understanding of the mechanism of cyclone separator operation. By considering the effects of radial instabilities in the boundary layers on the walls, he deduced that the boundary layer on the outer wall of the separator was unstable to radial disturbances and the random separation of this boundary layer was the source of the high turbulence in the separator. Furthermore, he postulated that the turbulence resulting from the unstable layer was inherent in any device employing a rotating flow within a stationary container.

Thordarson (56) made some observations of the air flow patterns in a transparent plastic vortex chamber having the geometry of a spray dryer. The model was 61 cm in diameter and was designed to permit observation of rotational or straight-line air flow. By injecting balsa dust in the air stream, it was possible to photograph air flow patterns for various air inlet arrangements; when the air entered through a single tangential inlet at the top of the tower, a steep spiral path was developed, but when the air entered through four inlets at an angle to the radius, the diameter of the spiral appeared to become smaller the more closely the inlets coincided with the radius. These observations are sketched in Figures 1, 2 and 3. When the air entered at an angle of

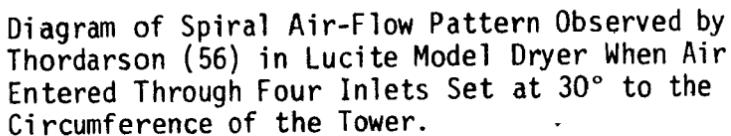


FIGURE 1

Diagram of Spiral Air-Flow Pattern Observed by Thordarson (56) in Lucite Model Dryer When Air Entered Through Four Inlets Set at  $30^\circ$  to the Circumference of the Tower.

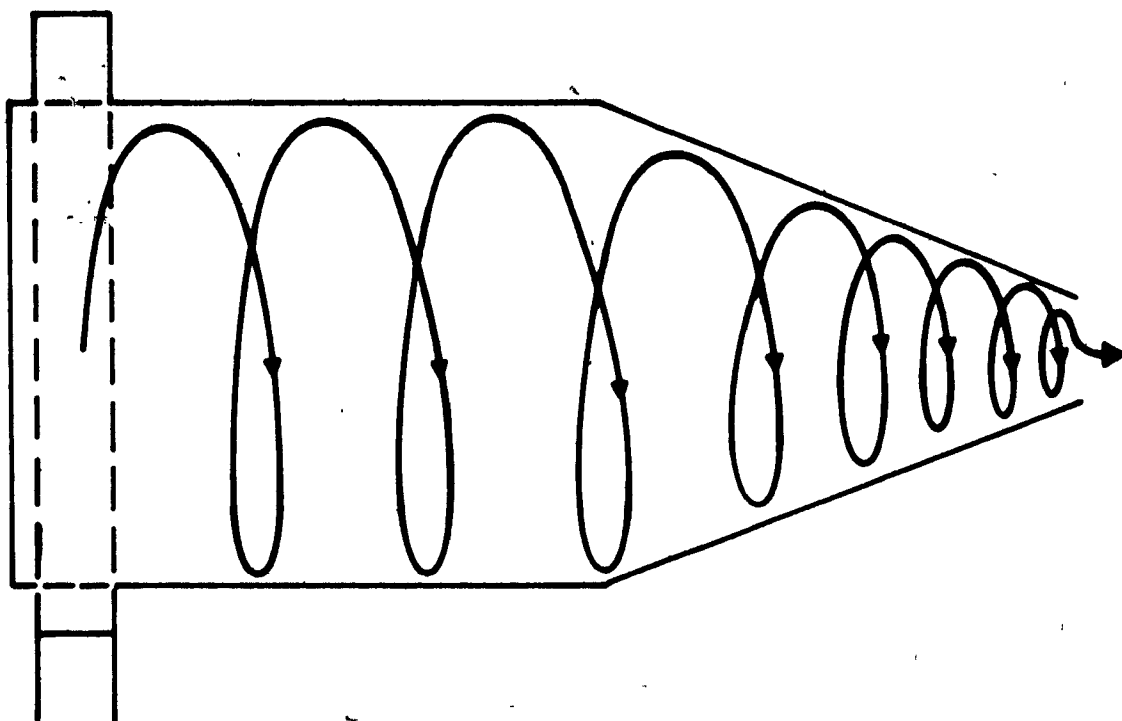
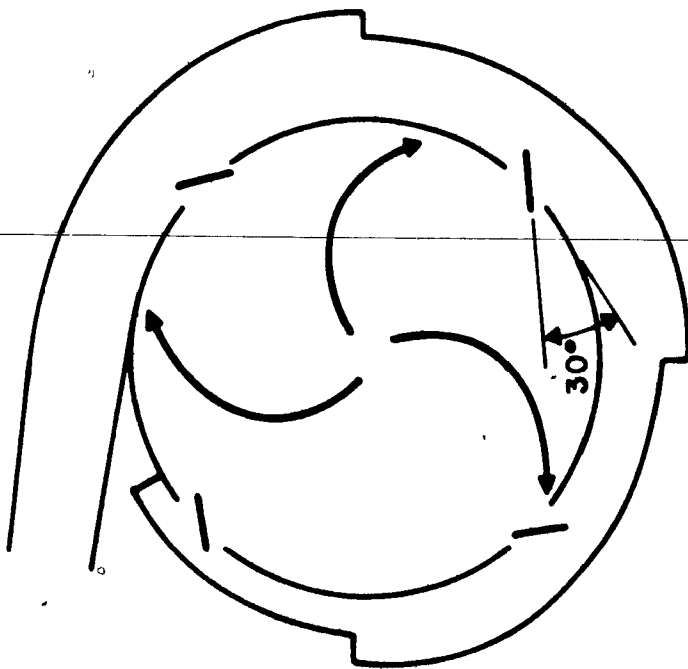




FIGURE 2

Diagram of Spiral Air-Flow Pattern in Lucite Model When Air Entered Through Four Inlets Set at  $45^\circ$  to the Tower Circumference (56).

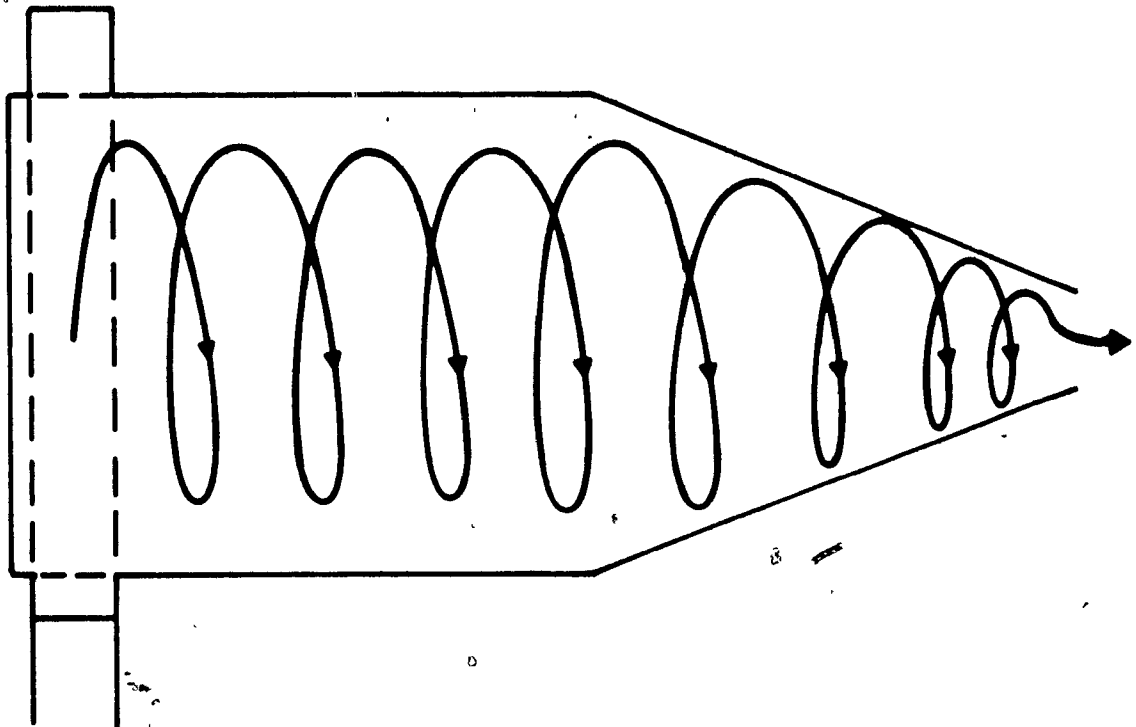
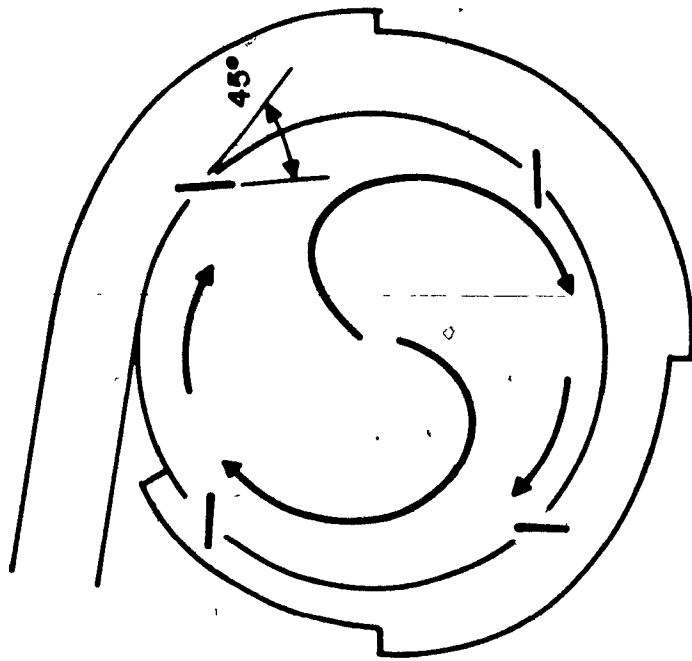
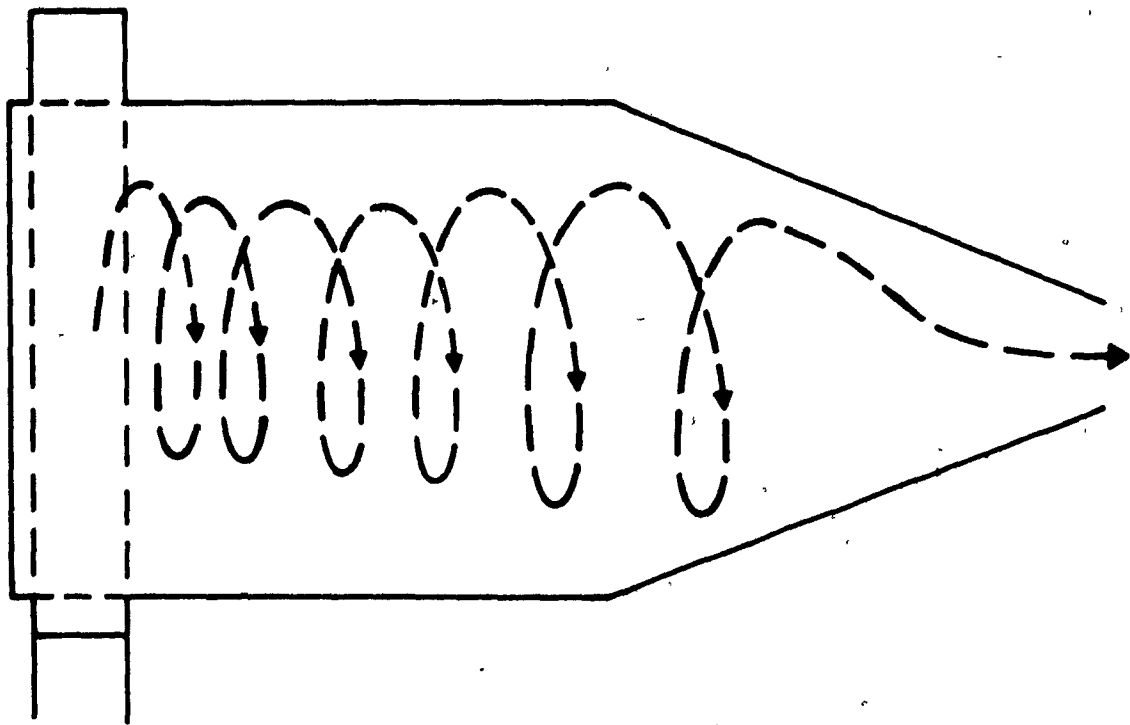
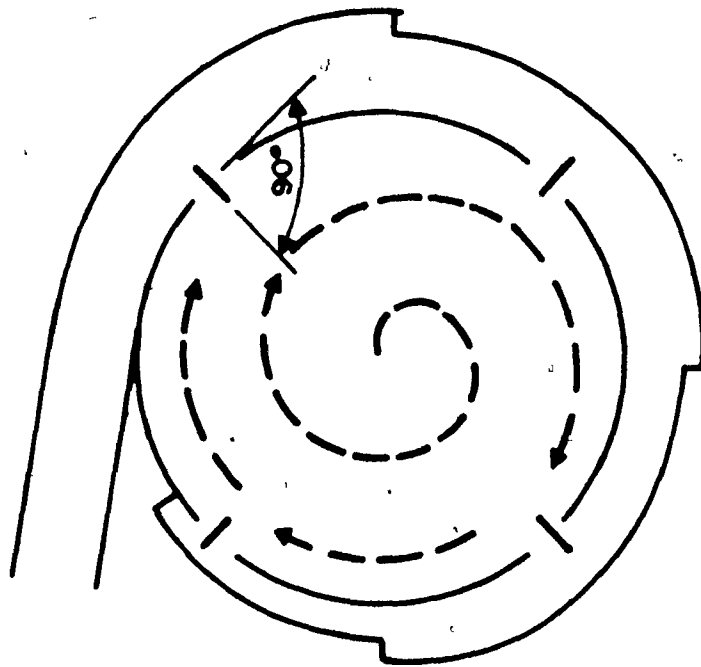




FIGURE 3

Diagram of Spiral Air-Flow Pattern in Lucite  
Model When Air Entered Through Four Inlets Set  
at 90° to the Tower Circumference.



30° to the circumference, Figure 1, the spiral diameter nearly equaled the diameter of the chamber. At 60°, Figure 2, the diameter of the vortex became smaller, while at 90°, Figure 3, the spiral motion was due mainly to the angular momentum the air possessed before entering the dryer. In other words, for this case the tendency of the air to move in a circumferential direction in the bustle duct was not completely removed when it was caused to enter the dryer through the perpendicular louvers.

An identical vortex chamber was also used earlier by Edeling (12) who did an elegant experimental and theoretical investigations on air and particle motions within the chamber.

An experiment was devised in 1973 by So (57) to study the behavior of rotating flow in a conical diffuser, with the primary objective of examining various vortex flow regimes. A secondary purpose was to gain an understanding of the mechanism of vortex decay\*. The first objective was sought entirely through experiments, whereas the second was aided by a mathematical model using the integral equations of mass, axial momentum, angular momentum, and moment of axial momentum. The flow considered was assumed to be steady, incompressible, and axially symmetric, and no energy consideration was made. So's study resulted in the establishment of five distinct flow regimes representing three basic types of vortex flow and two transitional phenomena.

---

\* The characteristic behavior of a decaying swirling motion is that the axial variation of the tangential velocity distribution is much greater than that of the axial velocity distribution.

So's results were presented in terms of strength of the vortex flow: weak swirl, medium swirl, and strong swirl; the amount of swirl was varied by adjusting the volumetric flowrate. He generalized his findings by postulating that for a weakly rotating motion (small swirl), a flow rate gradually increasing from zero slowly changed the laminar flow to a turbulent one, with a laminar vortex breakdown phenomenon bridging the two. If the amount of swirl was increased further, the transition from laminar to turbulent flow occurred in a shorter range of flow rate. The turbulent flow seemed to be the limiting flow pattern for a sufficiently small swirl.

For motion with a larger swirl, the transition from laminar flow to turbulent happened very rapidly, and the first phenomenon generally observed as the flowrate was increased was the formation of a small reversed flow, or two-celled, region nested on the centre of the end closure. Downstream of this region, the vortex flow remained one-celled.

Decay of swirl in turbulent flow has been studied recently for different geometries, and Wolf et al. (58) presented an experimental study of the decay of turbulent swirling flow in tubes. They determined the local values of the total and static pressures and flow direction with a cylindrical probe that spanned the tube diameter, and also investigated the structure of turbulence with a hot-wire anemometer. They showed that, unlike pipe flow, the turbulent intensity as well as the turbulent fluctuations themselves increased to very high levels near the axis of the tube and were relatively independent of axial position. About the decay of swirl, which was approximately exponential with axial position, they

concluded that it decreased with increasing axial Reynolds Number and was independent of initial swirl angle, and they postulated that as the swirl decayed, the point where the tangential velocity was maximum moved radially inward.

Vortex breakdown (an abrupt change in the structure of the core of a swirling flow) has been observed to occur under a variety of circumstances such as in cyclone separators. Its occurrence is marked by a rapid deceleration, deformation, flow reversal, and changes in the velocity and pressure distribution in the surrounding swirling flow. In connection with this phenomenon, Sarpkaya (59,60) studied swirling flows in a mildly-diverging cylindrical tube and reported the occurrence of three types of vortex breakdown: double-helix and spiral forms (followed by turbulent mixing), and axisymmetric form (often followed by a spiral breakdown, then by turbulent mixing). The type and location of the breakdowns were found to be dependent upon the Reynolds Number.

In 1968 Lineberry (61) experimentally studied the behavior of swirling air flow in a conical converging nozzle. He observed that the spherical radial component of velocity approached the same magnitude as the tangential component as the apex of the cone was approached. As did Ter Linden (48), Lineberry found areas of reversed radial flow in the core of the vortex. Internal flow characteristics of a swirling flow chamber or of a nozzle was also investigated by Batson and Sforzini (62). Flow direction was measured by miniature probes and observed by wool tufts. They assumed negligible radial velocities and with the knowledge of flow angle, Mach number and temperature, calculated the tangential and axial velocities.

## SURVEY OF ANALYTICAL STUDIES

In his pioneering paper, Hilsch (3) gave a qualitative description of the flow in the vortex tube and postulated an outward flow of kinetic energy due to internal friction. An analytical approach following the qualitative description of Hilsch was made by Kassner and Knoernschild (29). They assumed that the velocity profile of the air near the entrance was similar to that of a free vortex (constant angular momentum) and that as the air moved towards the exit of the tube the velocity profile was converted to that of a forced vortex (constant angular velocity or "wheel flow") by the action of viscosity. They also postulated an "adiabatic" temperature distribution due to turbulent mixing.

Another analytical approach was given by Scheper (22). He postulated a flow model based upon experimentally-determined flow patterns in which the vortex tube was considered to act as a counterflow heat exchanger. A third analytical approach was initiated in an Appendix due to Dornbrand (17). In this study the vortex tube is replaced by a steady two-dimensional, forced vortex having velocity and temperature profiles which are identical in all sections perpendicular to the axis of the vortex. The Dornbrand analysis considered only the momentum equation and the transfer of energy due to shear work, but included the effect of radial flow. A "two-dimensional vortex tube" based upon this flow model was built, but is stated to have been "unsuccessful".

Another two-dimensional vortex analysis with only circumferential flow was made by Van Deemter (63) who used the complete energy equation

to calculate the temperature distributions corresponding to several assumed velocity distributions.

One drawback of the two-dimensional approach to the vortex tube based upon purely circumferential flow is that the only steady velocity distribution which satisfies the momentum equation is that of constant angular velocity, and this leads, in the case of a stationary wall, to no velocity at all. It was perhaps consideration of this problem which led Pengelly (64) to consider again the two-dimensional vortex with radial inflow. His analysis extended Dornbrand's (17) solution to include the effects of dissipation but not of heat conduction.

The most complete solution of the steady vortex has been given by Deissler and Perlmutter (65), who included both radial and axial flow and used the complete energy equation. The solution is still essentially two-dimensional, however, in that the circumferential velocity and the temperature profiles are identical in all sections perpendicular to the axis of the vortex. In another paper, Deissler and Perlmutter (4) presented one-dimensional analytical investigations of the energy distribution in vortex flows, and neglected the thermal conductivity of the fluid in comparison with the transport of energy by the radial mass flow. As one would expect, the vortex energy transport in these cases was found to be a function of the radial mass flow. Deissler and Perlmutter's results showed that vortex energy separation cannot occur if the Reynolds Number based on radial mass flow is greater than four. Therefore, they reached the conclusion that turbulence is of the utmost importance to the energy separation process.

Mack (66) also presented a one-dimensional analytical study of the energy separation in cylindrical vortex flows. He neglected the radial mass flow in the vortex and found that the energy separation in the vortex is a function of the fluid Prandtl Number.

Swirling flow patterns in cyclones have been studied theoretically by Fontein and Dijkstra (67), Yoshiojta and Hotta (50), Rietema (68) and others. In all cases only the tangential velocity has been investigated although the outward radial velocity is also required. Fontein and Dijkstra assumed that the tangential velocity,  $W$ , is given by:

$$W = K_1/R + K_2R \quad (4)$$

where  $R$  is the radial distance and  $K_1$  and  $K_2$  are constants which were to be determined by the operation of the cyclone. No values of  $K_1$  and  $K_2$  were given. Rietema (68) assumed that  $W$  was independent of the height  $Z$ , and that the horizontal velocity was as obtained by Kelsall (49). He then solved the radial component of the Navier-Stokes equations for a range of Reynolds numbers based on the radial velocity, radius of cyclone and an eddy viscosity.

As part of a study on the hydrodynamics of a cyclone separator, a theoretical investigation of the flow pattern in a flat box cyclone (cylindrical box with a tangential inlet extending over the total height and only one central outlet) was carried out by Rietema and Krajenbrink (69). Expressions were derived for the tangential velocity profile as influenced by internal friction (eddy viscosity) and wall friction. The most important parameter controlling the tangential velocity profile was found to be:

$$\lambda = -u_0 R_0 / (\nu + \epsilon) \quad (5)$$

where  $u_0$  is the radial velocity at the outer radius  $R_0$  of the cyclone,  $\nu$  the kinematic liquid viscosity and  $\epsilon$  is the kinematic eddy viscosity. For values of  $\lambda$  greater than about 10, the tangential velocity profile was found to be nearly hyperbolic, while for  $\lambda$  smaller than 1 the tangential velocity decreased towards the centre. It was also shown how  $\lambda$  and also the wall friction coefficient could be obtained from experimental velocity profiles with the aid of suitable graphs. They finally pointed out that, because of the close relation between eddy viscosity and eddy diffusion, measurements of velocity profiles in flat box cyclones would also provide information on the fluctuating motion of particles in a cyclone, a motion reducing its separation efficiency.

Einstein and Li (70), after studying the "bath tub" vortex formed by emptying a container, proposed one of the earliest vortex models applicable to the vortex tube. In this model, it was assumed that the flow could be represented by a plane vortex which was divided into two areas: the area outside of the actual drain opening and the area inside the drain opening. Outside the drain opening, the mass flow across any concentric circumference is considered to be constant and inside the drain opening, the mass flow is assumed to vary inversely as the square of the radial distance from the centre. With these assumptions, it is not surprising that the authors found solutions that are a function of two non-dimensional parameters: the ratio of the radius to the drain radius and a Reynolds Number based on radial mass flow. The limiting forms of these solutions show that for very large radial Reynolds Numbers, the tangential velocity profile approaches that of a potential vortex (constant circulation) and

for very small radial Reynolds Numbers the tangential velocity profile approaches that of a forced vortex (wheel flow). Lewellen (71) showed that the solutions of Einstein and Li are the "zeroth order" terms of a power series expansion solution for confined vortex flows. In order to apply their model to turbulent flows, Einstein and Li made a "Boussinesq" type assumption. That is, they assumed that the turbulent Reynolds stresses could be presented by a constant eddy diffusivity (virtual viscosity) times the local rate of strain of the mean values of the flow viscosity. Unfortunately, a number of investigators who followed Einstein and Li attempted to experimentally measure this virtual viscosity without accounting for the effects of the wall boundary layers on the mainstream flow. Keyes (72), using the turbulent model proposed by Einstein and Li, calculated the eddy diffusivity necessary to match experimental values of the confined vortex flow.

Donaldson (25) in 1957 presented a particular class of vortex solutions to the incompressible Navier-Stokes Equations. These solutions were obtained in the following manner: Working in cylindrical coordinates, Donaldson assumed that the tangential velocity was axisymmetric and furthermore a function of radius only. With this assumed form of tangential velocity, an analysis of the general equations of motion showed that the radial velocity must be a function of the radius only, and that the axial velocity must be a function of the radius, times the axial distance, plus an arbitrary function of the cylindrical radius. Substitution of these forms of the velocity components into the general equations of motion transforms the equations to a set of nonlinear ordinary differential

equations. Donaldson applied these transformed equations of motion to the viscous, incompressible flow field inside a rotating, porous cylinder.

~~Closed form solutions~~ for the very viscous and nonviscous cases were obtained. General cases were then solved by means of a power series expansion about these limiting solutions. Donaldson and Sullivan (73) extended this work by numerically obtaining the complete class of solutions, five distinct types of solutions, which depend upon the radial Reynolds Number and an axial pressure gradient parameter, were obtained. Multi-celled vortex motions, that is, areas of reversed axial flow, seen in previous experimental studies were exhibited analytically in these solutions. The solutions of Burgers (74) were shown to be a special case of this complete set of solutions. These two investigations represent the earliest analytical evidence of the important effect of the viscous stresses on the three-dimensional character of confined vortex flows.

The three-dimensionality of swirling flows is also discussed by Loitsyansky (75), Görtler (76), and Steiger and Bloom (77) for the case of laminar flow, and solutions were obtained using the assumption of similarity of the velocity profiles. Turbulent swirling flow was considered by Chervinsky (78) who showed that similar solutions of the components of the velocity exist in the two limiting cases depending on whether the flow is controlled by linear or angular momentum.

Long (79), in his attempt to explain the large vertical velocities in a tornado, assumed that the vortex circulation approaches a constant as the cylindrical radius approaches infinity. From an analysis of the

momentum transfer, Long obtained a similarity transformation. He then combined the similarity transformation with the boundary layer assumptions to reduce the Navier-Stokes equations to a set of three ordinary differential equations. Although no numerical results were given, a qualitative discussion of the ordinary differential equations indicates that as the vortex becomes more concentrated (smaller vortex radius) near the vortex centreline, the vertical velocity continually increases. Lewellen (71), commenting on this solution, notes that even at large cylindrical radii, the axial velocity does not disappear; therefore, he doubts the usefulness of this solution for the prediction of tornado velocity profiles.

Lewellen (80,81) also considered a flow model which is composed of a strong cylindrical tangential rotation and a radial sink flow which exhausts axially inside a finite radius. With this model, the incompressible Navier-Stokes equations could be reduced to two coupled partial differential equations in terms of the stream function and circulation. These equations contained three nondimensional parameters, the radial Reynolds Number, the ratio of mass flow per unit length to circulation, and a ratio of characteristic axial and radial dimensions. Lewellen showed that for strong vortex flows the ratio of mass flow per unit length to circulation was very small. Thus, a solution of the two partial differential equations was obtained by means of a power series expansion in terms of the last two dimensionless parameters. The zeroth order terms of this expansion were shown to represent the solutions obtained by the vortex flow model of Einstein and Li (70), as mentioned above. The difficulty with this solution was that it could not be carried

into the side wall boundary layers. That is, inside the boundary layers the ratio of mass flow per unit length to circulation could no longer be considered small; thus, the series solution was invalid in the boundary layer region. A number of investigators: Rosenzweig et al. (82), Logan (83), and Linderstrom-Lang (84) had circumvented this difficulty by matching the power series solution for the vortex mainstream to a boundary layer solution near the container walls. In all three cases, however, only the zeroth order terms of Lewellen's power series had been used in the vortex mainstream.

Lilley (85) made a theoretical analysis to predict a swirl velocity field; his argument was based on a direct-finite difference solution and disputes the isotropy assumptions for turbulent swirling flows. Contributions on the behavior of the vortex flow at high swirls can also be attributed to Bossel (86). He formulated the problem by the method of weighted residuals, using Bessel functions as approximating functions, and this analytical approach showed that, at high swirls, the inviscid equation of rotating flow controlled the flow behavior of vortex flows. He developed a computational method for the solution of the above mentioned inviscid equation for a variable outer stream surface. His method explains the vortex breakdown bubbles in divergences, tubes and free flows.

Mathematical treatment of incompressible flow in a conical hydro-cyclone was presented by Bloor and Ingham (87) in 1973. Their theory presents a simple model for the determination of velocity components at various levels in the conical chamber, and can be used as a

basis for assessing theoretically the performance of equipment involving swirling flows.

Lawler and Ostrach (88), and Burton (89) studied the influence of gravity on the performance of a conical vortex separator. The former defined a Froude Number for the qualitative evaluation of the relative strength of the gravitational and inertial forces. Their analytical results were obtained by considering the body force to act on the fluid, both within and outside the boundary layer. Burton's work differs from Ref. (88) in that he neglected the effect of gravity in the thin region of fluid outside the boundary layer. Such an assumption allowed explicit prediction of the effect of a body force on the boundary-layer flow, and resulted in definition of the limiting condition for use of a vortex separator in an adverse gravity field.

The effects of the mainstream viscosity and that of the wall boundary layer were considered recently by Crow (90). He presented a composite solution for the flow field of a three-dimensional, incompressible, laminar, viscous vortex confined inside a conical converging nozzle. His confined vortex flow field was divided into mainstream and boundary layer regions. He used a particular class of solutions of the general equations of motion to represent the vortex flow in the mainstream region, then the velocity and pressure profiles from the mainstream region were used as boundary conditions to generate an integral momentum solution in the boundary layer region.

Converging nozzles were also studied analytically and experimentally by Norton et al. (91); they developed a correction for the effects of

viscous dissipation and derived governing equations for the rotating, inviscid, adiabatic and compressible flow of a perfect gas. Mager (92), also, analytically studied the incompressible, viscous swirling flow field in a converging-diverging nozzle. In this study, the nozzle flow field was divided into a vortex core and a mainstream region. In the vortex core near the nozzle centreline, a boundary layer integral momentum solution was matched to a potential vortex in the mainstream region. Conservation of total system mass flow and momentum was the criterion used to change this solution as the flow progressed axially through the nozzle. King (93) considered an inviscid, compressible case of the same problem and found that the mass flow through the nozzle was strongly dependent on the ratio of inlet tangential to radial velocity. Above a critical value of this ratio, reversed flow occurred in the subsonic portion of the nozzle, but no reversed flows were found to occur in the supersonic portion of the nozzle. Both of these studies neglected the effects of the nozzle wall boundary layers, which must be included if the analytical model is to describe confined vortex flows accurately.

Additional information on the subject of confined vortex motion can be found in references (94, 95 and 96). However, it is believed that the references briefly summarized in this literature review are the most significant in a body of vast published articles.

#### SUMMARY

Flow patterns and structure of turbulence have been shown to exert significant effect on the efficiency and operation of industrial equipment involving swirling flows.

In general, most investigations reported in the literature have been limited to measurements and predictions of temperature and concentration profiles, based on some assumed velocity fields. Although particular attention was paid to vortex tubes, none was given to other geometries. Very few investigators have tried to measure turbulence structures in a confined vortex flow, and none have attempted to define the turbulent pattern occurring in a spray-dryer type vortex chamber.

Comparison between results of different investigators is rendered difficult, if not impossible, since the test geometries (size and inlet and outlet geometries, etc.) are generally not similar and the measurement errors cannot be estimated with sufficient confidence owing to lack of details. Moreover, from a critical analysis of the literature, it is noted that adequate description of the experimental apparatus and specifications of the electronic instrumentation are generally not given by most authors, with the result that most available data are unduly biased owing to lack of complete information.

In general, experimental and theoretical results of most workers agree in demonstrating the following significant points about confined vortex flows:

(a) The confined vortex flow field is three-dimensional in nature (14,32,47,75,76,77,78).

(b) High turbulence is inherent in any device employing a rotating flow within a stationary container. Boundary layer on the outer wall of the container is unstable to radially inward displacement and the separation of this boundary layer in certain locations of the apparatus is

the source of high turbulence (40,43,52,55,70).

(c) The tangential component of the velocity is predominant in the entire vortex flow, with the exception of the turbulent core in the centre (47,48).

(d) In a swirl flow, the radial component of velocity is very small (26,27,28,32).

(e) In a confined vortex flow, the predominant axial velocity is concentrated in an annular region adjacent to the wall, while in the interior of the flow the axial velocities are small (25,26,27,28,32,37,38,79).

(f) In a confined vortex flow, the axial velocity falls off sharply toward the centre of the vortex, and may exhibit a reverse flow near the centre (26,27,32,39,47,61,73,93).

(g) Flow in the central portion of the vortex tube is one of nearly constant angular velocity (forced vortex) (28,29,30).

(h) In a vortex flow, there is a helical-shape dynamic axis of symmetry (28,34,43).

(i) Spiral flow patterns are quite insensitive to changes in the inlet velocities (26,27,28,32,53,54).

In conclusion, a survey of literature dealing with experimental and analytical studies on vortex flows transport points to the necessity of detailed turbulence measurements, which eventually will lead to more realistic analytical formulations.

METHOD OF MEASUREMENTS IN VORTEX FLOWS

## METHOD OF MEASUREMENTS IN VORTEX FLOWS

### INTRODUCTION

Many of the reported observations of vortex flows have been based on visualization of the flow giving qualitative descriptions of part of the flow field. Attempts to quantify these visual observations were rarely successful. Almost all the reported measurements of velocities in vortex flow field have been based upon the introduction of probes into the flow. However, the latter is particularly sensitive to the introduction of local disturbances which may trigger instabilities and cause vortex breakdown. When the probe dimensions are small with respect to the vortex core and particular care is taken to minimize the disturbing effect of the probe, accurate measurements of velocities can be obtained. Earlier measurements were made with pressure impact tubes such as the three-dimensional directional pressure probe while more recent measurements have been made with hot wire anemometers.

### THREE-DIMENSIONAL DIRECTIONAL PRESSURE PROBE

The three-dimensional directional pressure probe, sometimes referred to as a five-hole pitot tube, is used to measure yaw and pitch angles, and total and static pressures. Five pressure tappings are drilled in the hemispherical probe head, one on the axis and at the pole of the hemisphere, the other four spaced equidistant from the first and from each other at a latitude of  $30^\circ$  to  $50^\circ$  from the pole. The principle of operation of the probe (97) is based upon the surface pressure distribution around the probe tip. If the probe is placed in a flow field such

that the total mean velocity vector is at some angle to the axis of the probe, then a pressure differential will be set up across these holes, the magnitude of which will depend upon the geometry of the probe tip, relative position of the holes and the magnitude and direction of the velocity vector. Each probe requires calibration of the pressure differentials between holes as a function of yaw and pitch angle. For Mach numbers less than 0.2, calibration is independent of Mach Number, Reynolds Number and turbulence intensity (up to 30%).

If the system allows, it is preferable to rotate the probe until the yaw pressures are equal, measure the angle of probe rotation (yaw angle) and determine the pitch angle from the remaining pressure differentials. The probe can be used without rotation by using the complete set of calibration curves but the complexity of measurement and calculation is increased and accuracy is reduced. Difficulty is often found in obtaining accurate measurement near the vortex centre and interpolation through the vortex centre may be required. Measurements have been reported using tips with a diameter of 3.2 mm and holes with diameters of 0.25 mm. Use of a pressure transducer for measurement of pressure differentials is recommended, particularly for pressure differentials of the order of 0.10 mm water gauge which arise at various flow magnitudes and angles. Velocity components are calculated from total pressure, static pressure and yaw and pitch angle measurements.

#### FLOW SENSE INDICATOR

Flow reversal, as mentioned in the Literature Review, can arise in

some patterns of vortex flows and it is necessary to determine the general direction of the velocity vector before introducing a measuring instrument into the flow. For example, introducing a directional pressure probe, as described above, into a flow with the sensing head pointing in a direction opposite to the main flow direction will result in completely erroneous measurements. Flow sense can be detected by use of tuft grids, or alternatively a simple flow sense indicator can be constructed using a closed tube with two pressure tappings in the side walls facing in opposite directions ( $180^\circ$  spacing). Carrying out a traverse through the flow and measuring the pressure differential with such a probe indicates the main flow direction. Such a probe is also useful for determination of reverse flow boundaries in recirculation eddies.

#### STATIC PRESSURE MEASUREMENTS

Static pressure gradients occur in all vortex flows as a consequence of tangential velocity (and associated centrifugal force) gradients, as well as due to variations in turbulence intensity. Care is required in the measurement of static pressure in turbulent vortex flows in order to avoid erroneous contributions from the dynamic pressure components. This can be achieved by aligning the static pressure measuring surface so that the local velocity vector is in the plane of the surface. A disc static probe was used by Miller and Comings (98) for non swirling flows where they showed the reliability of results obtained with a disc probe in a single and dual jet flows by balancing pressure and shear terms (from hot wire anemometer measurements) in the equation of motion. The disc

probe has been modified for use in swirling flows (99), by fitting a simple yaw meter--two hypodermic tubes with edges sawn off at 45°--fitted to the underside of the disc. The disc is rotated until the pressure differential in the yaw tube is zero and then the static pressure is measured via the static pressure tapping.

Measurements of static pressure can also be made by using the five-hole pressure probe previously described, and calibrating the probe as a function of yaw and pitch angle.

#### THE HOT WIRE ANEMOMETER

The hot wire anemometer (the instrument used in the present study), has the particular advantages of small size (5-micron diameter wires) causing minimal disturbance to the flow coupled with high sensitivity at low flow velocities. The high frequency response of more than 100 KHz allows measurements of velocity, turbulence intensity, shear stress and correlation. Provided that sufficient care is taken to make frequent calibrations of voltage as a function of velocity, and that compensations for ambient temperature and density variations are made, measurements of mean velocity can be made with an accuracy of better than 1% with relative ease. In regions of high turbulence as encountered in vortex flows, time averaging as long as 2 to 3 minutes is required for each measuring point. Accuracy has been shown to be improved (100) by using higher order polynomials for fitting experimental calibration curves of the form:

$$E'^2 = A' + B'U^{1/2} + C'U \quad (6)$$

where  $E'$  is the mean voltage;  $U$  is the mean velocity and  $A'$ ,  $B'$  and  $C'$  are constants.

Curve fitting is improved if the zero velocity voltage is excluded, since spurious values of  $A$  are generated due to free convection effects. This leads to curve fits with a standard deviation of less than 1%. For a flow which is not normal to the probe wire the instantaneous velocity is given by\*:

$$U_i = (U_x^2 + g^2 U_y^2 + k^2 U_z^2)^{1/2} \quad (7)$$

where  $U_x$ ,  $U_y$ ,  $U_z$  are components of the velocity vector and  $g$  and  $k$  are constants which must be determined for each individual probe by calibration of the wire as a function of yaw and pitch angle. Careful prong spacing and gold plating of the sensing wire near the prongs results in values of  $g \rightarrow 1$  and  $k \rightarrow 0.05$ . Developments in manufacturing techniques of probes should, in the near future, lead to elimination of the necessity to calibrate for  $g$  and  $k$ .

For three-dimensional flow fields the components of the velocity vector have been determined by two methods. The first, developed at Sheffield University by Davies (100), Allen (101), and Syred (102) involves the introduction of single wires and varying the orientation of the probe to the main flow direction. Two probes are generally used--one with the wire inclined at  $45^\circ$  to the main flow direction and the other the standard probe with the wire normal to the main flow direction. Initially (100,101), measurements at each measuring point required orientation of the wire in six different positions. The instantaneous

---

\* This case is discussed in detail in Appendix I.

velocity vector was calculated from the set of six measurements, and subsequently by assuming that the six output voltages are of similar shape and frequency distribution, and also that the six output voltages are in phase, calculations were made of mean velocity components and normal and shear components of the Reynolds stress tensor.

Syred (102) has improved on the previous methods by taking four measurements at each point, using a single probe. He also discusses the significance of the effect of non-linearity of the calibration curve and the assumptions of similar regular shape and of similar frequency distribution of the four relevant voltages on the evaluation of the turbulent fluctuating velocity components.

A three-wire probe is also used for measuring vortex flows. It has the advantage that measurements with each wire are made at the same instant of time and this may be the critical factor in choosing a method for flows in which the vortex is not stationary with time. A separate anemometer circuit is required for each wire. It has the disadvantage that the fluid volume, in which the measurement is made, as well as the interference to the flow, are increased.

In the present study, as shall be described in the Experimental Section of this thesis, the components of the velocity vector and turbulence intensities were determined by means of a single-wire probe inclined at  $45^\circ$ , as described above. However, in the present work the dominant flow was not in the plane of the sensor-prong plane; hence, it was necessary to derive a new set of inclined hot-wire response equations from the assumption of the cosine law cooling, and the analysis substantiating this derivation is given in detail in Appendix I.

§  
EXPERIMENTAL SECTION

## EXPERIMENTAL SECTION

### INTRODUCTION

The review of the published literature which has been presented has made it abundantly clear that a knowledge of the characteristics and structure of a spiral turbulent flow is of prime importance in the design and performance of many industrial pieces of equipment. More specifically, this laboratory has been engaged for many years in a continuing program of research into the fundamental principles of the spray-drying process. Recent attempts to lay the foundations for the design of spray-drying chambers (14,15) have clearly demonstrated the importance of droplet trajectories which are in turn entirely dictated by the flow patterns of the entraining gas and by the magnitude of the three components of its mean-flow velocity. It is in support of this program that the present study was initiated and that the geometry of the vortex chamber--which resembles that of a spray dryer--was selected. Using ambient room air as the working fluid, the flow pattern and turbulence characteristics were studied as a function of the entrance velocity of the air.

### EXPERIMENTAL APPARATUS

A photograph of the chamber under investigation is given in Figure 4, and its diagrammatical presentation illustrated in Figure 5. This is typical of a down-flow, vertical spray-drying chamber, and it consists of two main sections: an upper jacketed cylindrical section and a lower conical part. The chamber had an overall internal height of six feet (183 cm), the upper cylindrical section being two feet (61 cm) in

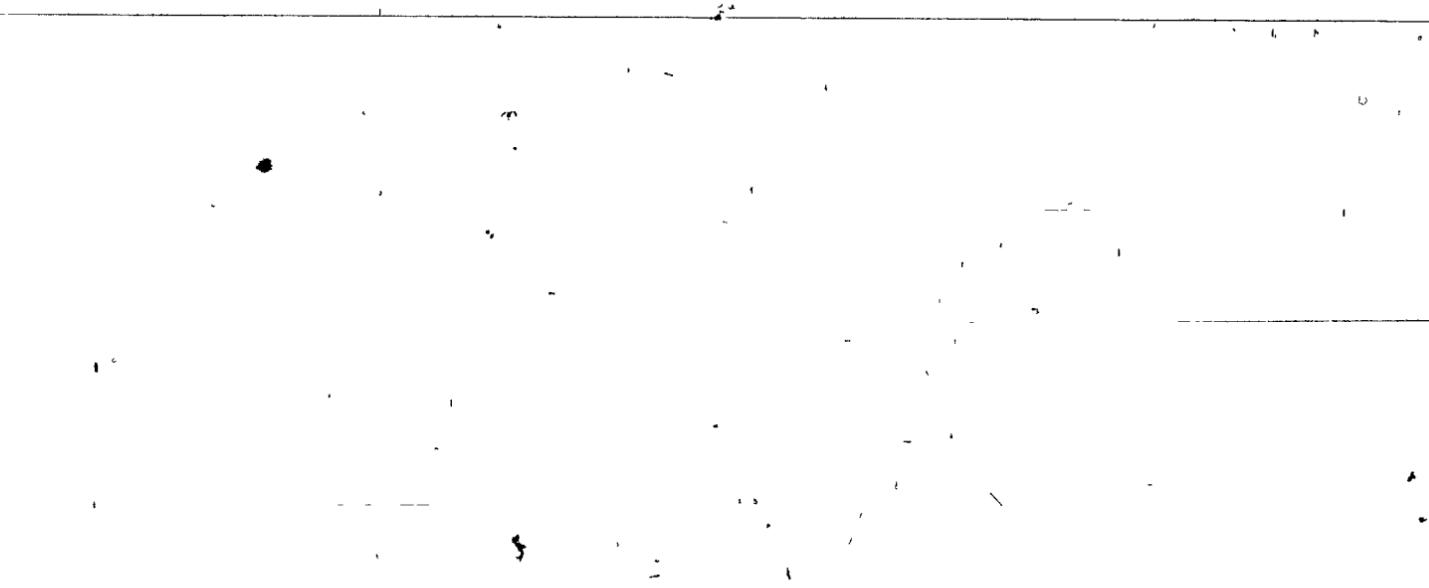


FIGURE 4

Photograph of the Chamber

ht

0



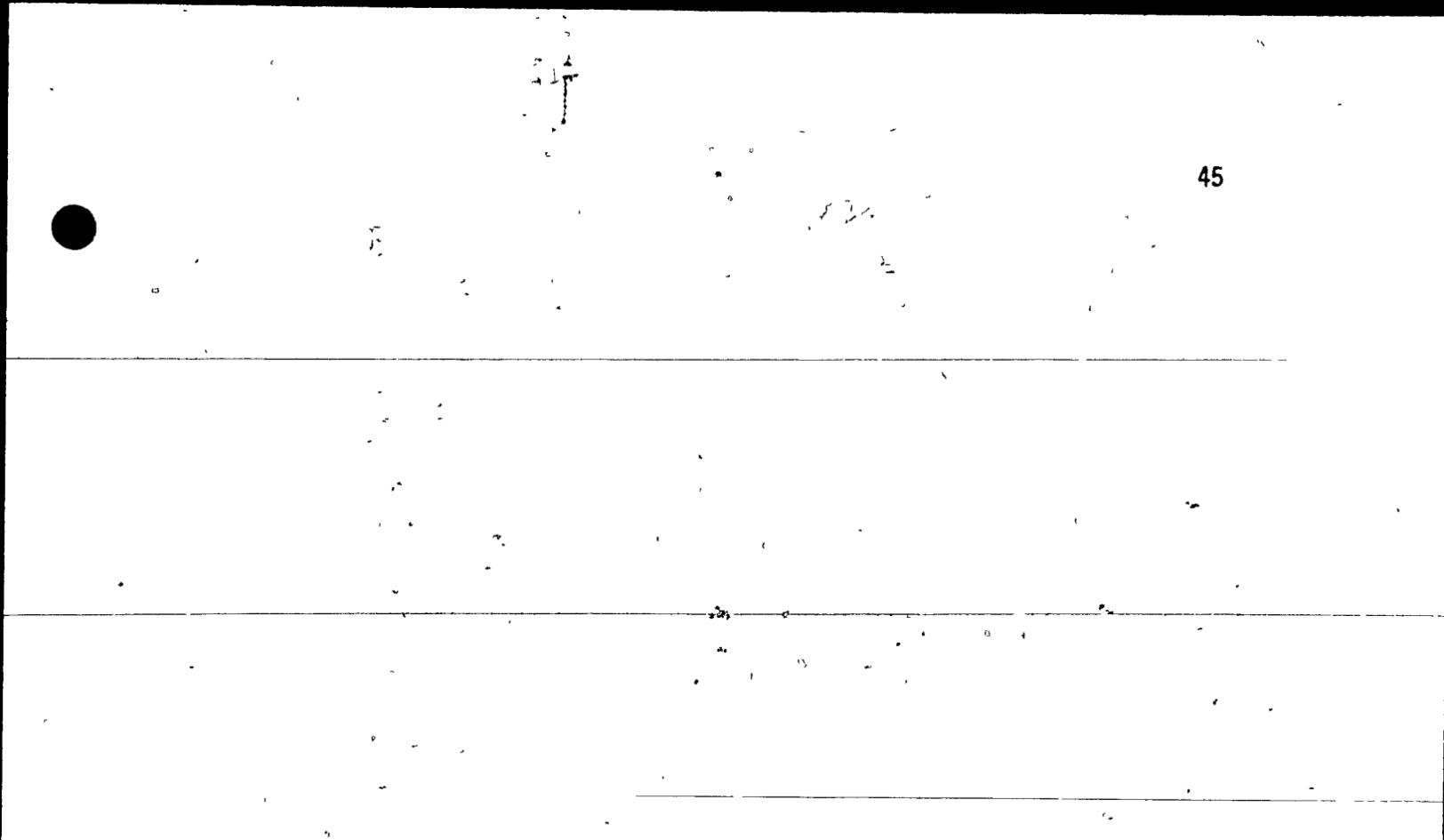
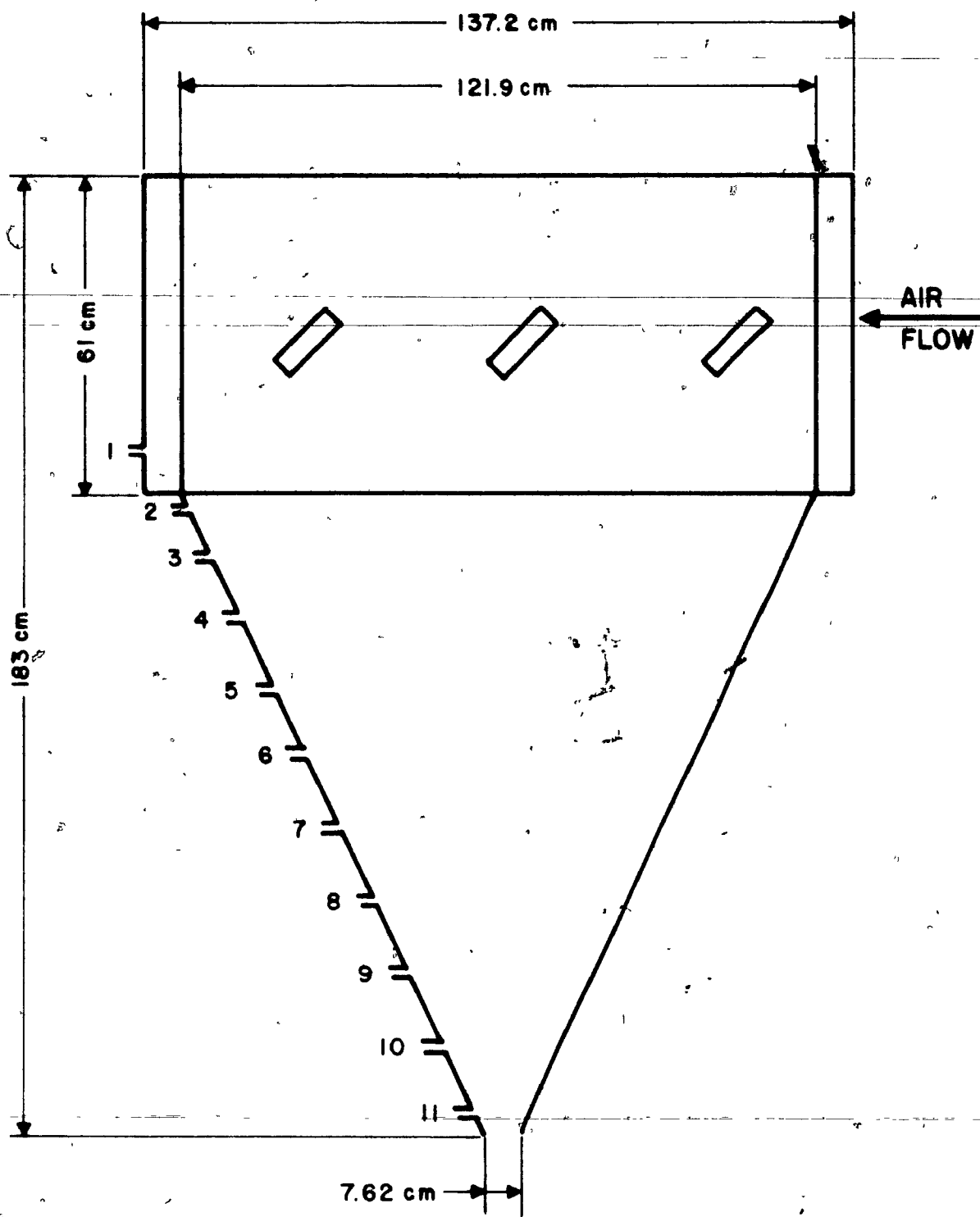
The diagram, which is missing from the page, would typically illustrate the internal structure of a chamber, possibly showing components like a piston, valves, or internal baffles, and their relative positions and movements.

FIGURE 5

Schematic Diagram of the Chamber



height and four and one-half feet (137.2 cm) in diameter. It was constructed of 20-gage galvanized steel.

A motor-blower assembly (Figure 6) consisting of a 3-H.P., 550-volt, 3-phase A.C. electric motor, connected to a V belt-driven blower, model 6 CI type SS wheel, made by Canadian Fans Limited, was used as a means of providing different air flowrates to the chamber. This could supply a maximum air flowrate of 931 cfm ( $584 \text{ m}^3/\text{s}$ ) at a static pressure of 7-in (17.8 cm) of  $\text{H}_2\text{O}$ . The inlet and outlet of the blower had outer diameters of 6-in (15.24 cm) and were connected, respectively, to an inlet blast gate for controlling the flow, and to an appropriate enlarging section to accommodate the 8-in (20.32 cm) galvanized duct entering the chamber. A 200-mesh stainless steel wire cloth was also attached to the inlet of the blower in order to filter the entering air.

The volumetric flowrate of air was measured and controlled by two square-edged orifices having 9.86 and 6.99 cms. These were placed, one at a time, in the outlet line of the blower, and their pressure differentials were measured between "Radius Taps" located on the same line, and were read on a U-type manometer filled with dyed ethanol. Two other U-type manometers filled with ethanol were used to read pressures in the inlet and the outlet pipes of the chamber; both were referred to the atmospheric pressure. These various manometers, together with a barometer (used to read atmospheric pressure necessary in the calibration of hot-wire probes), and a thermometer to record the ambient temperature, were installed on a single panel which is shown in Figure 7.

FIGURE 6

Photograph of the Motor-Blower Assembly

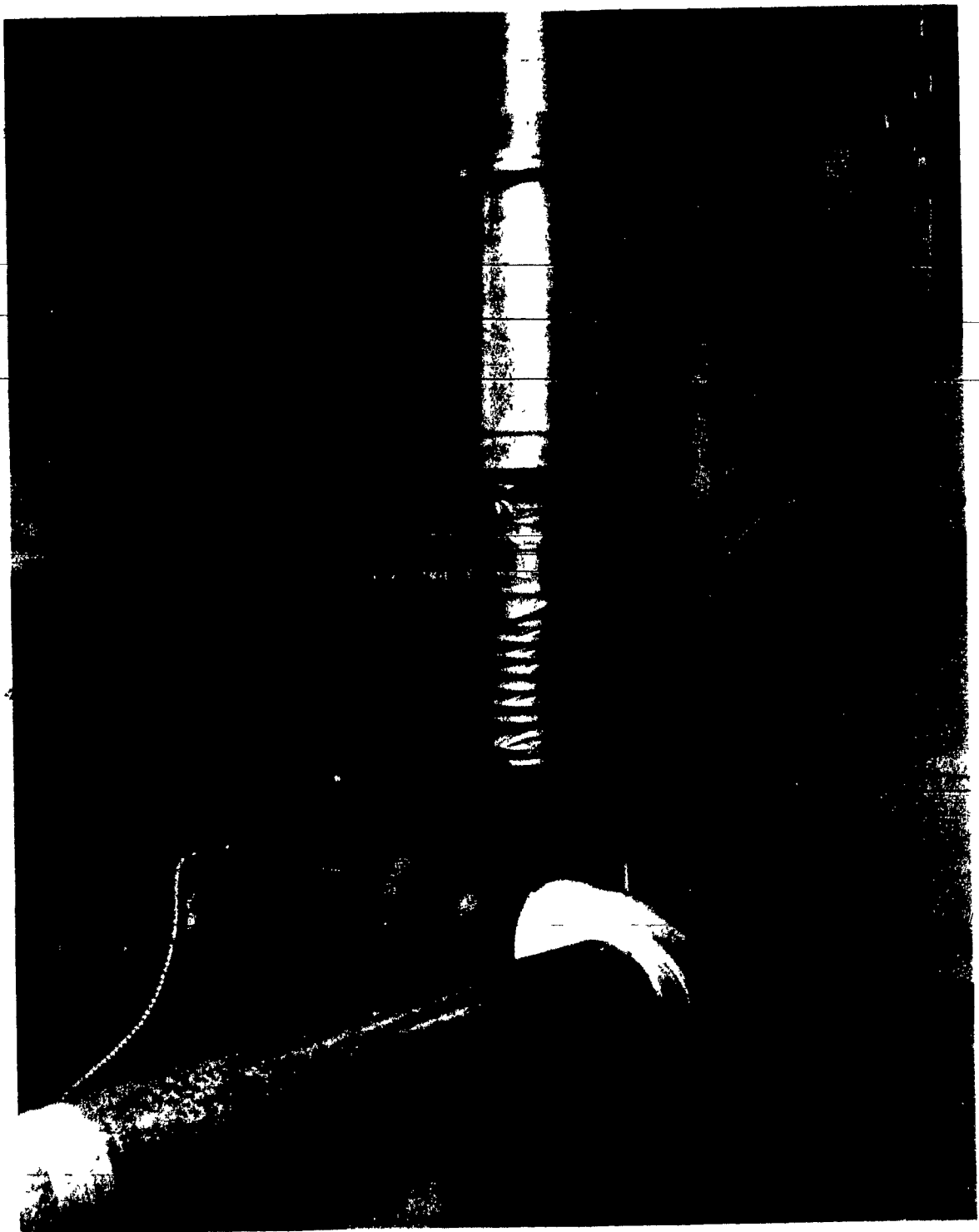
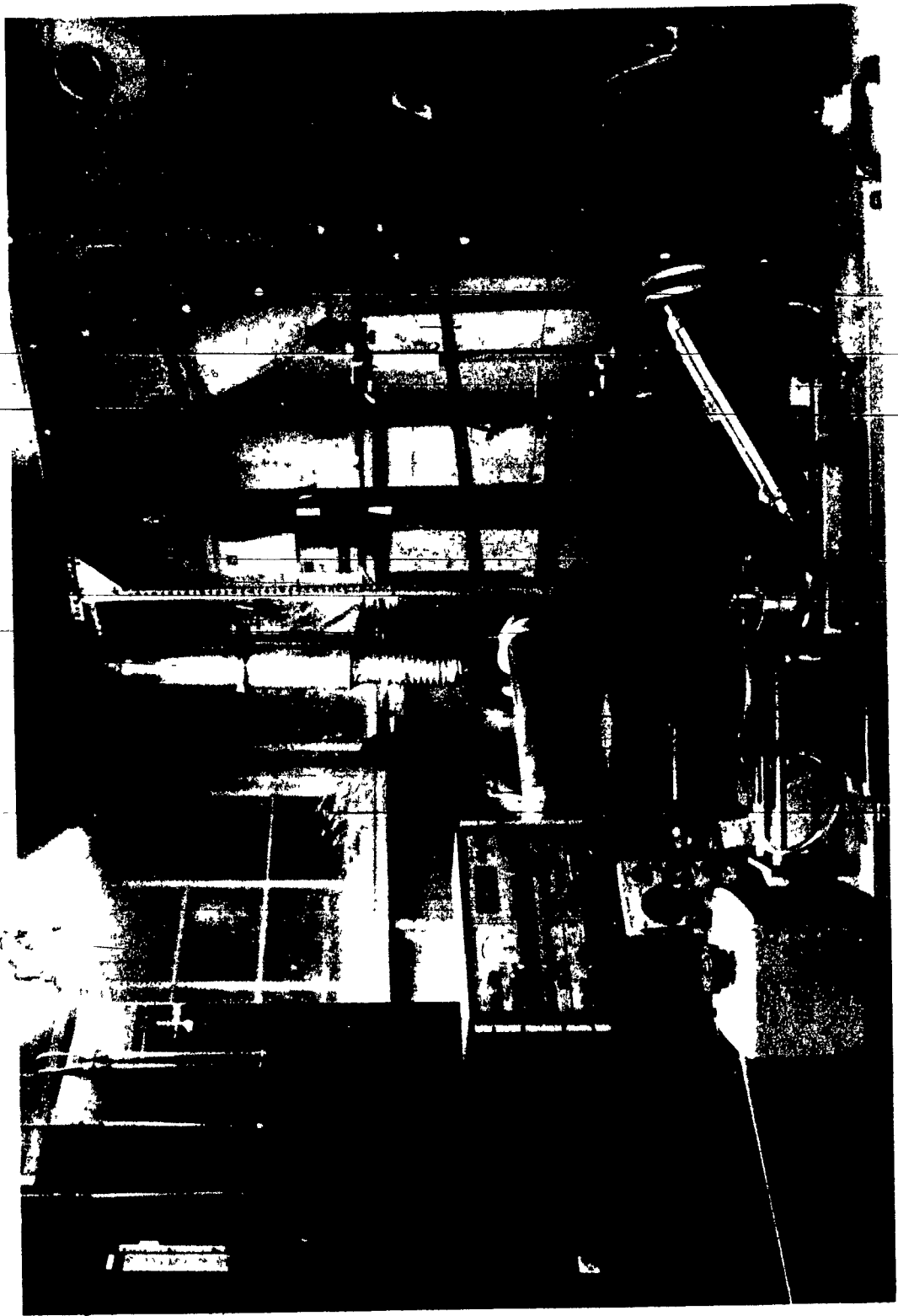


FIGURE 7

Photograph of the Experimental Equipment



The temperature of the inlet air to the chamber was also recorded during each run. This was done using a thermometer inserted in the suction line of the blower.

The air from the blower entered the jacketed cylindrical section tangentially, and was properly distributed to the chamber by six  $1\frac{1}{2}$ -in x 6 in (3.81 x 15.24 cm) slots in the inside wall at an angle of 45 degrees. The metal was not cut out, but was merely bent back along a vertical edge.

At points along the chamber wall, eleven holes were drilled (Figures 4 and 5), and  $\frac{7}{16}$ -in (1.11 cm) I.D. bushings were soldered to them for the insertion of the traversing mechanism and probes. Corks were used to plug the holes that were not in use, so that the internal flow patterns were not disturbed. The location of these holes relative to the top of the chamber is shown in Table I. It may be noted that only station 1 was located in the cylindrical part of the chamber. Six observation windows were also installed, one at the top and five on the side of the cone, for the purpose of lighting the inside of the chamber, and for flow visualization, respectively.

Finally, it should be mentioned that the vibration of the test section (chamber) induced by the fan was reduced to a negligible level by using a small section of light-weight flexible connection, made by "Flexaust Co.", in the outlet line of the blower. The fabric was impregnated and coated with neoprene compounds, and had a close pitch spiral wire reinforcement embedded within the fabric piles.

## SPECIFICATIONS OF MEASURING INSTRUMENTS

### Processing Equipment

The anemometer arrangement is shown in Figure 8. The mean and fluctuating velocity components were measured with a DISA type 55M01 constant temperature anemometer. The anemometer was operated at an overheat ratio  $R = 0.80$ , where

$$R = \frac{(\text{Operating Probe Resistance}) - (\text{Cold Probe Resistance})}{(\text{Cold Probe Resistance})} \quad (8)$$

No corrections were deemed necessary for small variations in ambient temperature.

The frequency response of the anemometer was always found to be such that its 3dB down point (roll-off frequency) was greater than 5KHz, a level much higher than the highest frequency of interest in the present investigation. The response of the anemometer was fed to a DISA type 55D10 linearizer which incorporated logarithmic amplifiers to give a response

$$V_{out} = X(V_{in}^2 - V_0^2)^{m'} \quad (9)$$

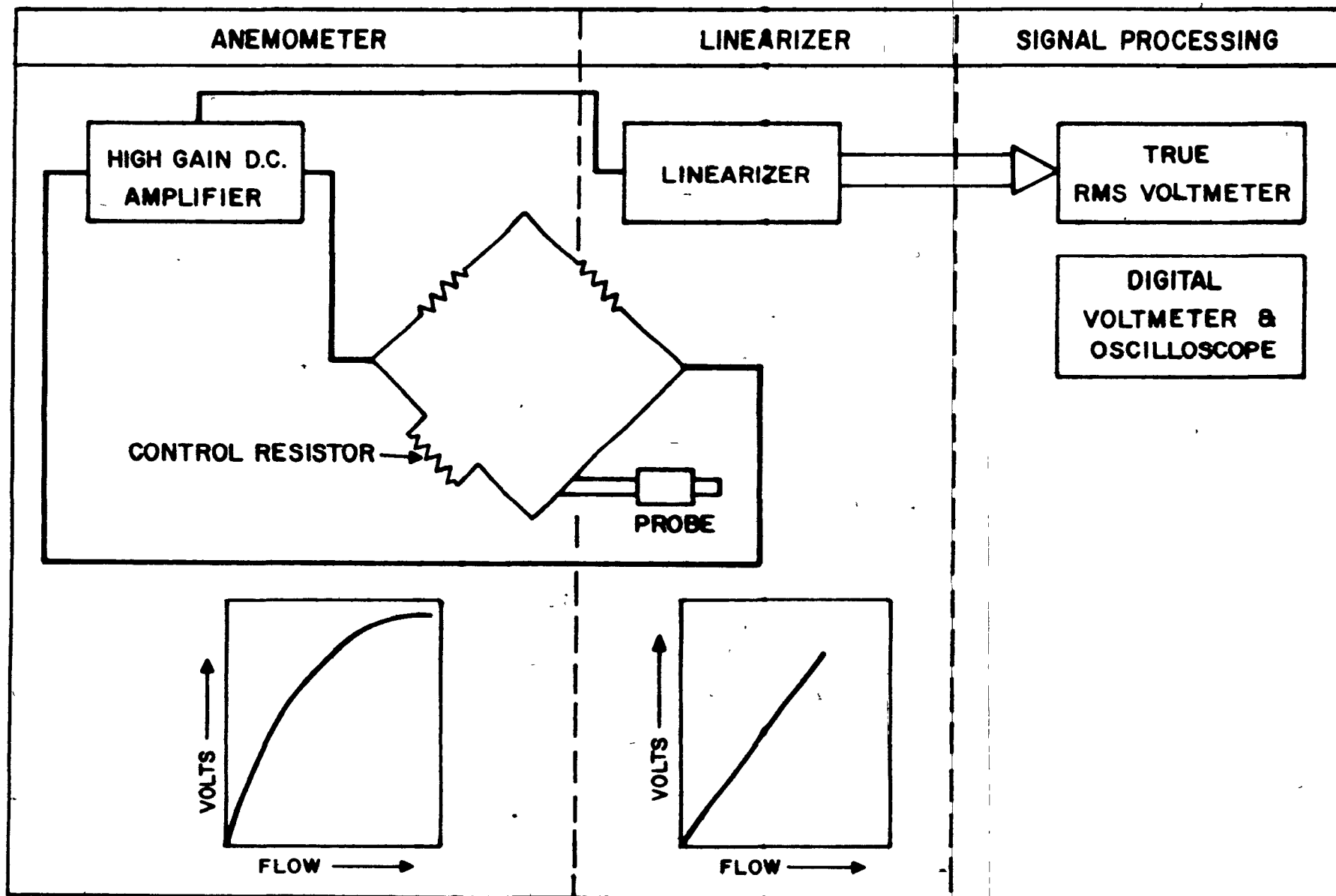
where  $X$ ,  $V_0$  and  $m'$  were all constants adjusted so that the output voltage was a linear function of the velocity of the gas flow past the wires.

The D.C. components of the signals were measured by a 55D31 digital voltmeter of the electronic type which read on a 100-volt scale to an accuracy of 0.1% of full scale  $\pm 1$  digit. Even at high flowrates, it was necessary to operate this with a smoothing filter of time constant = 3 seconds, in order to obtain an easily readable signal.

A DISA type 55D35 RMS voltmeter was also used, to measure the A.C. components, and the latter could be read to  $\pm 1\%$  within the wave-band

FIGURE 8

Block Diagram of the Anemometry System



10 Hz-100 KHz. This incorporated an integrator of variable time constant, and again was usually set to 3 seconds.

### Probes

Two probes were used: a DISA type 55A22 standard normal wire and a DISA type 55A25 inclined wire. Details of these are given in the manufacturers catalogue but a common feature is the 1.1 mm long platinum-coated tungsten wires, 0.005 mm in diameter, supported by nickel pins. The bodies of the probes were 7 mm in diameter.

The angle of inclined wires was measured with a 50X Nikkor profile projector, and the probes were calibrated using a DISA type 55A60 calibration unit, whose background turbulence was less than 0.15% at a flow rate of 300 f.p.s. (91.4 m/s). The wires, normal and inclined, were normalized to an output of 3.0 and 1.5 volts respectively, at a free stream velocity of 30.0 m/sec. A typical linearized calibration curve is shown in Figure 9. An oscilloscope was also used to visualize the responses from hot-wire probes.

A photograph of the whole processing equipment is shown in Figure 10.

### Traversing Mechanism

The probes were supported by a DISA type 55A42 pressure tight probe support, and the whole system was placed in the desired position in the test section by means of a manual traversing mechanism made by United Sensor and Control Corp.

The probe system was supported on a tripod of adjustable length for the vertical traverses, and Figure 11 represents a photograph of the whole traversing mechanism.

### Measurements of Distances

Distances were measured on the traversing unit in increments of 0.1-in (2.54 mm) on a vernier. Standard scale length of 24-in (61 cm) was chosen as appropriate for this work.

Linear movement was restricted by friction of flat springs sliding on the scale, adjustable by a thumb screw which could be tightened to lock the probe at any location (Figure 12).

### Measurements of Angles

Angle of rotation of the probe was measured over a full  $360^\circ$  on a protractor graduated in  $2^\circ$  divisions for easy readability and a special large scale vernier (Figure 12).

Both vernier and protractor were friction-loaded with adjustable springs and balls for easy, accurate rotation to any angle. The adjusting spring screw could be tightened by a thumb screw or an Allen wrench to lock the probe at any angle. The vernier was also fully adjustable, permitting the zero angle point to be set at any time without loosening the probe in the collet and losing the distance setting.

### OPERATING PROCEDURE

#### Orifice Calibration and Flow Rate Measurements

The orifice discharge coefficient is significantly affected by flow disturbances which originate in valves, bends, and other fittings located upstream from the orifice. It is less affected by downstream disturbances. As a general rule, the meter should be placed

FIGURE 9

Typical Linearized Hot-Wire Calibration Curve

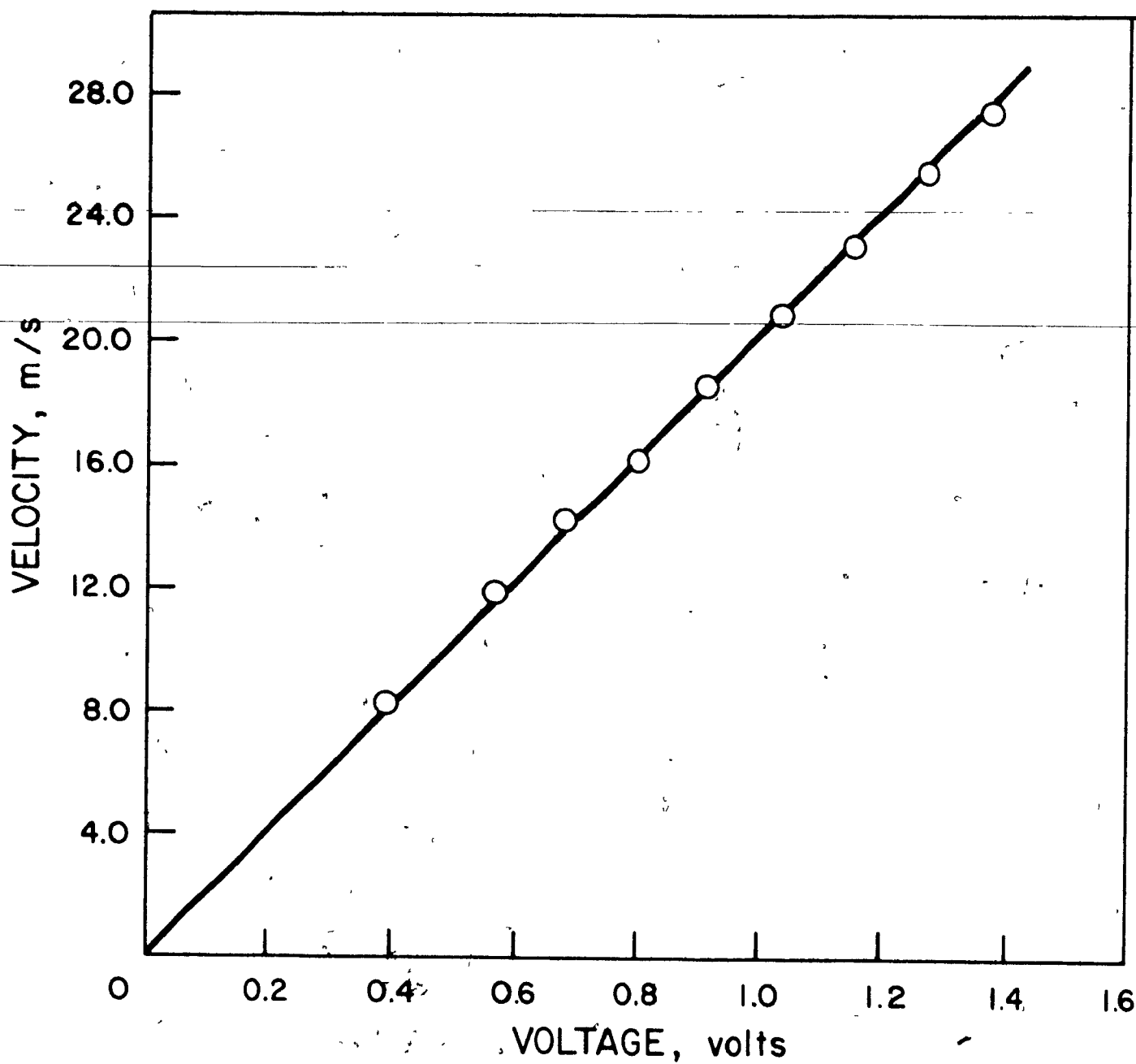


FIGURE 10

Photograph of the Anemometry System



FIGURE 11

Photograph of the Traversing Mechanism

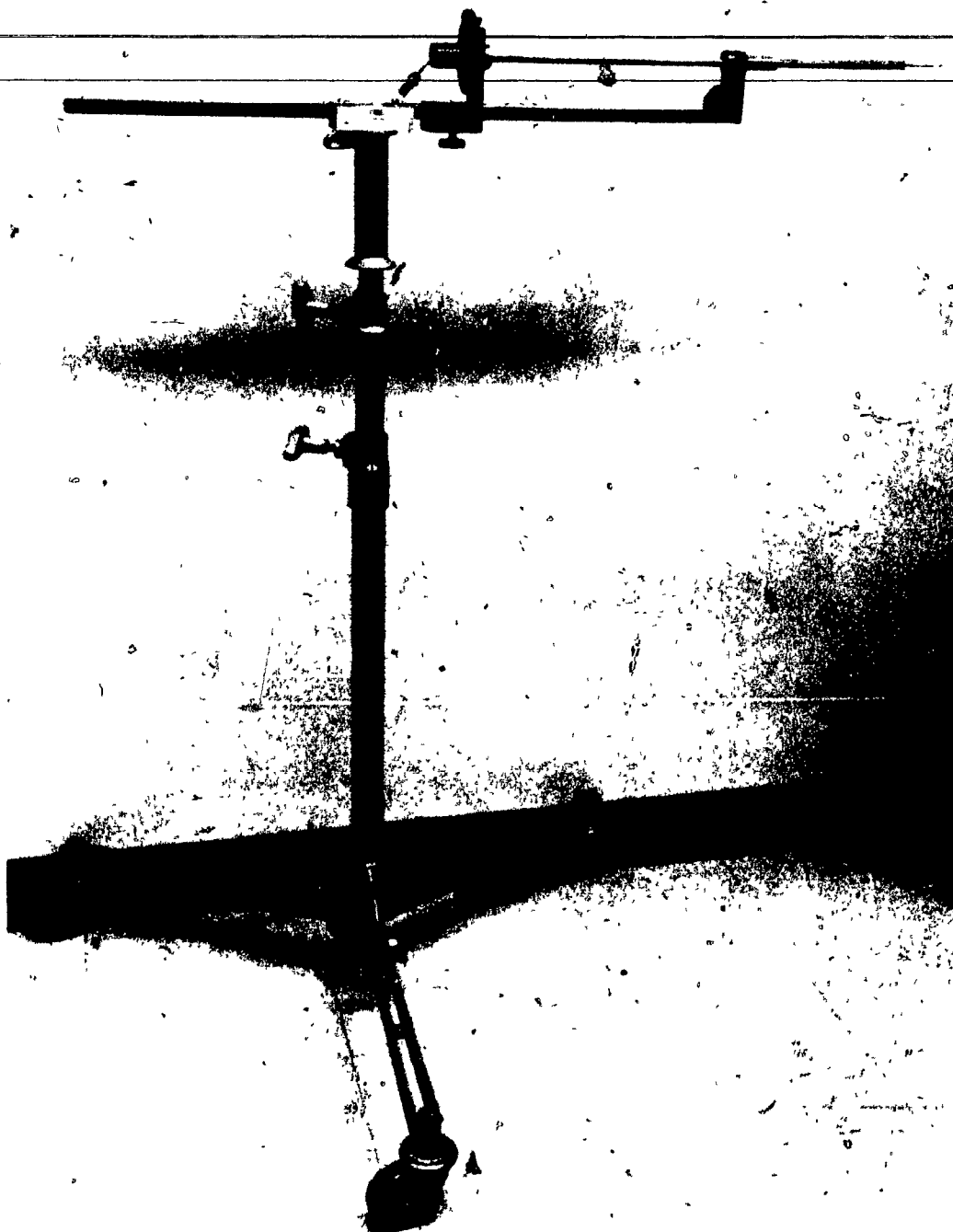
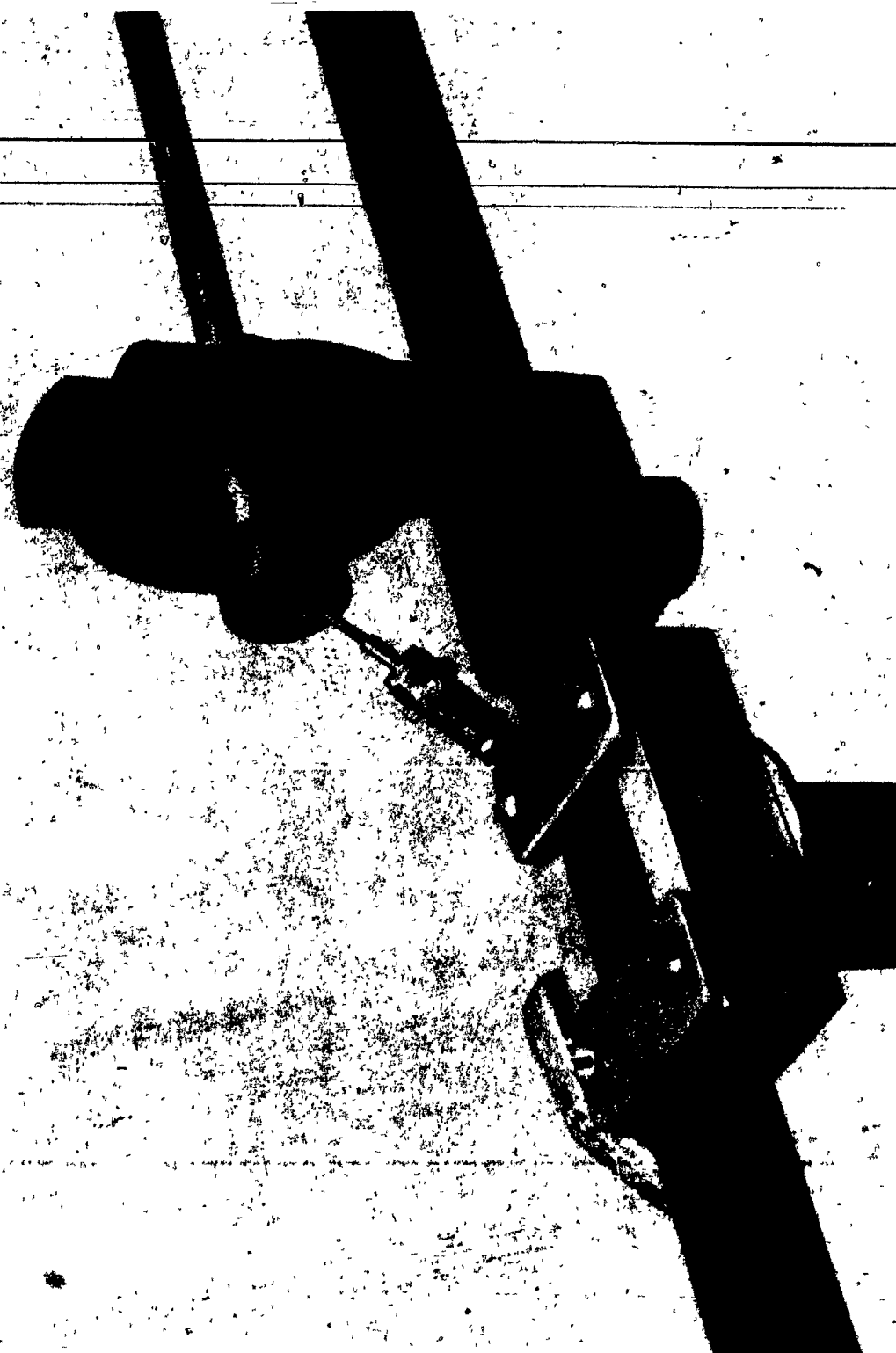


FIGURE 12

Close-up Photograph of the Traversing Device



50 pipe diameters downstream and 10 pipe diameters upstream from any disturbance. Since allowance for the above lengths was impossible in our laboratory, it was decided to calibrate the various orifice plates used in the orifice meter against a pitot tube.

A simple pitot tube of standard design was used. The velocity of flow was then calculated from the difference between the dynamic (or stagnation) pressure and the static pressure, by means of a precision inclined manometer, using methanol as the indicating fluid.

The local velocity was determined from the following equation:

$$u_o = c \sqrt{2g[(\rho_m - \rho_o)/\rho_o] \Delta H} \quad (10)$$

where  $u_o$  = the local velocity, ft/s

$c$  = a constant coefficient (assumed to be 1.0)

$\rho_m$  = density of manometer liquid (methanol) at ambient temperature, lbm/ft<sup>3</sup>

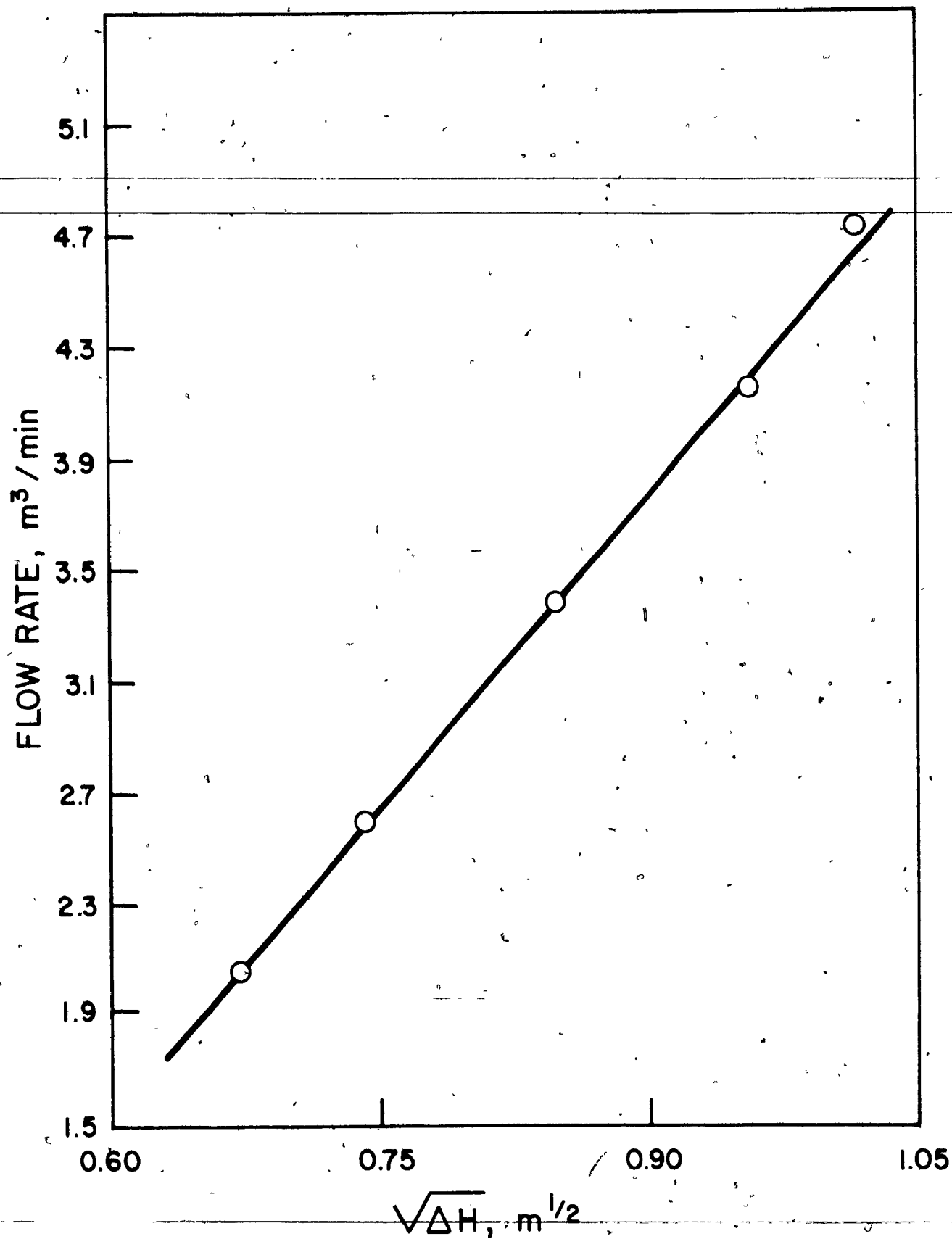
$\rho_o$  = density of flowing fluid (air) at ambient temperature, lbm/ft<sup>3</sup>

$\Delta H$  = difference in fluid levels in the manometer, ft.

A ten-point traverse was made across the duct in the suction line to the blower, from which the average velocity in the duct, and hence the volumetric flowrate to the chamber, were calculated. From simultaneous readings on the orifice manometer, an accurate calibration curve for the latter was obtained. A typical orifice calibration curve for the 6.99 cm orifice is presented in Fig. 13.

FIGURE 13

Typical Orifice Calibration Curve



### Flow Visualization and Determination of Flow Angles

To visualize the direction and pattern of flow, small wool tufts were fastened to the heads of eleven 3/16-in. (0.476 cm) diameter stainless steel rods, and inserted into the chamber through the measuring stations, at different radial distances. The directions of the tufts were then visually recorded through the plexiglass windows of the chamber wall. This procedure was used for the three different inlet velocities under investigation (1.6, 2.4 and 3.2 m/s).\*

It is, of course, realized that this method of determining the angle of flow was somewhat qualitative and the errors involved will be discussed in a later section.

An attempt was also made to measure the flow angles quantitatively by means of a single straight hot-wire probe. Since such a wire is virtually insensitive to a flow parallel to its axis, the direction of flow could be found as the direction of the wire for minimum D.C. output signal. The straight hot-wire probe was therefore rotated, in intervals of two degrees, at the desired location until the minimum D.C. voltage was read. The angle at which this minimum D.C. voltage occurred was read by means of a protractor, Figure 14, and then recorded as the flow angle.

---

\* All inlet velocities were average velocities based on the total cross sectional area of the (3.81 x 15.24 cm) slots in the inside wall of the jacketed cylindrical section.

This procedure was carried out for the three inlet velocities under investigation and also for different radial and axial positions throughout the chamber.

### Measurements of Velocities and Turbulence Intensities

An inclined hot-wire probe, described in a previous section, was used in these measurements. This was maintained at a constant temperature determined by its resistance, and the usual overheat ratio of 0.8 was employed, as this gave a wire temperature of about 300°C and the best sensitivity without danger of burning out. After the ambient temperature had reached a steady level, the cold wire resistance was measured ( $R_g$ ) and then the operating resistance set to  $R_w = 1.8 R_g$ .

Adjustments to the linearizing circuit were then carried out with the wire heated while the probe tip was still encased in its protective sheath. The reason for this procedure was that the wire should be surrounded by still air at the correct temperature. If this were indeed so and Collis' law (109,110) applied right down to zero velocity, then the voltage input to the linearizer would be  $\frac{AR_w(R_w - R_g)}{V_o^2}$  and by putting  $V_o^2$  equal to this (see equations (6) and (9))\* , a voltage signal proportional to the  $m^{th}$  power of velocity would be produced. In practice, the air is not still because of natural convection, although the sheath protects the wires from large eddy currents in the laboratory, and it is necessary to reduce  $R_w$  to  $R'_w$  so that when the

---

\* Equation (6) is also written as

$$V_{in}^2 / R_w (R_w - R_g) = A + BU^n$$

adjustment to the linearizer is made to give zero output voltage,

$V'_0$  is set equal to  $V'_{ino}{}^2$ , where

$$V'_{ino} = AR'_w(R'_w - R_g) + \text{the natural convection contribution}$$

Thus  $R'_w$  must be chosen so that the coefficient of heat transfer by natural convection at  $\theta'_w$  is equal to the theoretical "forced" convection coefficient for zero velocity at  $\theta_w$ . It was observed that a choice of  $R'_w$  so that

$$V'_{ino} = 0.9 V_{ino}$$

gave the closest extrapolation of  $V_{out}$  to the origin, where  $V_{ino}$  was the measured input voltage at zero velocity. It remained to put  $m' = 1/n$  in order to obtain a voltage signal linearly related to velocity, and  $m' = 2.3$  (corresponding to  $n = 0.435$ ) was found to give linearity over a large range (see Figure 9).

When the linearizer had been adjusted in the manner indicated, the sheath was removed and the wire temperature returned to  $\theta_w$ . Calibration was then carried out in the calibration unit previously described. It is interesting to note that some of these calibrations were observed to hold perfectly over a period of 48 hours.

At this stage, the inclined hot-wire probe was ready for measurements; it was then plugged into the probe support socket and the latter mounted on the traversing mechanism with the aid of a guide tube. The whole system of probe, probe support, and guide tube was then inserted into the chamber at a particular station and radial traverses made. This was repeated along the first nine measuring stations.

To deduce the velocity components and intensities of turbulence, mean and fluctuating (R.M.S. voltage) readings were required at different azimuthal,  $\theta$ , positions of the inclined wire. Readings were therefore taken at azimuthal angles of  $0^\circ$ ,  $45^\circ$ ,  $90^\circ$ ,  $135^\circ$ ,  $180^\circ$ ,  $225^\circ$ ,  $270^\circ$ , and  $315^\circ$ . The velocity components and turbulence intensities were then derived from the following equations (the detailed analysis substantiating these equations is given in Appendix I):

$$\bar{u}/W_0 = B_1(\bar{e}_0 - \bar{e}_{180})/2a_1a_3\cos\alpha W_0 \quad (11)$$

$$\bar{v}/W_0 = B_1(\bar{e}_{90} - \bar{e}_{270})/2a_1a_3\cos\alpha W_0 \quad (12)$$

$$\bar{w}/W_0 = B_1(\bar{e}_0 + \bar{e}_{180})/2a_1a_2\cos\alpha W_0 \quad (13)$$

$$- 1/a_2[1 + a_6(\bar{u}^2 + \bar{u}'^2)/W_0^2 + a_8(\bar{v}^2 + \bar{v}'^2)/W_0^2]$$

$$\begin{aligned} \bar{w}'^2/W_0^2 &= 1/a_2^2[B_1^2(\bar{e}_0 + \bar{e}_{180})/(2a_1^2\cos^2\alpha W_0^2) - a_3^2(\bar{u}'^2/W_0^2) \\ &\quad - 4a_2a_8(\bar{v}/W_0)(\bar{v}'/W_0) - 4a_2a_6(\bar{u}/W_0)(\bar{u}'/W_0)] \end{aligned} \quad (14)$$

$$\begin{aligned} \bar{v}'^2/W_0^2 &= 1/a_3^2[B_1^2(\bar{e}_{90} + \bar{e}_{270})/(2a_1^2\cos^2\alpha W_0^2) - a_2^2(\bar{w}'^2/W_0^2) \\ &\quad - 4a_2a_8(\bar{u}/W_0)(\bar{u}'/W_0) - 4a_2a_6(\bar{v}/W_0)(\bar{v}'/W_0)] \end{aligned} \quad (15)$$

and

$$\begin{aligned} \bar{u}'^2/W_0^2 &= 1/a_3^2[B_1^2(\bar{e}_{45} + \bar{e}_{225})/(a_1^2\cos^2\alpha W_0^2) \\ &\quad - 2a_2^2(\bar{w}'^2/W_0^2) - a_3^2(\bar{v}'^2/W_0^2) - 2a_3^2(\bar{u}'\bar{v}'/W_0^2) \\ &\quad - (\bar{v}'/W_0)\{( \bar{v}/W_0)(4a_2a_8 + 4a_2a_6) + (\bar{u}/W_0)(4a_2a_6 - 4a_2a_8)\} \\ &\quad - (\bar{u}'/W_0)\{( \bar{v}/W_0)(4a_2a_6 - 4a_2a_8) + (\bar{u}/W_0)(4a_2a_8 + 4a_2a_6)\}] \end{aligned} \quad (16)$$

Equations (14), (15) and (16) are, of course, the normal Reynolds stress components; therefore the corresponding turbulence intensities will be:

$$[\sqrt{(w'^2/w_0^2)} / (\bar{w}/w_0)] \times 100 \quad (17)$$

$$[\sqrt{(v'^2/v_0^2)} / (\bar{v}/v_0)] \times 100 \quad (18)$$

and

$$[\sqrt{(u'^2/u_0^2)} / (\bar{u}/u_0)] \times 100 \quad (19)$$

In the analysis, the mean velocity readings were taken to the second order, and the fluctuating to the third, and it can be seen that  $\bar{u}$  and  $\bar{v}$  were derived from the difference between two readings  $180^\circ$  apart, and  $\bar{w}$  from the sum of two readings at  $\theta = 0^\circ$  and  $\theta = 180^\circ$ . The fluctuating velocities  $w'$ ,  $v'$  and  $u'$  were obtained from the sum of two readings at  $\theta = 0^\circ$  and  $180^\circ$ ,  $\theta = 90^\circ$  and  $270^\circ$ , and  $\theta = 45^\circ$  and  $225^\circ$ , respectively.

Every set of the above mentioned readings (at different  $\theta$ 's corresponded only to one radial position only at a particular station (i.e., only one axial position); hence, to obtain the radial distribution of mean velocities and intensities of turbulence, radial traverses were made and D.C. and A.C. (R.M.S.) voltages were recorded at the first nine stations (see Figure 5) down the chamber (Table I), and Appendix II presents the collected experimental data. Data for runs with inlet velocities of 1.6 m/s are shown in Tables I to IX of Appendix II. Tables X to XVIII of the same Appendix present the data for an inlet velocity

TABLE I

LOCATION AND RADIUS OF THE MEASURING STATIONS

<u>Station Number</u> <u>see Fig. 5</u>	<u>Axial Distance from</u> <u>the Top of the Chamber</u> <u>(cm)</u>	<u>Radius</u> <u>(cm)</u>
1	50.20	61.60
2	64.20	61.00
3	74.30	57.80
4	84.50	52.70
5	94.60	47.00
6	109.90	40.00
7	125.10	32.40
8	140.40	24.80
9	155.60	17.80
10	170.80	10.16
11	181.00	3.80

of 3.2 m/s (flowrate of 5.66 m<sup>3</sup>/min), and finally Table XIX shows the data for a run with a third inlet velocity of 2.4 m/s (4.25 m<sup>3</sup>/min). These latter data are only for station 7, and were collected for comparison purposes.

It should be mentioned that during each run the inlet and outlet pressures of the chamber, and also the entering air temperatures were constantly monitored and their average values for each run are also presented in Tables I to XIX of Appendix II.

## RESULTS AND DISCUSSION

### FLOW PATTERNS - VISUALIZATION AND MEASUREMENTS

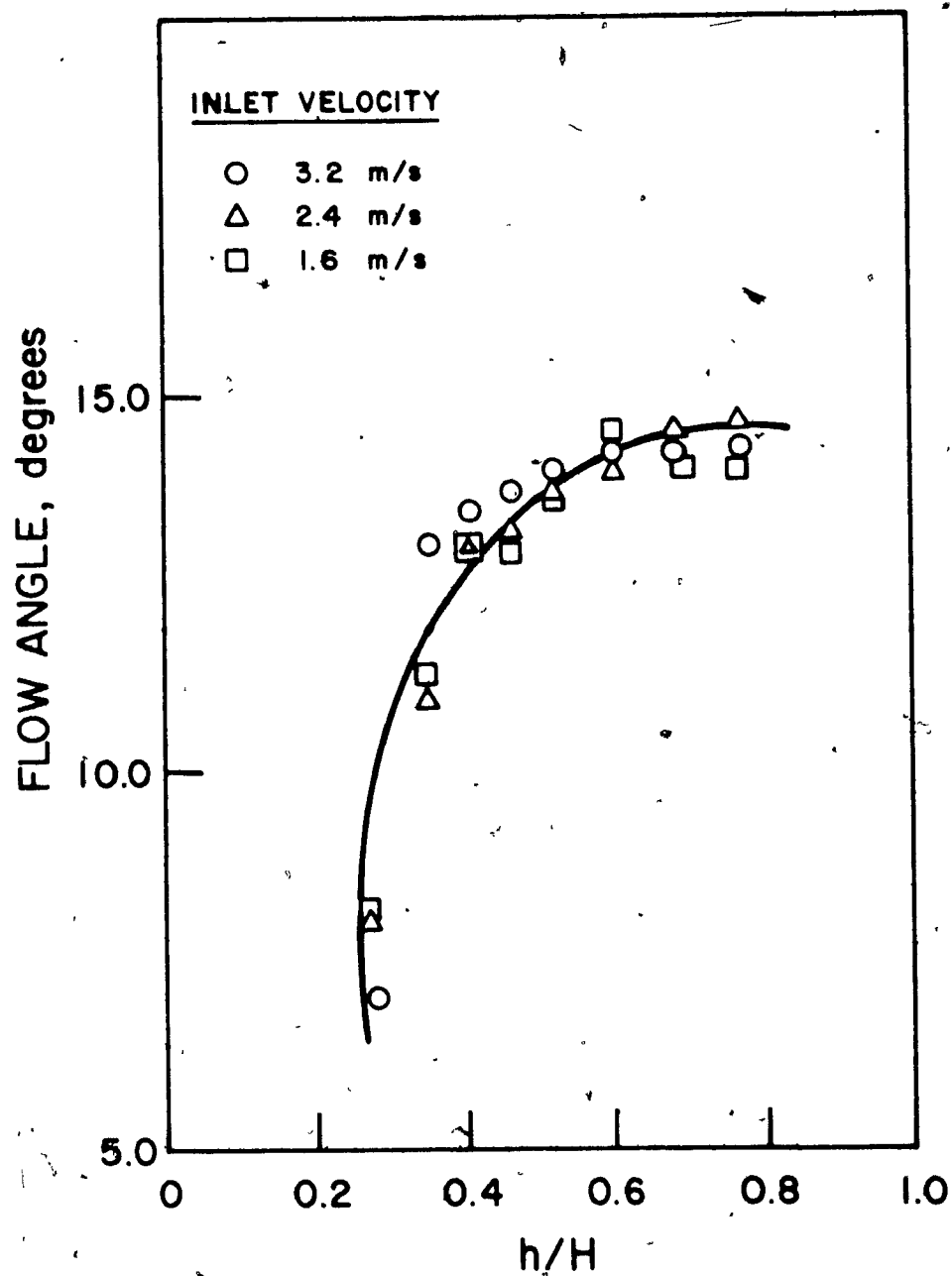
The results of flow angle measurements, for the test inlet velocities, are presented in Fig. 14, as the flow angle versus the dimensionless axial distance,  $h/H$ . The latter was obtained, for a particular radial position, from the ratio of the distance of a measuring station from the top of the chamber ( $h$ ) to the total height of the chamber ( $H$ ).

The curve shows that, going down the chamber, the angle of flow increases sharply to a maximum value of 15° and then becomes steady, yielding a pattern of almost parallel circular streamlines. This agrees with the results of Schowalter and Johnstone (28).

Another important finding shown in Fig. 14 is the insensitivity of the flow patterns to changes in the inlet velocities, an observation reported by many previous investigators (26, 27, 28, 32, 53, 54).

FIGURE 14

Flow Angles for Inlet Velocities of 1.6, 2.4 and 3.2 m/s.



These results were also observed qualitatively with the tuft probes described in the previous section. However, the procedure is subject to the following error: the connection between the thread and the probe had a certain stiffness, so that the position of the probe influenced the indicated direction. This fact could easily be seen by turning the probe by several degrees. Within a range of about two degrees the thread would follow the rotation of the probe. Only at larger angles would it adjust itself to a different position. Other errors could be due to the drag of the thread in connection with the spiral paths of the air.

Near the wall, the wool tufts indicated a flow direction with a large circumferential component and a small axial component. This flow was probably caused by the boundary layer at the wall. As the tufts were moved away from the boundary layer region, the axial component became negligible and the tufts behaved erratically, implying the existence of a central turbulent core.

#### MEAN VELOCITIES

Mean velocity measurements were made for different radial and axial points in the flow field at inlet air velocities of 1.6 and 3.2 m/s. A few additional measurements were also conducted for different radial locations but at one axial position only (i.e., station 7 (see Fig. 5)) at an inlet velocity of 2.4 m/s. All inlet velocities are average velocities based on the total cross sectional area of the (3.81 x 15.24 cm) slots in the inside wall of the jacketed cylindrical section.

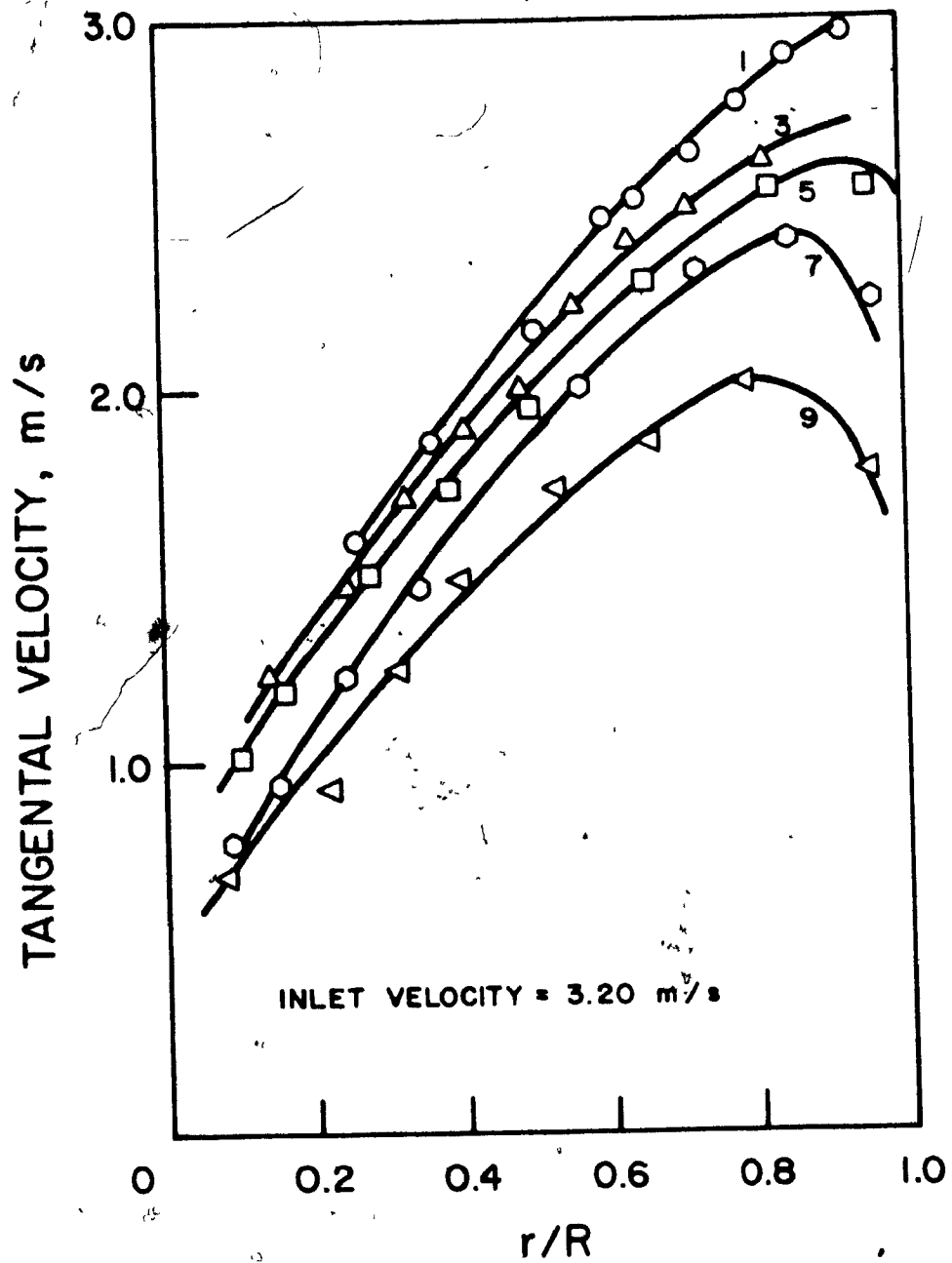
Radial profiles of the tangential mean velocities are shown in Fig. 15 and 16, at nine axial locations (stations 1 to 9 (see Fig. 5 and Table I for location)) for flow with an inlet velocity of 3.20 m/s. No data were taken in the region near the chamber centreline because of the relatively high turbulence, and the high disturbance of the flow caused by the probes. It is seen that the tangential velocity increases with increasing radius and reaches a maximum value near the wall and then falls off sharply to meet the requirement of zero rotation at the wall.

As shown in Fig. 15 and 16, instead of flow with constant angular momentum expected in a true vortex the tangential velocity distribution near the wall approaches the one of nearly constant angular velocity (i.e., the velocity varies approximately as  $1/r$ ). This, as suggested in Ref. (28), indicates the appearance of a high eddy viscosity in the central region. At smaller radii, the motion resembles a solid body rotation, where the tangential velocity is proportional to the radius. The boundary between these two regions of flow, marked by maximum tangential velocity, moves radially inward as one goes down the chamber. This gradual downstream decrease of the slope of the tangential velocity in the order of stations is an indication of decaying vortex (57).

Radial profiles of the axial velocities are presented in Fig. 17, 18 and 19, at nine locations (stations 1 to 9) for flow with an inlet velocity of 3.20 m/s. It is seen that the axial velocity approaches zero at the chamber centreline. This is characteristic of

FIGURE 15

Radial Profiles of the Tangential Mean Velocities  
at Stations 1, 3, 5, 7 and 9.



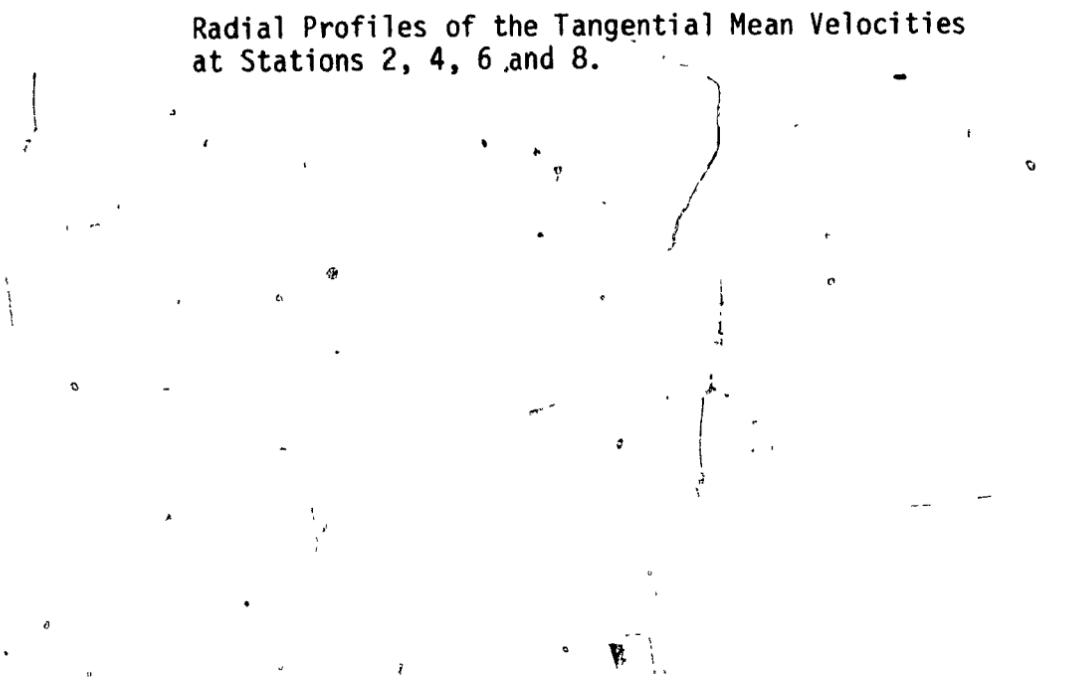


FIGURE 16

Radial Profiles of the Tangential Mean Velocities  
at Stations 2, 4, 6, and 8.

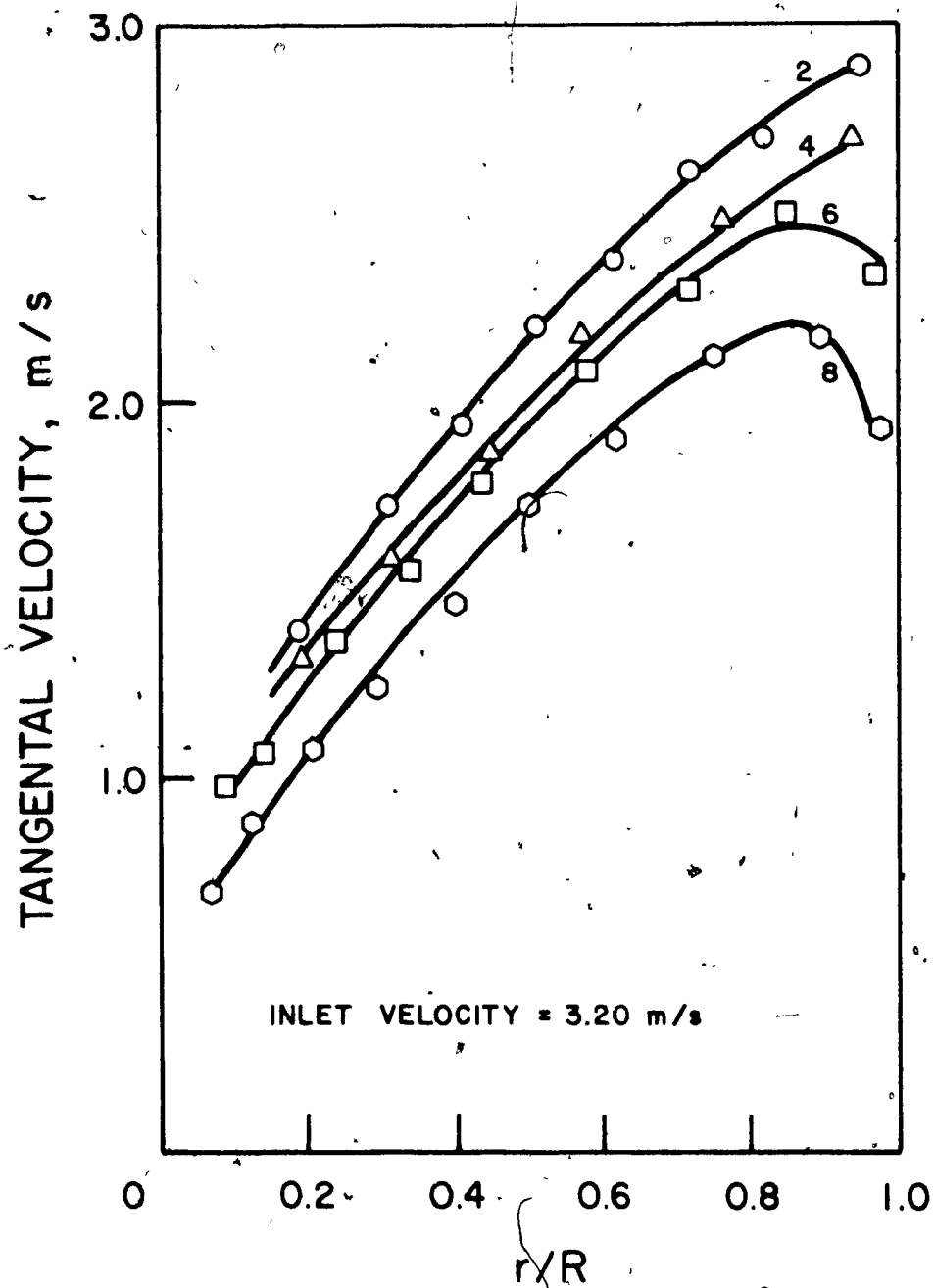


FIGURE 17

Radial Profiles of the Axial Mean Velocities  
at Stations 7, 8 and 9.

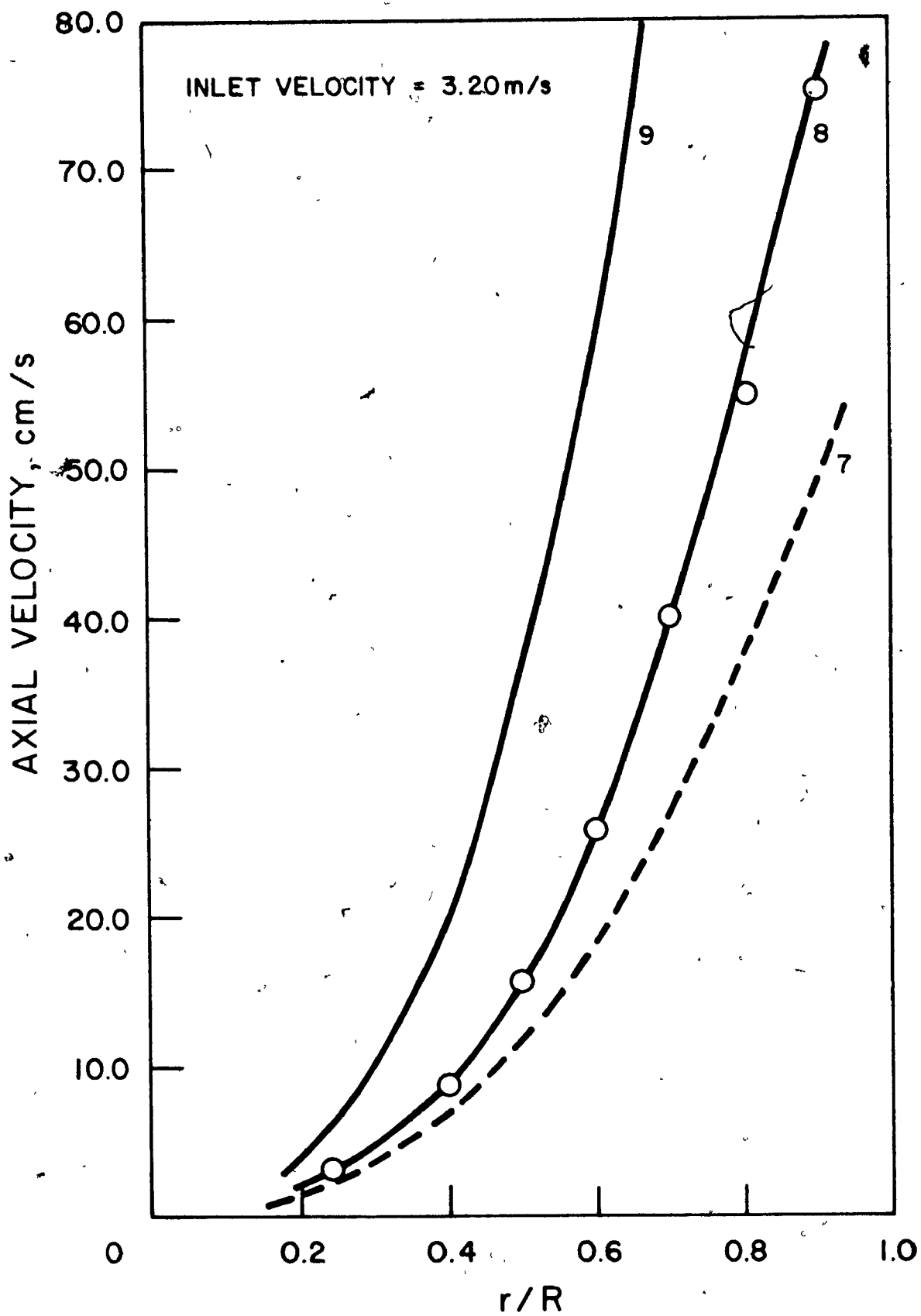


FIGURE 18

Radial Profiles of the Axial Mean Velocities  
at Stations 1, 3 and 5.

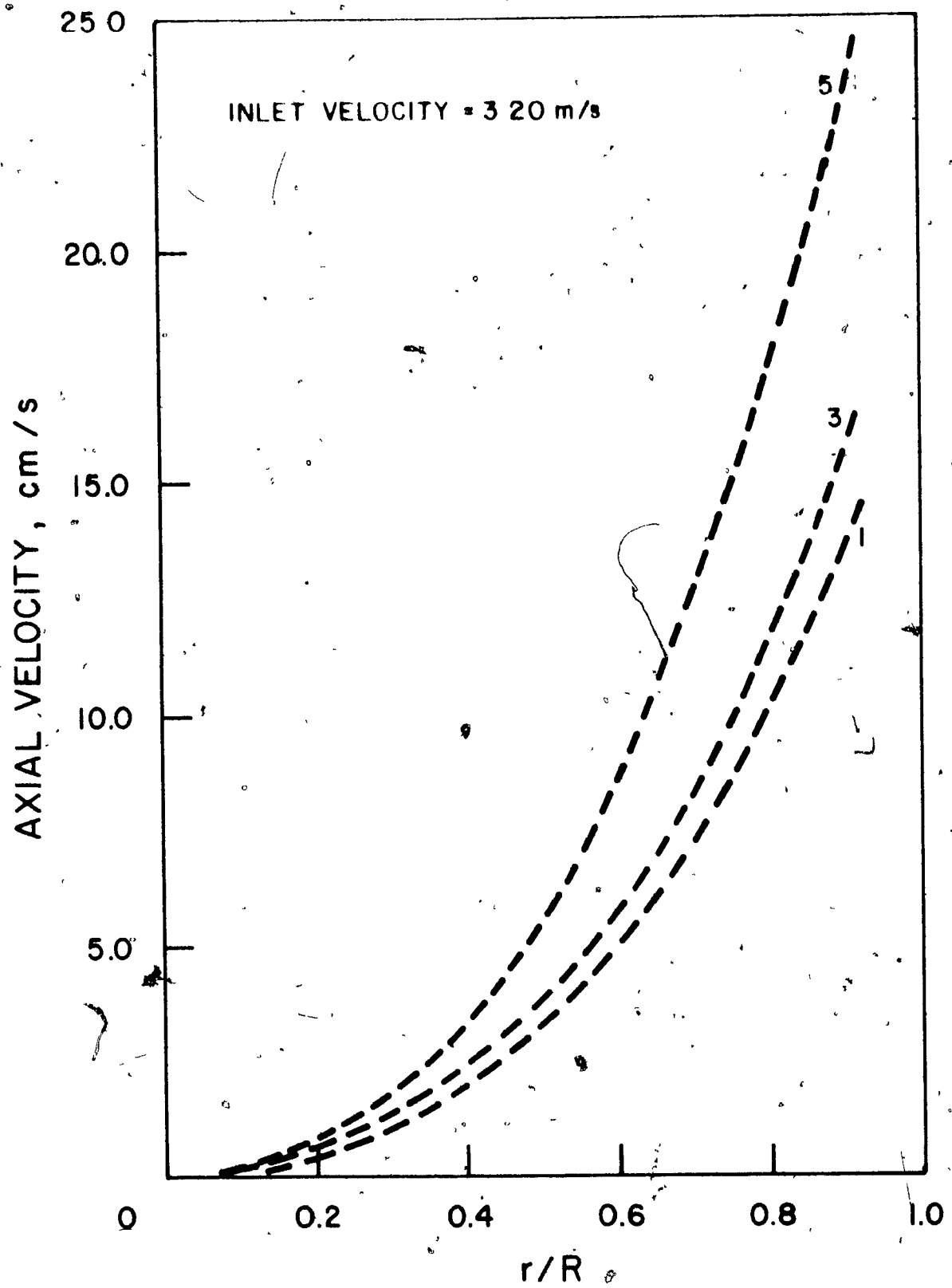
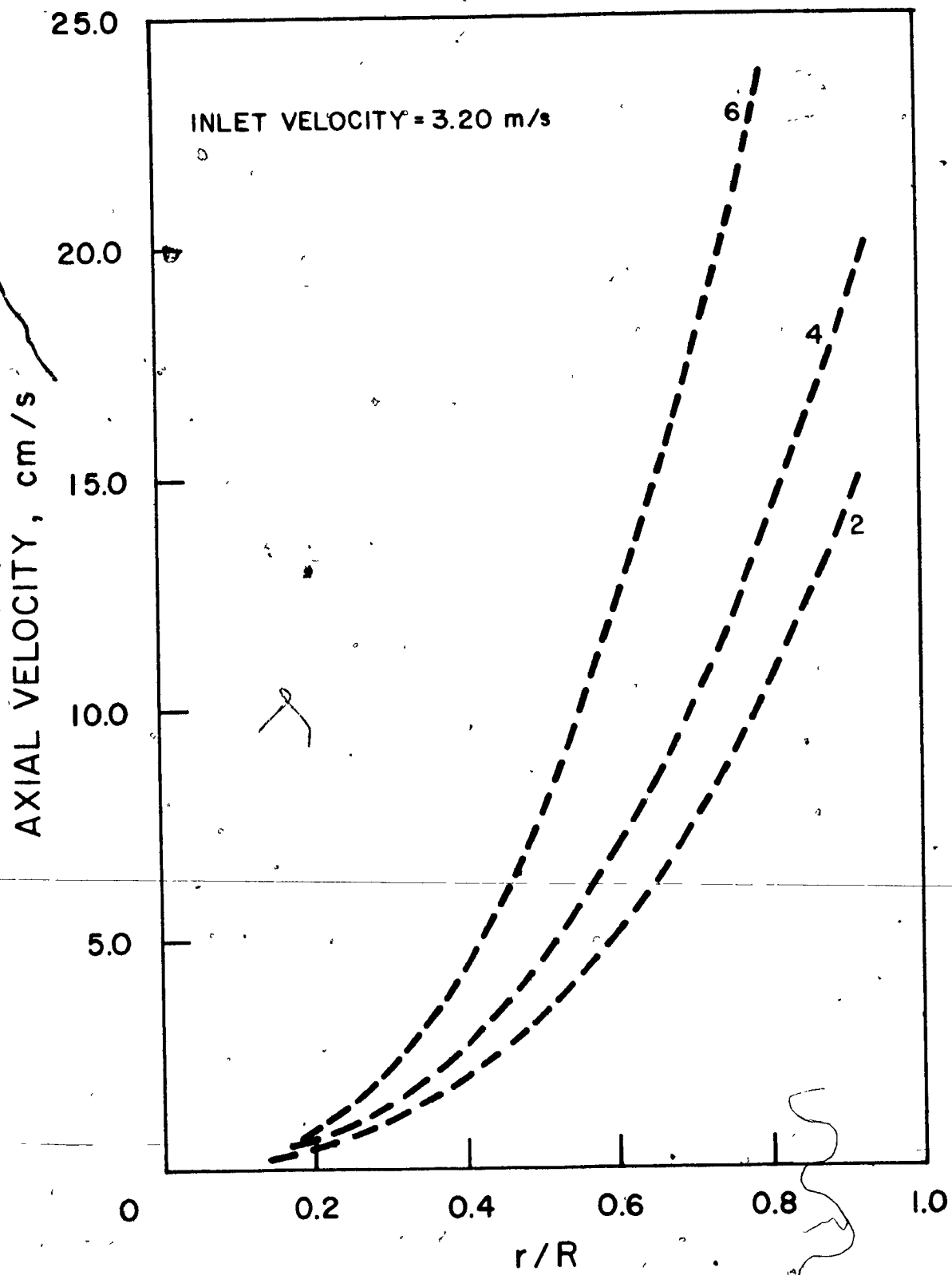




FIGURE 19

Radial Profiles of the Axial Mean Velocities  
at Stations 2, 4 and 6.



swirling flow that enters a stationary container. It should be noted that the axial variation of the tangential velocity distribution is much greater than that of the axial velocity distribution. This may be explained from a pressure increase near the axis and pressure decrease near the wall which tends to counteract the development of the axial profile. This was demonstrated analytically by Lavan (103) and Talbot (104) for laminar swirling flows and was one of the assumptions made by Kreith (105) and Rochino (106) in their studies of turbulent swirling flows.

It should be mentioned that some problems were encountered in the measurement of axial velocities at very low values, owing to the poor response of the hot wire anemometer under these conditions. For this reason, measurements at higher velocities which are considered valid are indicated in Fig. 17, 18 and 19 in solid lines. They can easily be verified from a mass balance on the total flow. Values at low velocities were calculated from the mass balance, according to the equation of the valid lines,  $V_{av} = C(r/R)^{2.5}$  and are shown in dotted lines.

Comparison of Fig. 15 and 16 with Fig. 17, 18 and 19 shows that the axial velocities are small when compared to tangential velocities, and also that the tangential velocity peaks do not coincide with the axial velocity peaks, but are located more toward the centre of the tube. This can be explained on the basis that wall friction causes a decrease in both the axial and tangential velocities near the wall as the flow moves along. From continuity considerations, this results in an increase in axial and tangential velocities in regions farther away from the wall.

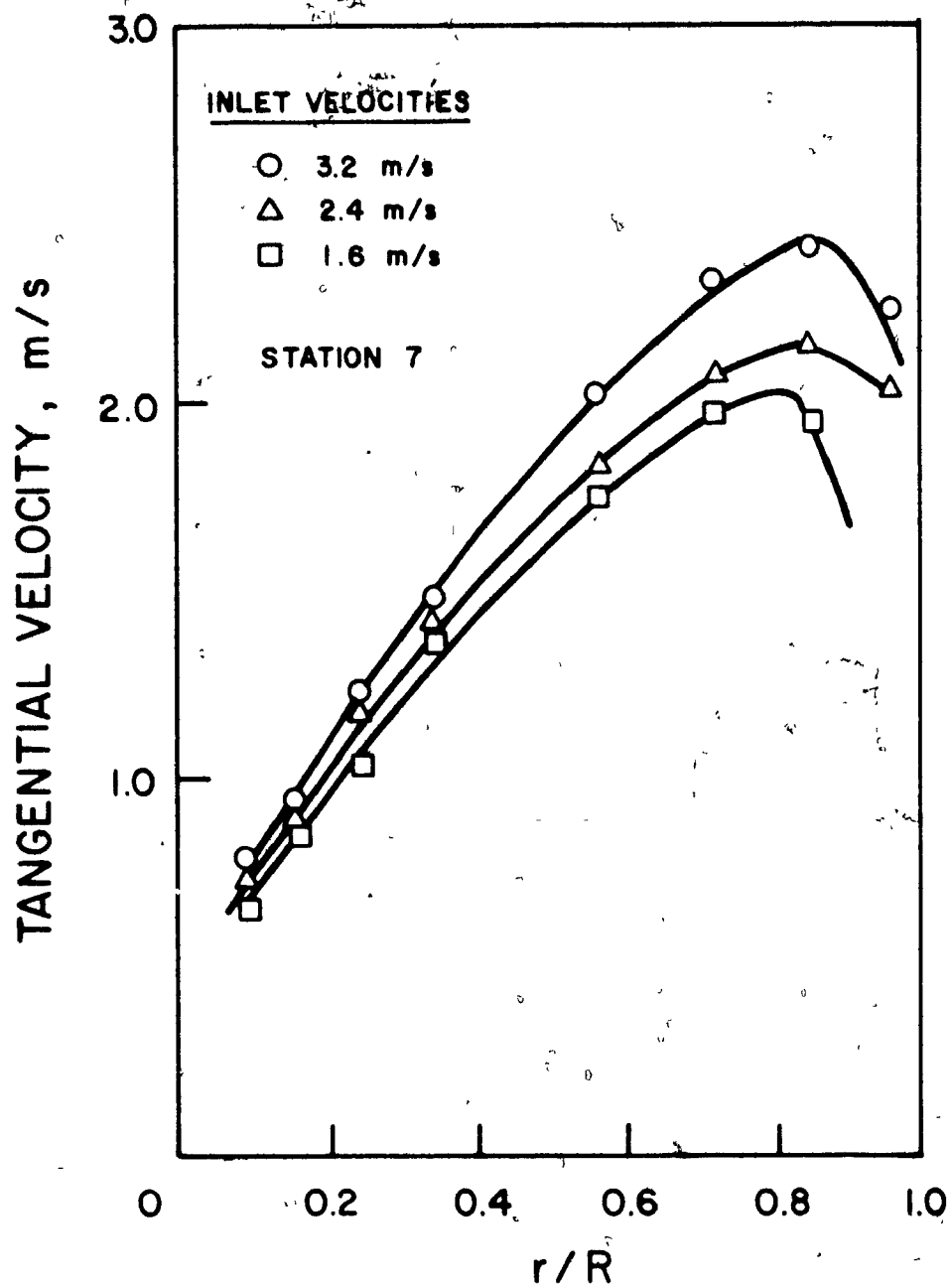
It indicates that some air must move in toward the centre as flow progresses down the chamber. In so doing, the air tends to conserve its angular momentum, thereby resulting in an increase in angular velocity in those regions farther away from the wall. The tangential velocity, as seen above, drops off at the centre of the chamber, for as was shown by Lay (33), there is theoretically only axial flow in that region.

Fig. 20 and 21 present the radial profiles of tangential and axial velocities at station 7, for three different inlet velocities. As it can be seen, these velocities are larger in the case of larger inlet velocity, but their distributions are almost similar indicating once more the insensitivity of the flow patterns to changes in inlet velocities.

It should be mentioned that the radial component of the velocity was also determined, for each run, from equation (A49) of Appendix I, but no attempt was made to present these data graphically, since the values were very small and would present an almost straight line distribution close to the axis of zero velocity. For the same reason, the radial distributions of the radial intensities of turbulence will not be presented in the following section, for in this study the ratio of the R.M.S. fluctuating velocity to the mean velocity at a point will define the intensity of turbulence at that point. Since negligible radial velocities occurred, such a ratio would yield radial intensities of turbulence of the order of 300 to 400%. Of course, one can plot the root-mean-square of turbulent radial velocity and in fact this result

FIGURE 20

Radial Distributions of Tangential Velocity  
at Station 7, for Different Inlet Velocities.



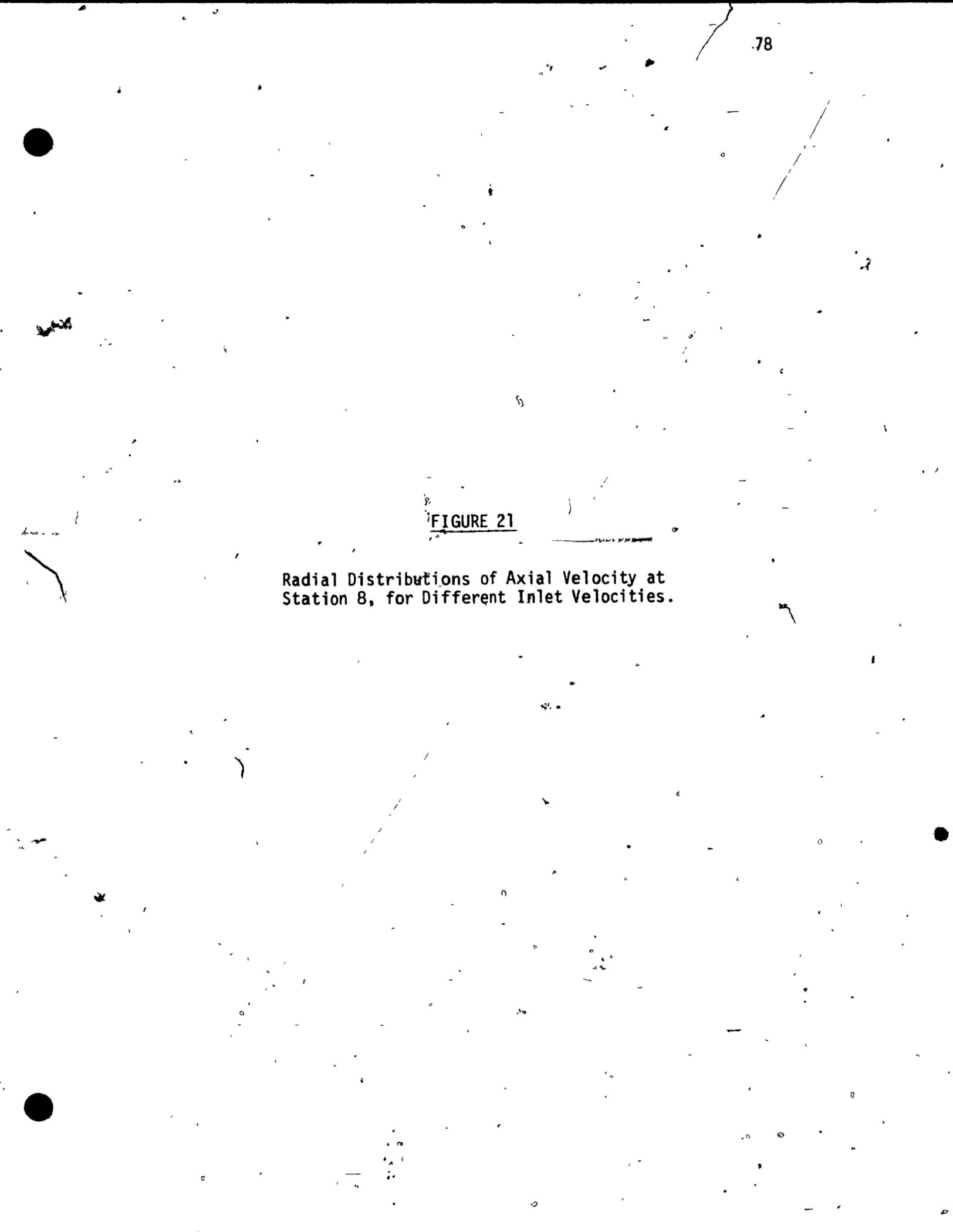
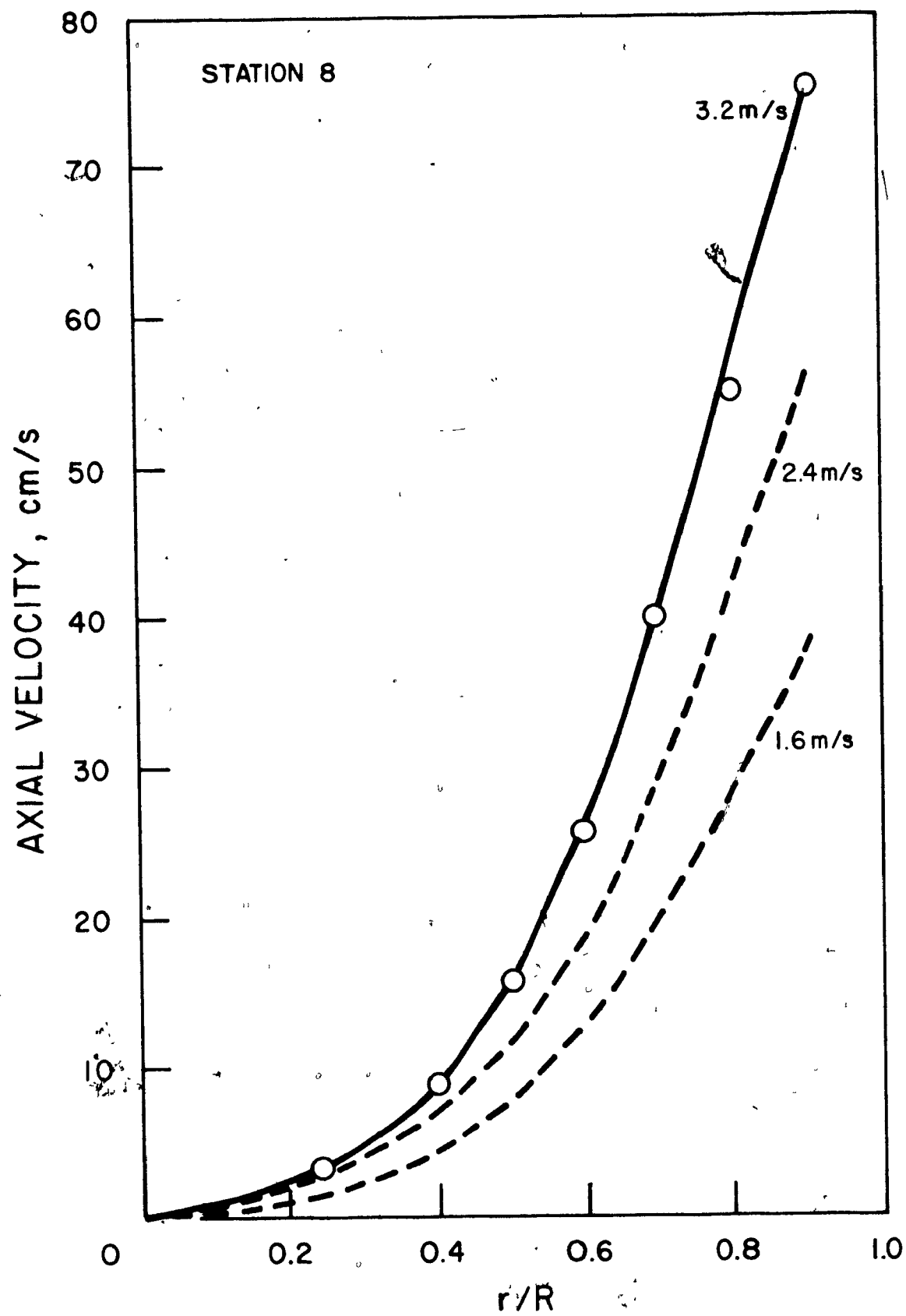


FIGURE 21

Radial Distributions of Axial Velocity at  
Station 8, for Different Inlet Velocities.



is presented for station 7 in the following section (Fig. 28).

### TURBULENCE INTENSITIES

Radial distributions of the tangential components of the turbulent intensities are plotted as functions of the radial-distance in Fig. 22 and 23, for various axial distances from the top of the chamber (stations 1 to 9). Again, these curves are only for the inlet velocity of 3.20 m/s. It can be seen that these intensities tend to increase with decreasing distance from the centreline. The increase in intensity is caused more by the rapidly decreasing mean tangential velocity than by the intensity in  $\sqrt{w'^2}$ . Unfortunately, no data are available for stresses, for the behavior of intensities could be explained in terms of these parameters using the turbulent energy equations of Eskinazi and Yeh (107), but one would expect to have relatively large values of  $\overline{w'v'}$  in this region.


Actually, using equations 60A, 61A and 62A of Appendix I, in conjunction with equations 49A to 58A of the same Appendix, and the tabulated experimental data presented in Appendix II, one can obtain the three Reynolds shear stresses ( $\overline{w'v'}$ ,  $\overline{u'v'}$ , and  $\overline{w'u'}$ ), but due to the highly non-linear nature of these response equations, one has to use a special iteration technique to solve all nine equations simultaneously. A few attempts were made to do this, but had to be abandoned because of time limitation.

In contrast with the mean tangential velocity profiles, the tangential intensity profiles show some dissimilarities in the sense



FIGURE 22

Radial Distribution of Tangential Intensities  
of Turbulence at Stations 1, 3, 5, 7 and 9.



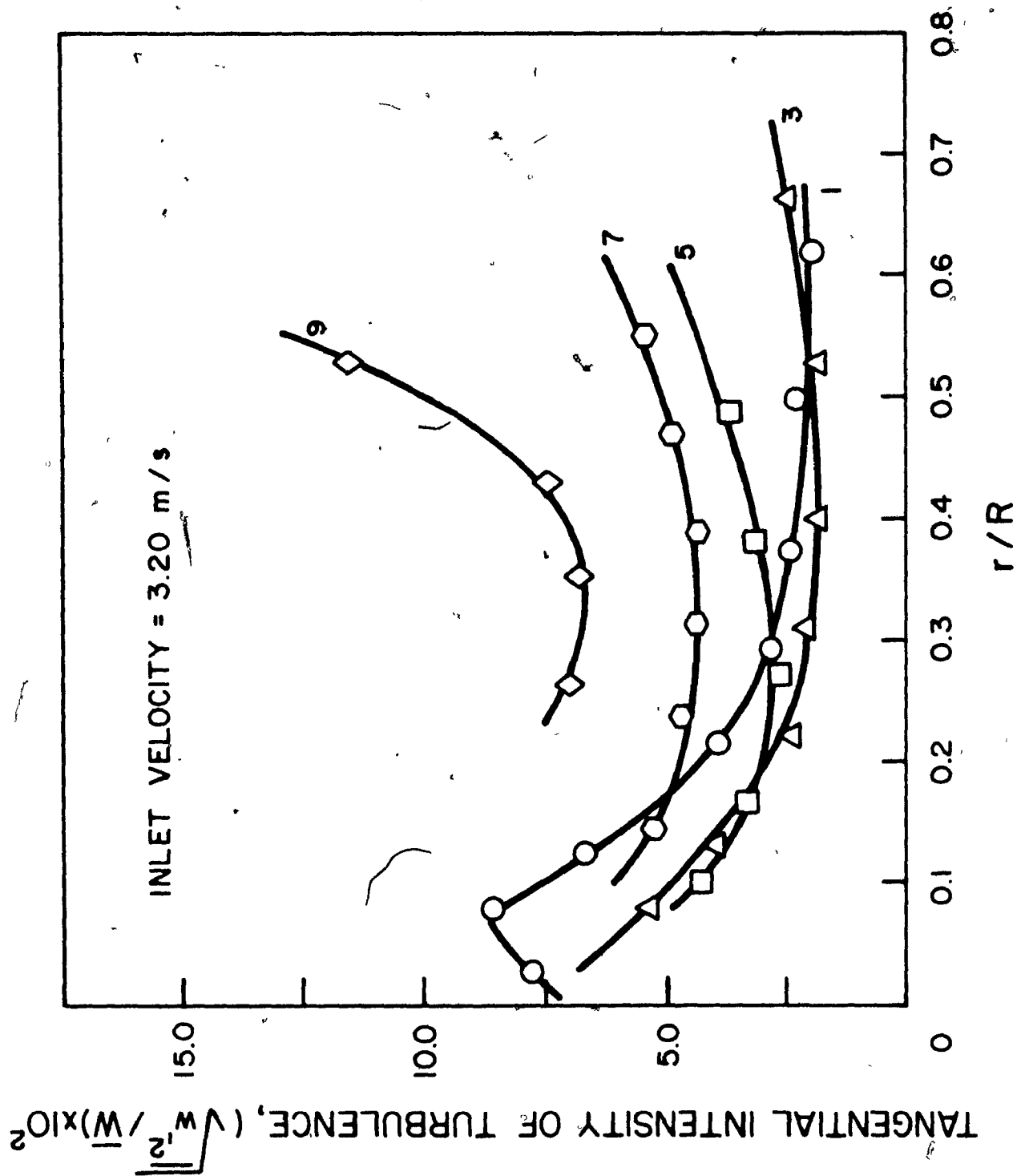
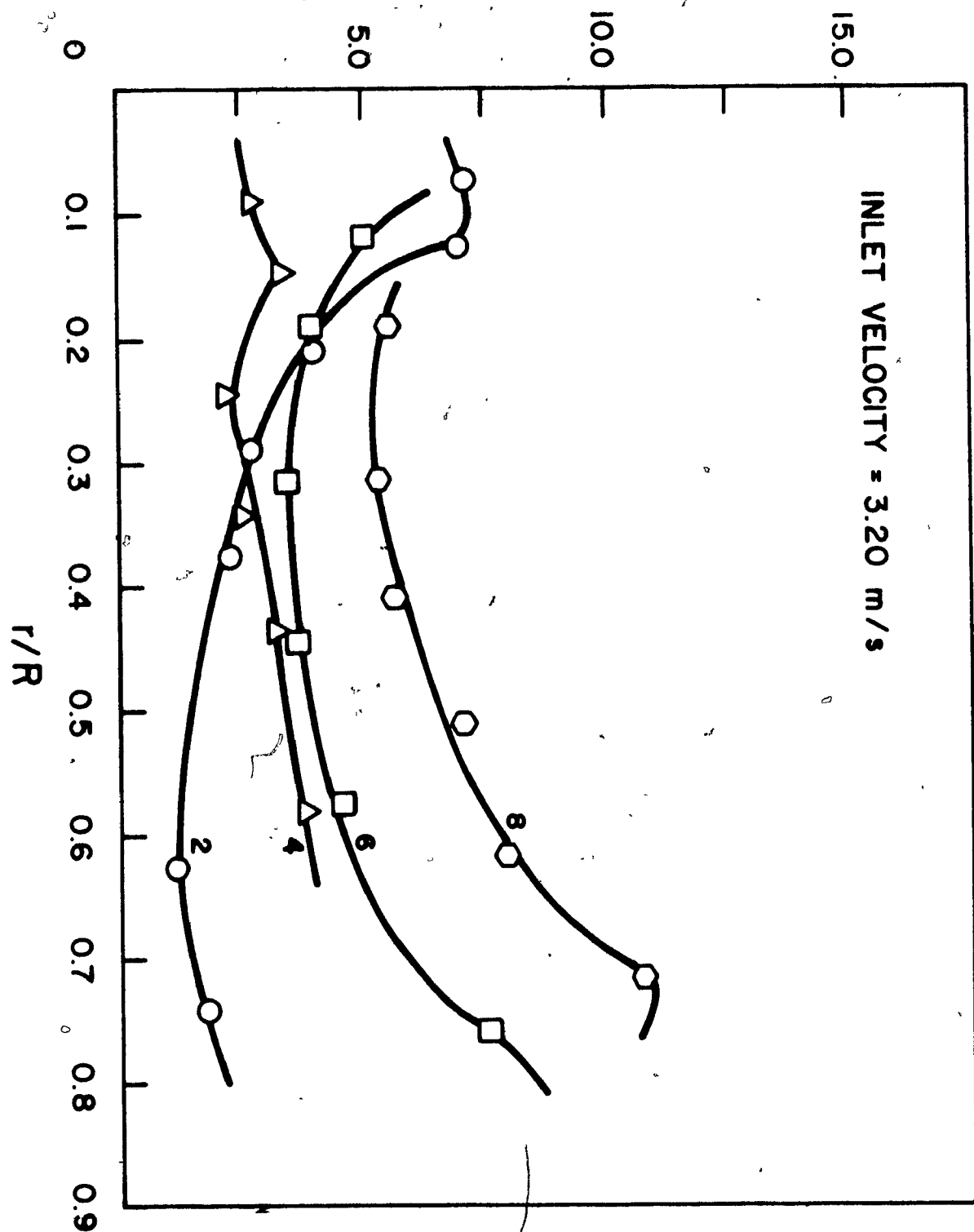


FIGURE 23.

Radial Distribution of Tangential Intensities  
of Turbulence at Stations 2, 4, 6 and 8.

TANGENTIAL INTENSITY OF TURBULENCE,  $(\sqrt{w'^2}/\bar{w}) \times 10^2$



that they show a stronger dependence on the axial position. In fact, the tangential intensity of turbulence increased with increasing axial distance from the top of the chamber, and the highest levels, about 11-12%, were obtained at stations 8 and 9.

Figures 24 and 25 show radial profiles of axial intensities of turbulence at stations 1 to 9, and for the same inlet velocity of 3.20 m/s. Here, the intensities are expressed as Root-Mean-Square values of the axial fluctuating velocities,  $\sqrt{v_1'^2}$ . The behaviour of these curves is seen to be somewhat similar, indicating an increase in  $\sqrt{v_1'^2}$  as one goes from centre to the wall, but their dependence on the axial direction does not follow a regular pattern. The suppression of  $\sqrt{v_1'^2}$  near the centre disagrees with the results obtained in other bounded shear flows (108).

Fig. 26 and 27 present the distribution of tangential intensity of turbulence and R.M.S. values of axial fluctuating velocities, respectively, at station 7, for different flow rates. Again the relative insensitivity to changes in inlet velocities is to be noted, although there seems to be some departure in the case of axial fluctuating velocity for the highest inlet velocity (Fig. 27). For both parameters, however, larger inlet velocity produced lower turbulence levels, indicating an indirect relationship. This is again because of the larger values of mean velocities obtained at larger inlet velocities.



FIGURE 24

Radial Distribution of R.M.S. Fluctuating  
Axial Velocity at Stations 1, 3, 5, 7 and 9.

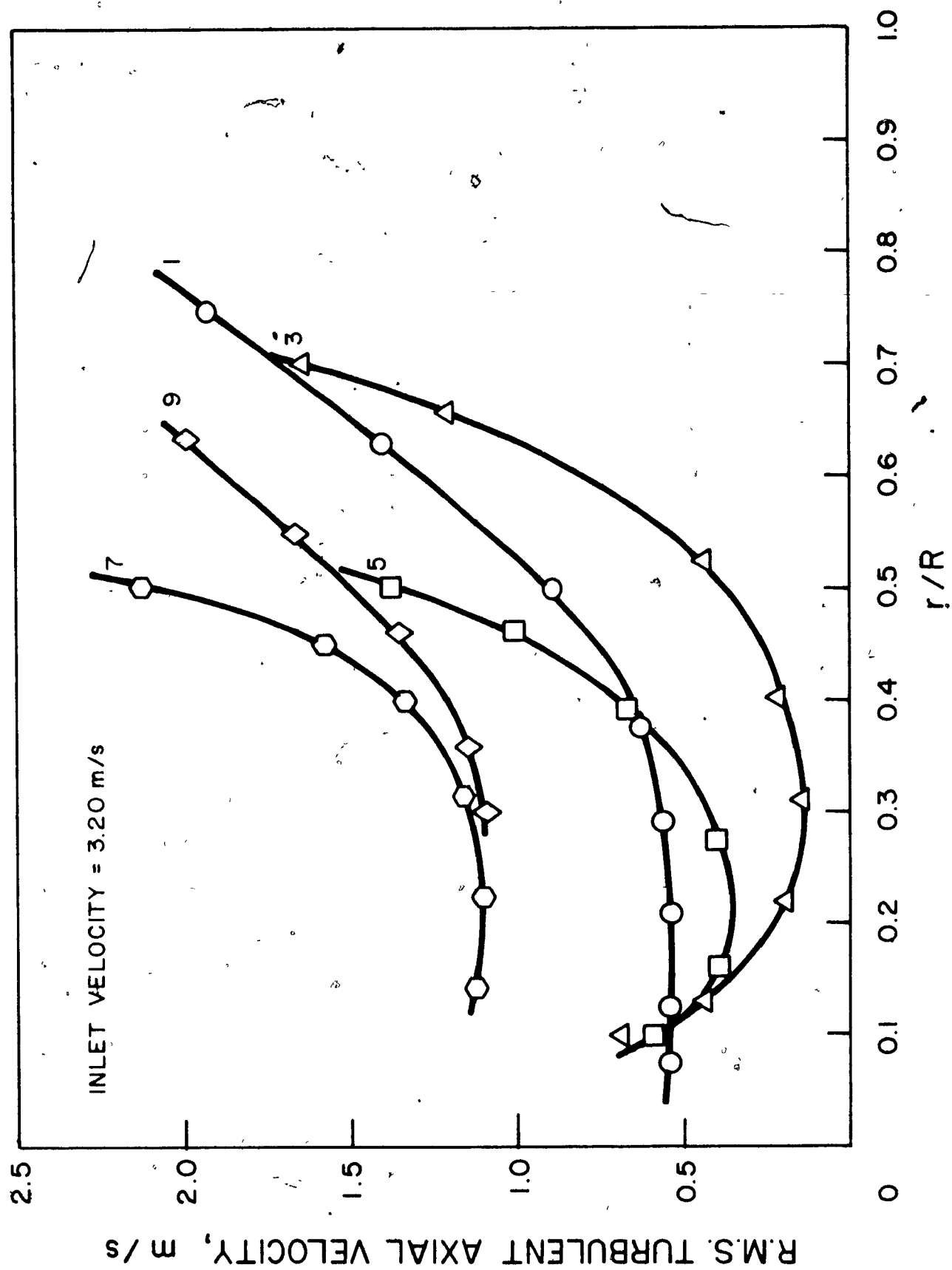


FIGURE 25

Radial Distribution of R.M.S. Fluctuating  
Axial Velocity at Stations 2, 4, 6 and 8.

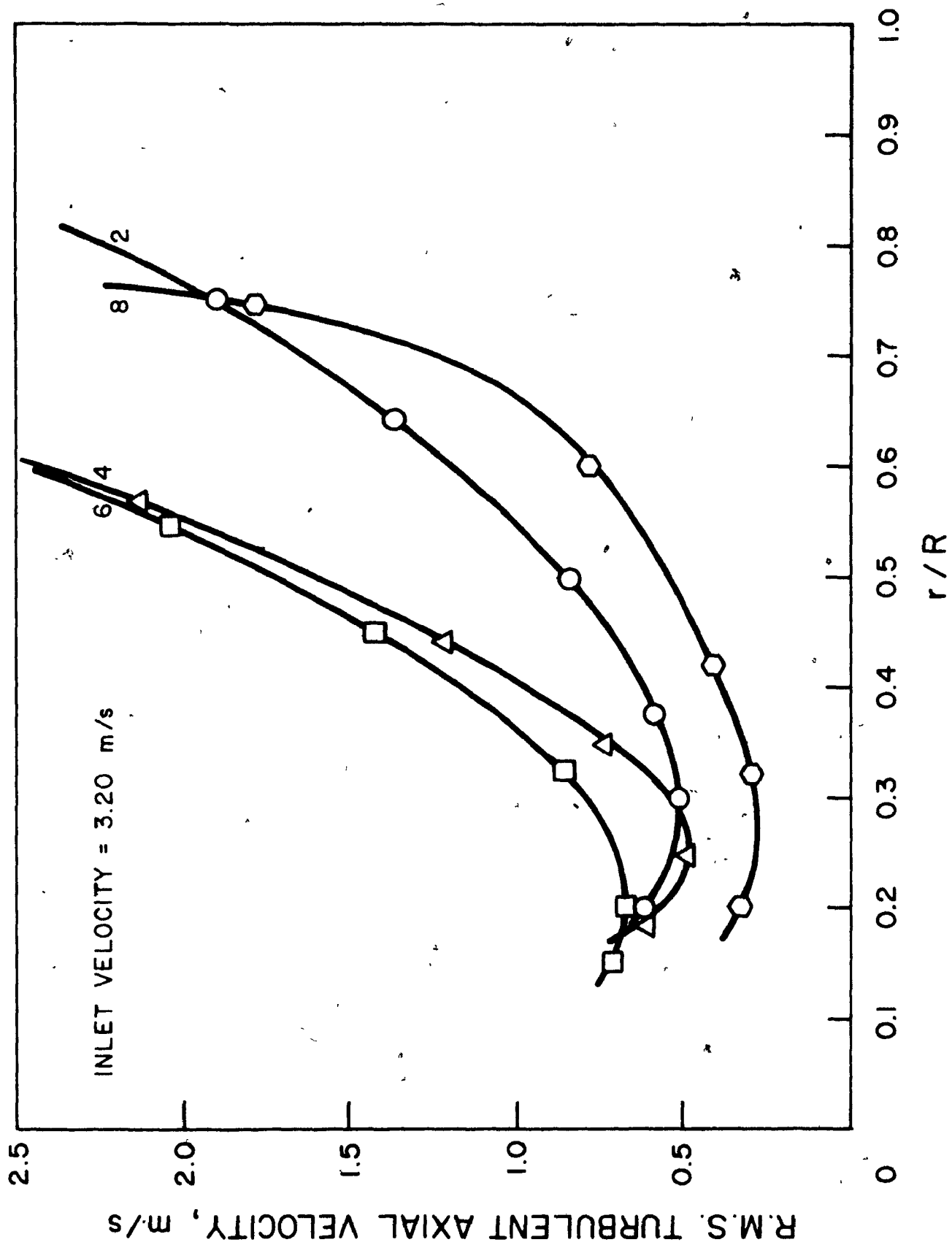


FIGURE 26

Distribution of Tangential Intensity of  
Turbulence at Station 7, for Different Inlet  
Velocities.

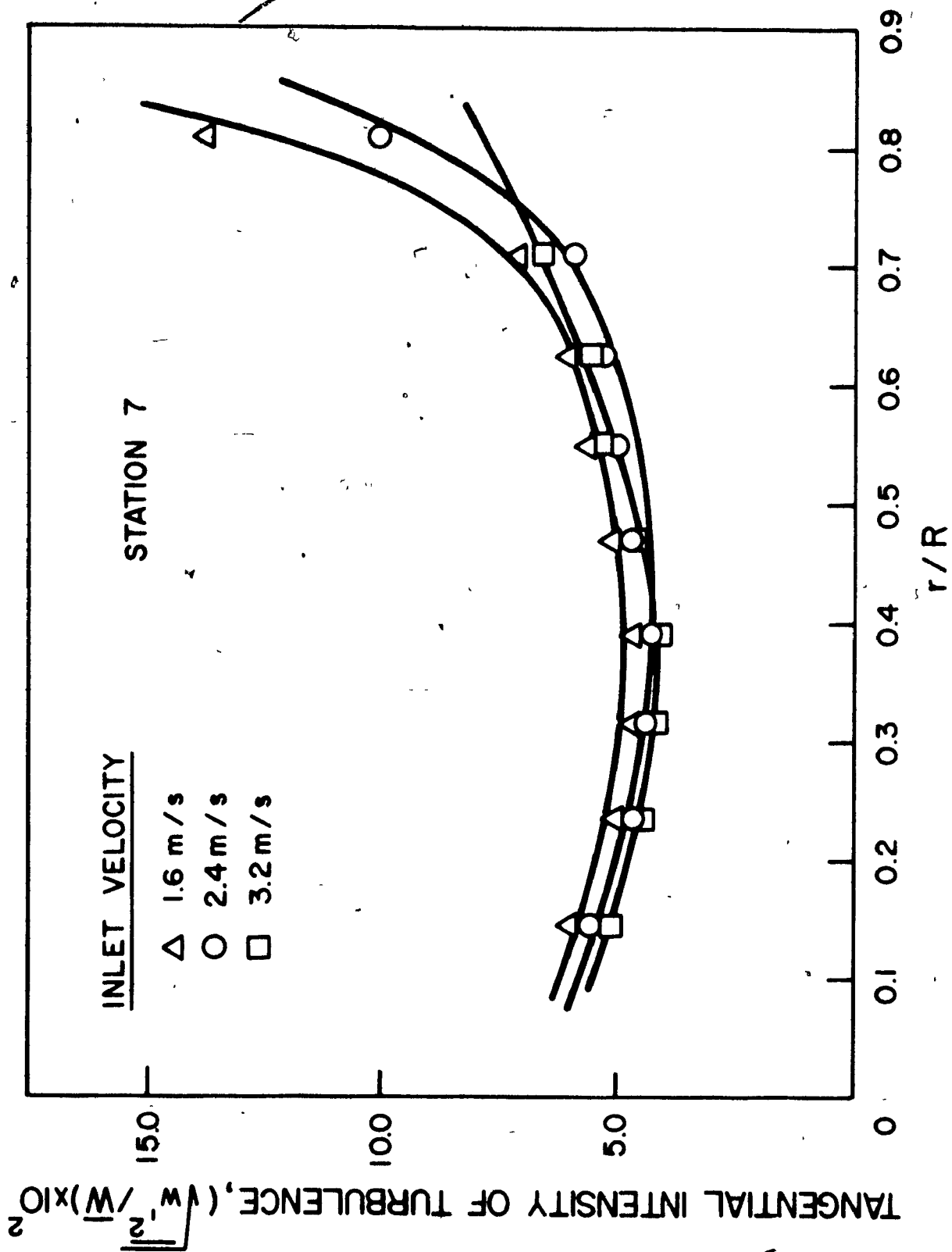
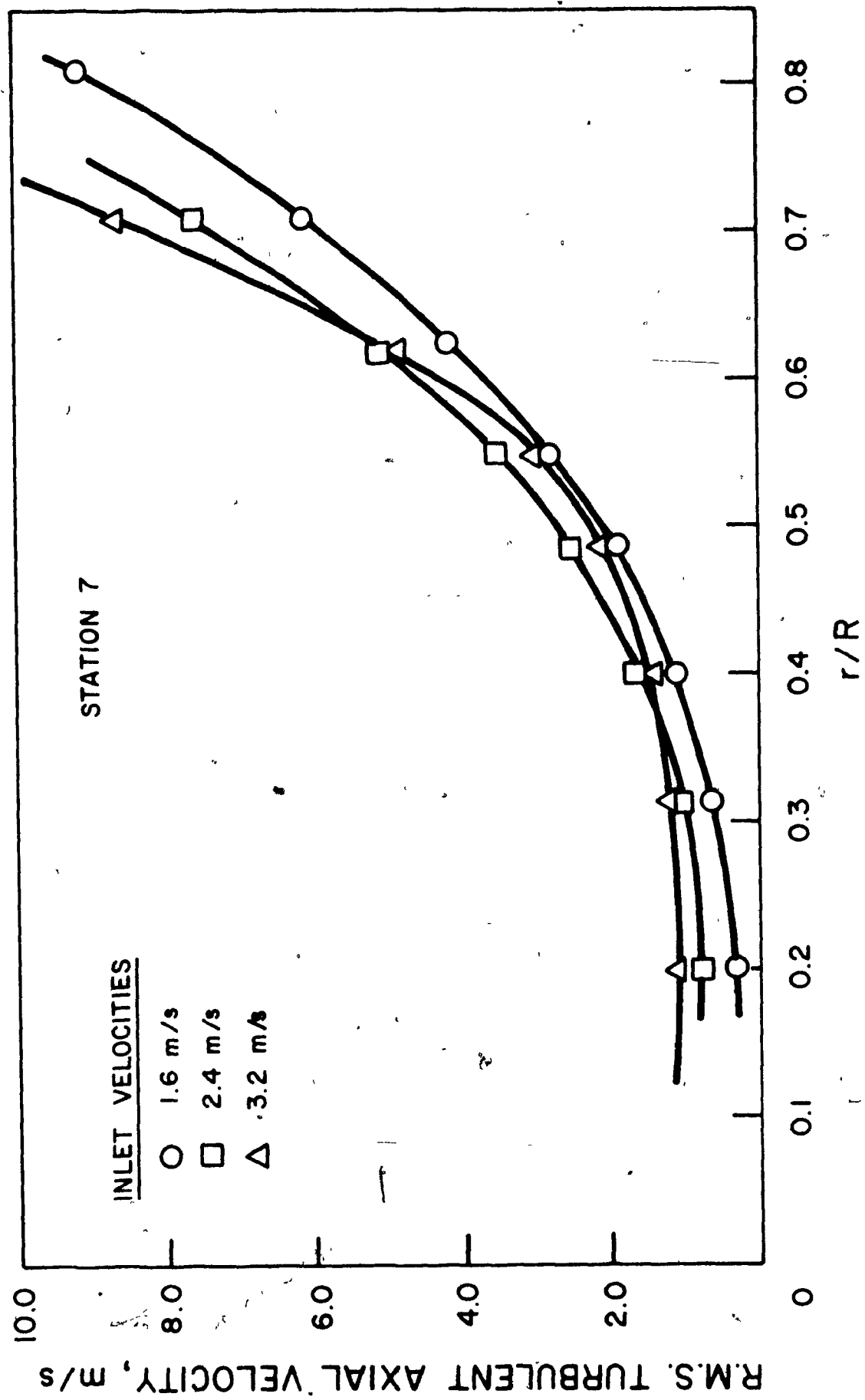




FIGURE 27

Distribution of R.M.S. turbulent Axial Velocity  
at Station 7, for Different Inlet Velocities.



Finally, Fig. 28 presents the root-mean-square value of the radial fluctuating velocity,  $\sqrt{u'^2}$ , at station 7, and for an inlet velocity of 3.20 m/s. Tangential and axial intensities of turbulence, at the same conditions, are also presented for purposes of comparison. The radial turbulent velocity is very small compared with the other two components, and it varies very little with radial distance.

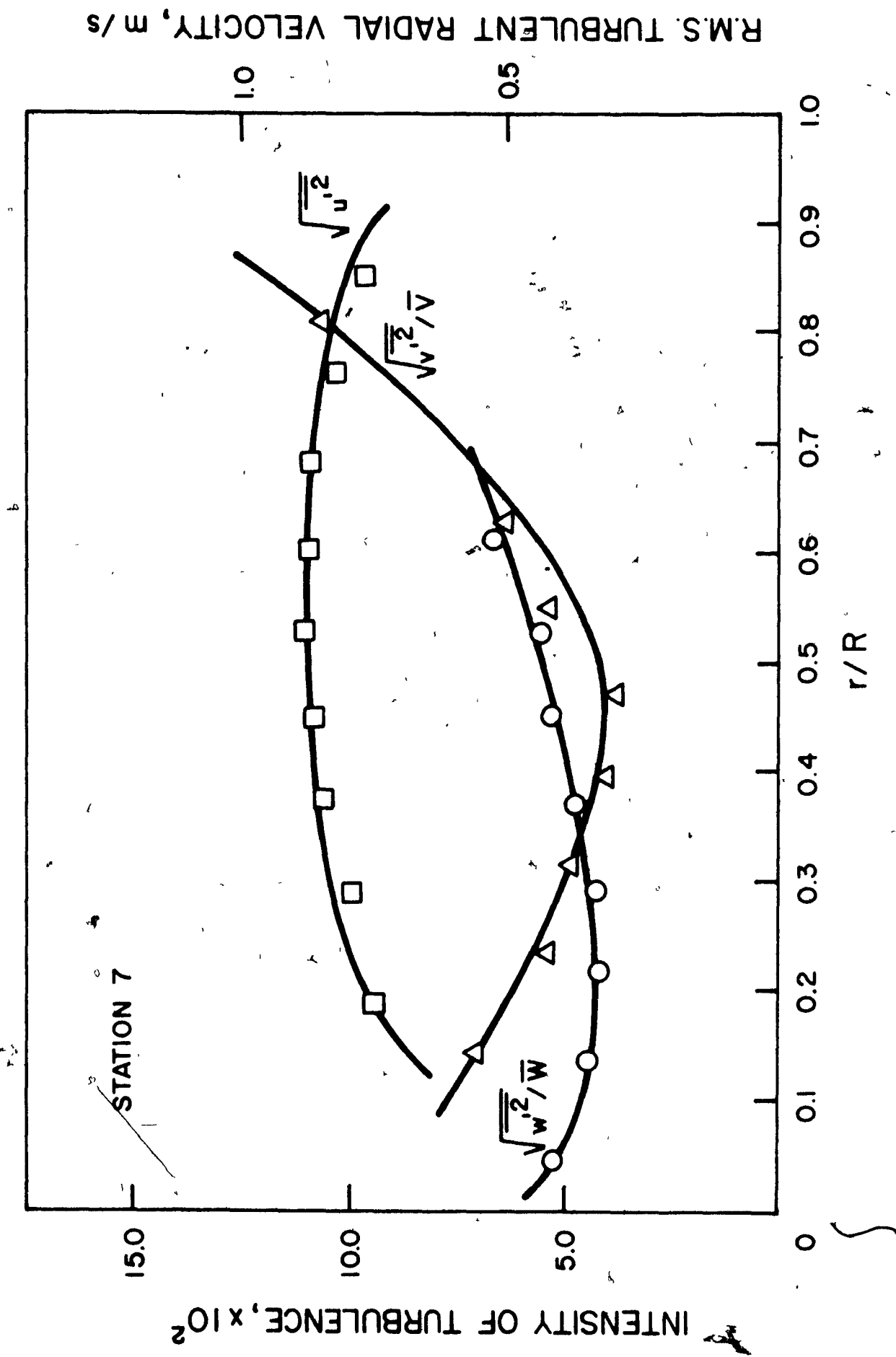
### CONCLUSIONS

It is believed that the data which have been presented on flow angles, profiles of mean tangential and axial velocities and radial distributions of tangential and axial intensities of turbulence represent one of the most exhaustive attempts ever made to characterize the vortex flow occurring in a chamber of the design under study, as a function of the inlet velocity as the main variable. The experimental approach depended on the use of a single inclined hot-wire probe which, in turn, relied on a set of response equations which have been derived in the analysis presented in Appendix I. Although the experimental technique is not new in itself, it is felt that the theoretical analysis, and hence the response equations derived from it, are more accurate than those which have been proposed so far in the literature.

In general, the quantitative results of the present study confirm the theoretical predictions and the experimental trends reported in the literature. In particular, they fully support the conclusion that the flow pattern is relatively insensitive to the entrance volumetric flowrate. They also show that the value of the mean outward radial

FIGURE 28

Root-Mean-Square Fluctuating Radial Velocity  
at Station 7, for Inlet Velocity of 3.20 m/s.



velocity is very small and could be neglected for design purposes. Taken together, these two facts should greatly facilitate future attempts to derive generalized equations of motion for vortex flow.

One of the great-and-remaining difficulties in the complete characterization of vortex flow is the large dependence of the flow pattern on the entrance conditions, as illustrated in Figures 1, 2 and 3 shown in the Literature Review section of this thesis. A more striking example is afforded by a comparison between the results of the present work and those reported by Gauvin, Katta and Knelman (14), who studied the motion of entrained droplets in a chamber of exactly the same geometry and dimensions as the present one, with the single and important difference that the entrance slots were inclined in the opposite direction. Although the quantitative data on tangential and axial mean velocity reported by these earlier authors are rather meagre, they are sufficient to show that the flow patterns, and in particular the flow angles, were completely different. In view of these findings, no attempt was made in the present work to derive generalized equations for tangential and axial motions, since a proper entrance parameter was lacking.

Before the complete characterization of the flow in a vortex chamber, and hence its design for industrial applications, can be attempted, it is obvious that more information must be obtained on the effect of entrance conditions. It can be predicted that the initial flow angle will be an important parameter, but will it be the only one?

Further work will obviously be needed to answer this question, and studies along those lines will be continuing in this laboratory. In the meantime, it is hoped that the present investigation has provided useful information towards an understanding of this interesting field.

BIBLIOGRAPHY

1. Beams, J.W., and Kuhlthau, A.R. "Present Status of the Gas Centrifuge Method for the Separation of Isotopes," Univ. of Virginia, Report EP 1779-59-TR6, (Nov. 1959).
2. Kerrebrock, Jack L., and Mèghreblian, V. Robert. "Vortex Containment for the Gaseous-Fission Rocket," J. Aerospace Sci., Vol. 28, No. 9, (Sept. 1961), 710.
3. Hilsch, R. "The Use of Expansion of Gases in a Centrifugal Field as a Cooling Process," Review of Scientific Instruments, Vol. 18, No. 2, (Feb. 1947), 108.
4. Deissler, Robert G., and Perlmutter, Morris. "An Analysis of the Energy Separation in Laminar and Turbulent Compressible Vortex Flow," Proceedings of Heat Transfer and Fluid Mechanics Institute, Berkeley, Calif., (June 1958).
5. Donaldson, Coleman DuP. "The Magnetohydrodynamic Vortex Power Generator, Basic Principles and Practical Problems," Aeronautical Research Associates of Princeton, Inc., A.R.A.P. Rept. No. 30, (March 1961).
6. Applegate, M. "Vortex Tube Applications," Proceedings of the Conference on Cooling of Aircraft Electronic Equipment, Ohio State University, Engineering Bulletin No. 148, (July 1952).
7. Taylor, G.I. "The Boundary Layer in the Converging Nozzle of a Swirl Atomizer," Quarterly Journal of Mechanics and Applied Math., Vol. 3, (1950), 129.
8. Havemann, H.A. "A Theory of Cyclone Combustion Chamber Design", National Gas Turbine Est., Report No. R53, (May 1949).
9. Kerrebrock and Lafyatis. "Analytical Study of Some Aspects of Vortex Tubes for Gas-Phase Fission Heating," ORNL, CF-58-7-4, (July 21, 1958).
10. Gillespie, T.D. "An Analytical and Experimental Study of the Influence of Swirl on Choked Nozzle Flow," Ph.D. Thesis, Pennsylvania State University, (1970).
11. Mensing, A.E., Stoeffler, K.D., Davison, W.R., and Hoover, T.E. "Investigation of the Use of a Vortex Flow to Separate Oil from an Oil-Water Mixture," United Aircraft Research Laboratories, Report 714/03/A/001, (Nov. 1970).
12. Edeling, C. Beihefte Angew. Chem., Vol. 57, No. 1, (1949).
13. Masters, K. "Spray Drying," Leonard Hill Books, London, England, (1972).

14. Gauvin, W.H., et al. "Drop Trajectory Predictions and their Importance in the Design of Spray Dryers," (to be published in Int. J. Multiphase Flow, in press).
15. Katta, S., and Gauvin, W.H. "Some Fundamental Aspects of Spray Drying," A.I.Ch.E., Journal, Vol. 21, No. 1, (1975), 143.
16. Chigier, A.N. "Velocity Measurement in Vortex Flows," A.S.M.E., Paper No. 5-1-31, (May 1971).
17. Dornbrand, H. "Theoretical and Experimental Study of Vortex Tubes," Republic Aviation Corporation, Air Force Tech. Rep., No. 6123, (1950).
18. Martynovskii, V.S., and Alekseev, V.P. "Investigation of the Vortex Thermal Separation Effect for Gases and Vapors," Soviet Phys.-Tech. Physics 1, translated from Zhur, Tekh. Fi., Vol. 26, (1956).
19. Westley, R. "A Bibliography and Survey of the Vortex Tube," College of Aeronautics, Granfield, Note No. 9, (1954).
20. Westley, R. "Vortex Tube Performance Data Sheets," College of Aeronautics, Granfield, Note No. 67, (1957).
21. Suzuki, M. "Theoretical and Experimental Studies on the Vortex Tube," Sci. Papers I.P.C.R. (Japan), Vol. 54, (1960), 43-87.
22. Scheper, G.W. "The Vortex-Tube Internal Flow Data and a Heat Transfer Theory," Refrigerating Engineering, Vol. 59, (1951), 985-9, and 1018.
23. Taylor, G.I. "Experiments with Rotating Fluids," Proceedings Royal Soc. of London, A100, (1921), 114.
24. Ranque, G.J. "Method and Apparatus for Obtaining from a Fluid Under Pressure Two Currents of Fluid of Different Temperatures," U.S. Patent Office, No. 1,952,281, (1932).
25. Donaldson, Coleman DuP. "Solutions of the Navier-Stokes Equations for Two and Three-Dimensional Vortices," Ph.D. Thesis, Princeton University, (1957).
26. Hartnett, J.P., and Eckert, E.R. "Experimental Study of the Velocity and Temperature Distribution in a High Velocity Vortex Type Flow," Heat Transfer and Fluid Mechanics Inst., Stanford University Press, Stanford, Calif., (1956).
27. ibid., Trans. A.S.M.E., Vol. 79, (1957), 751.

28. Schowalter, W.R., and Johnstone, H.F. "Characteristics of the Mean Flow Patterns and Structure of Turbulence in Spiral Gas Streams," A.I.Ch.E. Journal, Vol. 6, No. 4, (1960), 648.
29. Kassner, R., and Knoernschild, E. "Friction Laws and Energy Transfer in Circular Flow," Wright Patterson Air Force Base, Tech. Rep., No. F-TR-2198-ND, (1948).
30. Marshall, W.R., Jr. "Atomization and Spray Drying," Chem. Eng. Progress, Monograph Series, Vol. 50, No. 2, (1954).
31. Soo, S.L. "Some Basic Aspects of Cyclone Separators," Proceedings of the First International Conference in Particle Technology, IIT Research Institute, Chicago, Illinois, (Aug. 1973).
32. Lay, J.E. "Experimental and Analytical Study of Vortex-Flow Temperature Separation by Superposition of Spiral and Axial Flow," Journal of Heat Transfer, Trans. of A.S.M.E., Series C, Part 1, Vol. 81, (1959), 202.
33. Lay, J.E. "Study of Vortex Flow Temperature Separation by Superposition of Spiral and Axial Flows," Journal of Heat Transfer, Trans. of A.S.M.E., Series C, Part 2, Vol. 81, (1959), 213.
34. Holman, J.P., and Moore, G.D. "An Experimental Study of Vortex Chamber Flow," Journal of Basic Engineering, Trans. of A.S.M.E., Series E, (Dec. 1961), 632-6.
35. Savino, J.M., and Ragsdale, R.G. "Some Temperature and Pressure Measurements in a Confined Vortex Flow," Preprint 60-SA-4, A.S.M.E., (1960).
36. Ragsdale, R.G. "Applicability of Mixing Length Theory to Turbulent Vortex System," NASA TND-1051, (1961).
37. Kendall, J.M., Jr. "Experimental Study of a Compressible Viscous Vortex," J.P.L. Rep. TR 32-290, (1962).
38. Donaldson, C. duP., and Williamson, G.G. "An Experimental Study of Turbulence in a Driven Vortex," Aeronautical Research Associates of Princeton, Inc., A.R.A.P. Tech. Memo 62-2, (1962).
39. Pivrotto, T.J. "Binary Diffusion in a Compressible Three-Dimensional Turbulent Vortex," J.P.L. Space Programs Summary 37-18, Vol. IV, (Dec. 1962), 129-132.
40. Schulz-Jander, B. "Determination of the Flow Field in a Confined Vortex Chamber," M.S. Thesis, Rice University, Houston, Texas, (1963).

41. Collins, J.C., and Stubbs, T.F. "Qualitative Experimental Investigations on Various Vortex Tube Configurations," University of California, Lawrence Radiation Laboratory, U.C.R.L.-12045, (Aug. 1964).
42. Blatt, and Trusch, R. "An Experimental Investigation of an Improved Vortex Cooling Device," A.S.M.E., Paper No. 62-WA-200, (1960).
43. Travers, A., and Johnson, B.V. "Measurements of Flow Characteristics in an Axial Flow Vortex Tube," NASA, CR-277, (Aug. 1965).
44. Travers, A., and Johnson, B.V. "Measurements of Flow Characteristics in a Basic Vortex Tube," NASA, CR-278, (1965).
45. McFarlin, D.J. "Experimental Investigation of the Effect of Peripheral Wall Injection Technique on Turbulence in an Air Vortex Tube," United Aircraft Research Laboratories, U.A.R.L. Report D-910091-5, (Sept. 1965), also appears in NASA, CR-68867.
46. Nakamura, Takashi. "Experimental Study of a Single Confined Vortex Flow," M.S. Thesis, Massachusetts Institute of Technology, (1966).
47. Ter Linden, A.J. "Cyclone Dust Collectors for Boilers," A.S.M.E., Paper No. 52-FU-1, (1952).
48. Ter Linden, A.J. "Investigations into Cyclone Dust Collectors," A.S.M.E., Vol. 75, (1953), 433.
49. Kelsall, D.F. Trans. Instn. Chem. Engrs., Vol. 30, (1952), 87.
50. Yoshioka, H., and Hotta, Y. Chem. Engng. Japan, Vol. 19, (1955), 632.
51. Bradley, D., and Pulling, D.J. Trans. Instn. Chem. Engrs., Vol. 37, (1959), 34.
52. Smith, J.L., Jr. "An Experimental Study of the Vortex in the Cyclone Separator," Journal of Basic Eng., Trans. A.S.M.E., Series E, Vol. 84, (Dec. 1962), 602.
53. First, M.W. "Fundamental Factors in the Design of Cyclone Dust Collectors," Sc.D. Thesis, Department of Industrial Hygiene, Harvard University, (1950).
54. Iinoya, K. "Study of the Cyclone", Memoirs of the Faculty of Engineering, Nagoya University, Vol. 5, (1953), p. 131.
55. Smith, J.L., Jr. "An Analysis of the Vortex Flow in the Cyclone Separator," Journal of Basic Eng., Trans. A.S.M.E., Series E, Vol. 84, (Dec. 1962), 609.

56. Thordarson, R. M.S. Thesis, Univ. Wisconsin, (1952).
57. So, L. Kwan. "Vortex Phenomena in a Conical Diffuser," A.I.A.A. Journal, Vol. 5, No. 6, (June 1973), 1072-78.
58. Wolf, L., Lavan, Z., and Fejer, A.A. "Measurements of the Decay of Swirl in Turbulent Flow," A.I.A.A. Journal, Vol. 7, No. 5, (May 1969), 971-3.
59. Sarpkaya, T. "On Stationary and Travelling Vortex Breakdowns," Journal of Fluid Mech. Vol. 45, Pt. 73, (Feb. 1971), 545.
60. Sarpkaya, Targut. "Vortex Breakdown in Swirling Conical Flows," A.I.A.A. Journal, Vol. 9, No. 9, (Sept. 1971), 1792-9.
61. Lineberry, C.W. "A Study of Swirling Air Flow in a Converging Nozzle," M.S. Thesis, University of Missouri-Rolla, (1968).
62. Batson, J.L., and Sforzini, R.H. "Swirling Flow through a Nozzle," Journal of Space Craft and Rockets, Vol. 7, No. 2, (Feb. 1970), 159-163.
63. Van Deemter, J.J. "On the Theory of the Ranque-Hilsch Cooling Effect," Appl. Sci. Res., A,3, (1952), 174-96.
64. Pengelly, C.D. "Flow in a Viscous Vortex," J. Appl. Phys. Vol. 28, (1957), 86-92.
65. Deissler, Robert G. and Perlmutter, Morris. "Analysis of the Flow and Energy Separation in a Turbulent Vortex," Int. J. Heat and Mass Transfer, Vol. 1, (1960), 173-91.
66. Mack, L.M. "The Compressible Viscous Heat-Conducting Vortex," Journal of Fluid Mech., Vol. 8, (June 1960), 184.
67. Fontein, F.J., and Dijkman, C. "Recent Developments in Mineral Dressing," London: Institution of Mining and Metallurgy, (1953), 229.
68. Rietema, K. Chem. Engng. Sci., Vol. 15, (1961), 298.
69. Rietema, K., and Krajenbrink, H.J. "Theoretical Derivation of Tangential Velocity Profiles in a Flat Vortex Chamber--Influence of Turbulence and Wall Friction," Appl. Sci. Res., Section A, Vol. 8, (1959), 177.
70. Einstein, H.A., and Li, H.L. "Steady Vortex Flow in a Real Fluid," Proceedings of Heat Transfer and Fluid Mech. Inst., Stanford University, (1951), 483.

71. Lewellen, W.S. "Three-Dimensional Viscous Vortices in Incompressible Flow," Ph.D. Thesis, University of California, Los Angeles, (1964).
72. Keyes, J.J., Jr. "Experimental Study of Gas Dynamics in High Velocity Vortex Flow," Proceedings of Heat Transfer and Fluid Mech. Inst., (1960), 31-46.
73. Donaldson, C. duP., and Sullivan, R.D. "Behavior of Solutions of Navier-Stokes Equations for a Complete Class of Three-Dimensional Viscous Vortices," Proceedings of Heat Transfer and Fluid Mech. Inst., Stanford, (1960), 16.
74. Burgers, J.M. "The Effect of Stretching of a Vortex Core," University of Maryland Inst. for Fluid Dynamics and Applied Mechanics, Tech. Dept. BN-80, (1956).
75. Loitsyansky, L.G. "The Propagation of a Twisted Jet in an Unbounded Space Filled with the Same Fluid," Prikladnaya Matematika i Mekhanika, Vol. 17, (1953), 3-16.
76. Görtler, H. "Decay of Swirl in an Axially Symmetrical Jet Far from the Orifice," Revista Matematica Hispani Americanas, Vol. 14, Nos. 4 and 5, (1954), 143-178.
77. Steiger, M.H., and Bloom, M.H. "Axially Symmetric Laminar Free Mixing with Swirl," Proceedings of the Heat Transfer and Fluid Mechanics Institute, Stanford University Press, Stanford, Calif., (1961).
78. Chervinsky, Amnon. "Similarity of Turbulent Axisymmetrical Swirling Jets," A.I.A.A.J., Vol. 6, No. 5, (May 1968), 912-914.
79. Long, R.R. "Vortex Motion in a Viscous Fluid," Journal Meteor., Vol. 15, (1958), 108.
80. Lewellen, W.S. "A Solution for Three-Dimensional Vortex Flows with Strong Circulation," Journal of Fluid Mechanics, Vol. 14, (1962), 420.
81. Lewellen, W.S. "Linearized Vortex Flows," A.I.A.A. Journal, Vol. 3, No. 1, (Jan. 1965), 91-97.
82. Rosenzweig, L.M., Lewellen, W.S., and Ross, D.H. "Confined Vortex Flows with Boundary Layer Interactions," A.I.A.A. Journal, Vol. 2, No. 12, (Dec. 1964), 2127.
83. Logan, S.E. "An Approach to the Dust Devil Vortex," A.I.A.A. Journal, Vol. 9, No. 4, (April 1971), 660.

84. Linderstrom-Lang, C.U. "The Three-Dimensional Distributions of Tangential Velocity and Total Temperature in Vortex Tubes," Journal of Fluid Mechanics, Vol. 45, Part 1, (1971), 161.
85. Lilley, David, G. "Prediction of Inert Turbulent Swirl Flows," A.I.A.A. Journal, Vol. 11, No. 7, (July 1973), 955-9.
86. Bossel, Hartmut, H. "Swirling Flows in Streamtubes of Variable Cross Section," A.I.A.A. Journal, Vol. 11, No. 8, (Aug 1973), 1161-4.
87. Bloor, M.I.G., and Ingham, B. Robert. "Theoretical Investigation of the Flow in a Conical Hydrocyclone," Trans. Instn. Chem. Engrs., Vol. 51, No. 1, (Jan. 1973), 36-41.
88. Lawler, M.T., and Ostrach, S. "A Study of Cyclonic Two-Fluid Separation," Fluid, Thermal and Aerospace Sciences, Engineering Division, Case Institute of Technology, AFOSR65-1523, Cleveland, Ohio, (June 1965).
89. Burton, K.R. "Influence of Gravity on the Performance of a Conical Vortex Separator," A.I.A.A. Journal, Vol. 8, No. 5, (May 1970), 956.
90. Crow, D.E. "An Analytical Study of a Confined Viscous Vortex," Ph.D. Thesis, University of Missouri-Rolla, (1972).
91. Norton, David, J., et al. "An Analytical and Experimental Investigation of Swirling Flow in Nozzles," A.I.A.A. Journal, Vol. 7, No. 10, (Oct. 1969), 1992-2000.
92. Mager, A. "Incompressible, Viscous, Swirling Flow Through a Nozzle," A.I.A.A. Journal, Vol. 9, No. 4 (April 1971), 649.
93. King, W.S. "A Theoretical Investigation of Swirling Flows Through a Nozzle," Ph.D. Thesis, University of California, Los Angeles, (1967).
94. Lewellen, W.S. "A Review of Confined Vortex Flows," NASA CR-1772, (1971); or N71-32276, M.I.T. Press, (1971).
95. Timm, George, K. "Survey of Experimental Velocity Distributions in Vortex Flows with Bibliography," Boeing Scientific Research Laboratories, Document DI-82-0683 (Nov. 1967).
96. Dobratz, Brigitta, M. "Vortex Tubes, a Bibliography," University of California, Lawrence Radiation Laboratory, Report UCRL-7829, (April 1964).

97. Lee, J.C., and Ash, J.E. Trans. A.S.M.E., Vol. 78, (1956), 603-608.
98. Miller, R.D., and Comings, E.W., J. Fluid. Mech., Vol. 7, No. 2, (1960), 237-256.
99. Chigier, N.A., and Beer, J.M., Journal of Basic Eng. Trans. A.S.M.E., Series D, Vol. 86, No. 4, (1964), 788-796.
100. Davies, T.W. Ph.D. Thesis, Dept. Chemical Engineering, Sheffield University (1969).
101. Allen, R.A. Ph.D. Thesis, Dept. Chemical Engineering, Sheffield University (1971).
102. Syred, N., Dept. Chemical Engineering, Sheffield University FTCE/27/NS/12, (1970).
- ~~103. Lavan, Z. and Fejer, A.A. "Investigations of Swirling Flows in Ducts," Aerospace Research Lab., ARL 66-0083, U.S. Air Force, Wright-Patterson Air Force Base, Ohio, (May 1966).~~
104. Talbot, L. "Laminar Swirling Pipe Flow," Journal of Applied Mechanics, Trans. A.S.M.E., (March 1954), p. 1.
105. Kreith, F. and Sonju, O. "The Decay of Turbulent Swirl in a Pipe," Journal of Fluid Mechanics, Vol. 22, Pt. 2, (1965), p. 257.
106. Rochino, A.P., "Analytical Investigation of Incompressible Turbulent Swirling Flow in Pipes," M.S. Thesis, Illinois Institute of Technology, (1968).
107. Eskinazi, S., and H. Yeh., J. Aeronaut. Sci., Vol. 23, No. 23, (1956).
108. Cohen, M.F. "Turbulence in Water During Pipe Flow," M.S. Thesis, The Ohio State University, (1962).
109. Collis, D.C., Aero. Quart., Vol. IV, (1952).
110. Collis, D.C., J. Aero. Sci., (July 1956).

APPENDIX I

HOT WIRE ANALYSIS

LIST OF FIGURES IN APPENDIX I

<u>Figure</u>		<u>Page</u>
A-1	Different Yaw Situations	A-3
A-2	Coordinate System Used	A-6
A-3	Diagram for Derivation of Hot-Wire Response Equations	A-7

## APPENDIX I

### HOT WIRE ANALYSIS

#### YAW CALIBRATION

For a complete description of the hot wire response, we have to determine the instantaneous effective cooling velocity. This will not be the component of velocity normal to the wire, but will take account of the component along it. If the ratio of the efficiency of the two components in cooling the wire is denoted by  $K$ , then

$$q_e = q_i (\cos^2 \beta_s + K^2 \sin^2 \beta_s)^{1/2} \quad (A1)$$

where  $q_i$  is the instantaneous velocity vector making an angle  $\beta_s$  with the normal to the wire. Even when the effect has been reduced to these terms, the determination of the magnitude of  $K$  for a particular situation is extremely complicated.

According to Champagne, Sleicher and Wehrmann (1) and Davies and Davis (3), Equation (A1) gives the best representation of the effective cooling velocity  $q_e$  of a hot wire inclined to the mean flow. They also concluded that the velocity component along a wire of finite length results in an asymmetric distribution of heat transfer coefficient, and an increase in average heat transfer coefficient with increasing yaw angle for a fixed normal velocity. The temperature of the gas flowing around the wire increases downstream along the wire, but the temperature distribution on the wire itself is not appreciably asymmetric, nor is the difference in the end conduction losses to the two supports

significant. Careful studies by the above researchers using various support sizes and a flow visualization technique respectively have also shown that the distortion of the flow by the supports is not a factor that need be considered. Thus results for different probe support geometries should be comparable, but the yaw effect is likely to be influenced by the value of mean wire temperature above ambient, by the length-to-diameter ratio of the wire, and by the velocity of the flow.

By considering overheat ratios of 0.8 only, we can eliminate the first of these factors. The dependence of  $K$  on the second is shown in the results of Champagne et al. (1), who measured  $K = 0.21 \pm 0.04$ , when  $l/d = 200$ , falling steadily as the wire-length increases to approximately zero for  $l/d = 600$ , at a velocity of 35 m/sec. However, Webster (4), who yawed his probe in a different way from Champagne (see Figure A1), reported a mean value of  $K = 0.20 \pm 0.01$  with no significant dependence on  $l/d$  over a range from 86 to 1456. Neither Champagne nor Webster found any really significant dependence on velocity (for a statistical analysis of Webster's results, see Kjellstrom and Larsson (5)) but Webster's were in a narrow range around 5 m/sec. Taken with the suggestion of Rasmussen, quoted by Kjellstrom and Larsson (5), that  $K = 0.26 \pm 0.03$ , the results suggest that 0.23 is most appropriate for DISA probes ( $l/d = 200$ ) at velocities of the order of 30 m/sec.

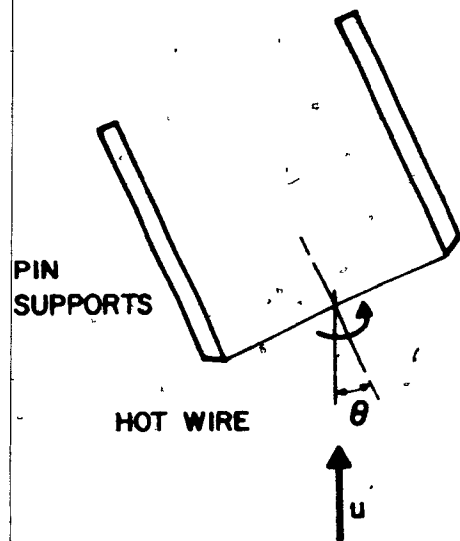
Another effect complicates the analysis of the yaw calibration. This is the increase in measured velocity by 18% when the pin supports are rotated through  $90^\circ$  about the axis of a wire which is normal to the

FIGURE A-1

Different Yaw Situations

a

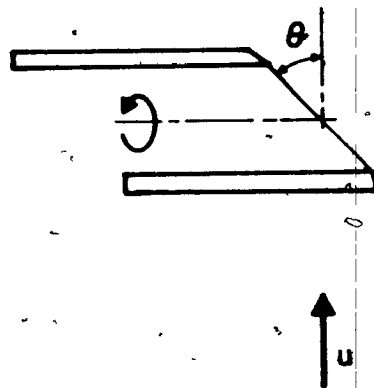
CHAMPAGNE ET AL (1967)



$$u_{\text{eff}}^2 = u^2 (\cos^2 \theta + k_1^2 \sin^2 \theta)$$

b

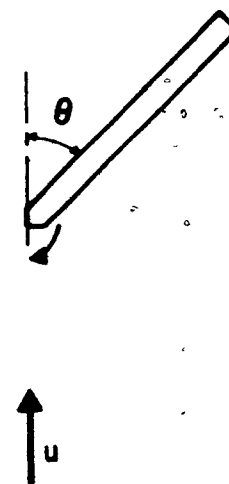
WEBSTER (1962)



$$u_{\text{eff}}^2 = u^2 (\cos^2 \theta + k_2^2 \sin^2 \theta)$$

c

ROOLE & CALVERT (1967)  
EYRE (1967)



flow, to a position perpendicular to the flow (see Figure A1-C). It has been reported by Hoole and Calvert (6), and Eyre (7), who shows theoretically that it could be due to varying end losses by conduction when different parts of the supports lie within the wake of the wire. Thus the probe must be calibrated in the position in which it is to be used, or a further correction must be applied. This mechanism of changing end conduction loss would be expected to apply to the other yawing situations (a and b in Figure A1), so it is surprising that it was not measured by Champagne et al.

#### ANALYSIS

The wire calibration gives a mean voltage corresponding to a mean uniform velocity normal to, or at a known angle, to the wire, the turbulence in the calibrating stream being negligible. Measurements in the chamber give a mean voltage as well as the R.M.S. value of the fluctuating voltage, and one has to relate these voltages to mean and fluctuating velocities using the calibration.

The present analysis is an attempt to obtain a modified set of response equations (using the calibration data), which would permit the determinations of the components of the mean velocity vectors, turbulence intensities and Reynolds stresses, from a single inclined hot-wire probe introduced in various orientations in a flow field having a "dominant tangential velocity component". In what follows, the corrections for blockage and pitch are neglected, and the yaw factor is denoted by  $K$ .

The coordinate system used and the velocity component diagram are shown in Figures A-2 and A-3 respectively. In the diagram  $q_i$  represents the instantaneous resultant velocity vector\*, and  $q_x$ ,  $q_y$ , and  $q_z$  are the component instantaneous velocities in X, Y, and Z directions.  $Q_z$  is a fictitious dominant mean velocity, included for the purpose of normalizing the final response equations.

As mentioned in the previous section, the instantaneous effective cooling velocity is given by the cosine law as

$$q_e = q_i (\cos^2 \beta_s + K^2 \sin^2 \beta_s)^{1/2} \quad (A1)$$

where  $\beta_s$  is the angle between the instantaneous velocity vector and the normal to the wire axis.

The sketch of Figure A-2 shows the hot-wire oriented at an angle  $\alpha'$  relative to the mean velocity  $Q_z$ , and at an angle  $\beta'_s$  relative to the instantaneous velocity, then it can be shown that

$$\beta_s = 90 - \beta'_s \quad (A2)$$

and

$$\alpha = 90 - \alpha' \quad (A3)$$

where  $\alpha$  is the angle between the normal to the wire and the mean flow direction.

Equation (A1) can also be written as

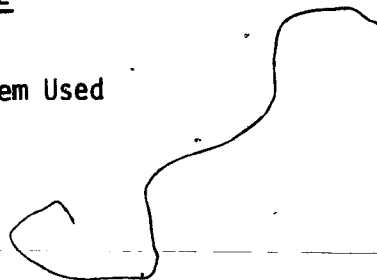
$$q_e^2 = q_i^2 [\cos^2 \beta_s + K^2 \sin^2 \beta_s] \quad (A4)$$

---

\* The direction of this resultant instantaneous velocity vector is mistakenly presented in References (2) and (9).

FIGURE A-2

Coordinate System Used



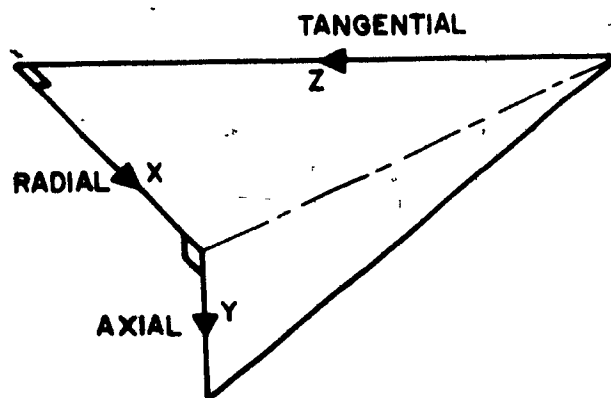
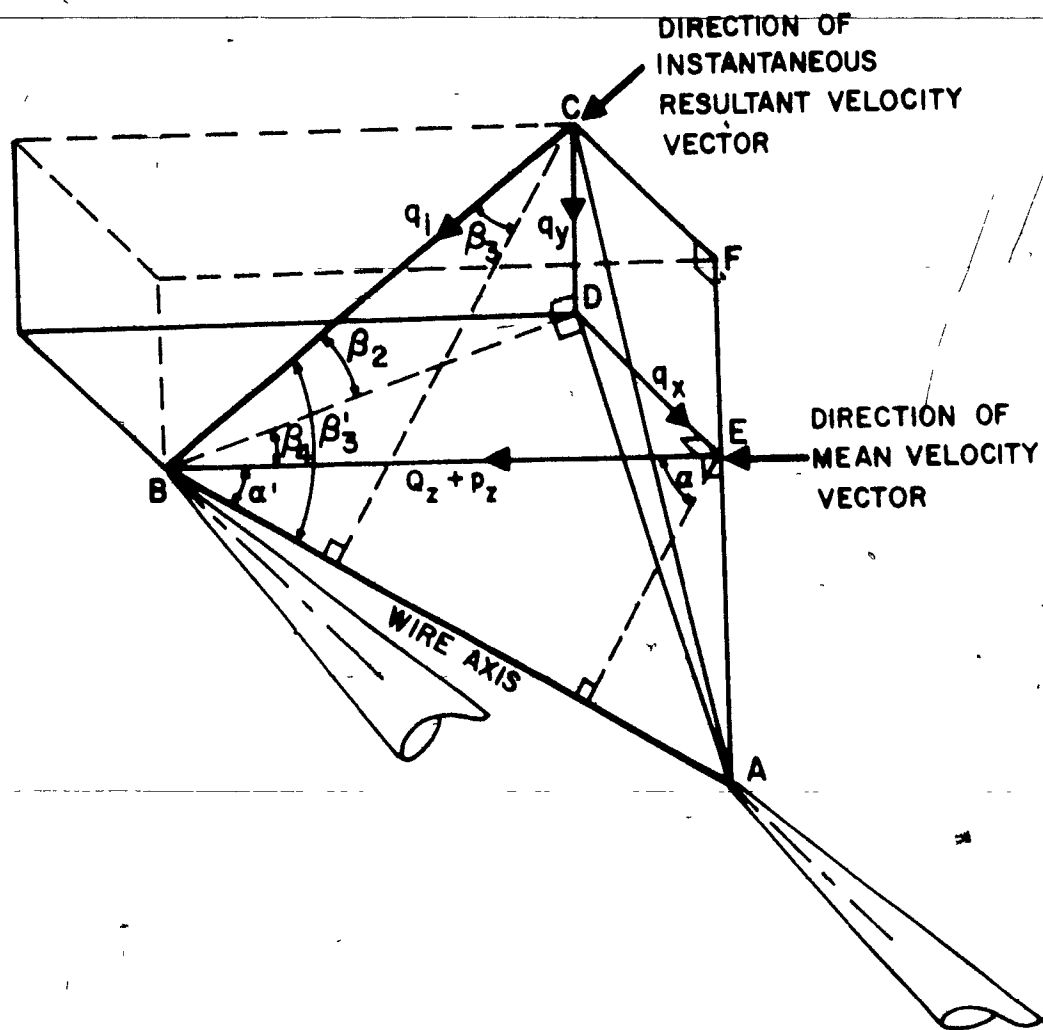


FIGURE A-3

Diagram for Derivation of Hot-wire Response Equations



but

$$\begin{aligned}
 \cos^2 \beta_s + K^2 \sin^2 \beta_s &= 1 + (K^2 - 1) \sin^2 \beta_s \\
 &= \cos^2 \alpha + \sin^2 \alpha + (K^2 - 1) \sin^2 \beta_s \\
 &= \cos^2 \alpha [1 + \tan^2 \alpha + (K^2 - 1) \sin^2 \beta_s / \cos^2 \alpha] \\
 &= \cos^2 \alpha [1 + K^2 \tan^2 \alpha + (K^2 - 1) (\sin^2 \beta_s / \cos^2 \alpha - \tan^2 \alpha)]
 \end{aligned}$$

or

$$\cos^2 \beta_s + K^2 \sin^2 \beta_s = \cos^2 \alpha [1 + K^2 \tan^2 \alpha + (K^2 - 1) \left\{ \frac{1}{\cos^2 \alpha} (\sin^2 \beta_s - \sin^2 \alpha) \right\}] \quad (A5)$$

and hence,

$$q_e^2 = q_i^2 \cos^2 \alpha [1 + K^2 \tan^2 \alpha + (K^2 - 1) \left\{ \frac{1}{\cos^2 \alpha} (\sin^2 \beta_s - \sin^2 \alpha) \right\}] \quad (A6)$$

Having defined  $\alpha$  and  $\beta_s$  as above, our immediate objective will be to express  $\beta_s$  in terms of  $\alpha$ , and defined angles  $\beta_2$ , and  $\beta_4$  (Fig. A-2). This can be obtained from the cosine law of trigonometry as follows:

Considering triangle ABC, we can write

$$AC^2 = AB^2 + BC^2 - 2(AB)(BC) \cos \beta_s \quad (A7)$$

or

$$c^2 = a^2 + b^2 - 2ab \cos \beta_s' \quad (A8)$$

Now we have to find  $b$  and  $c$ :

from triangles BCD, BDE, and ABE, we get

$$b = (a \cos \alpha' / \cos \beta_2) \cos \beta_4 \quad (A9)$$

and from triangles ACF we will have

$$c^2 = (AE)^2 + (EF)^2 + 2(AE)(EF) + (FC)^2 \quad (A10)$$

Substituting for AE, EF, and FC from triangles ABE, BCD, and BDE respectively, yields

$$c^2 = a^2 [\sin^2 \alpha' + \cos^2 \alpha' \cdot \tan^2 \beta_2 / \cos^2 \beta_4 + 2 \sin \alpha' \cos \alpha \tan \beta_2 / \cos \beta_4 + \cos^2 \alpha \tan^2 \beta_4] \quad (A11)$$

Substituting equations (A9) and (A11) into (A8) and dividing through by  $a^2$  we will have

$$\begin{aligned} -\cos \beta_3 = & [\cos \beta_2 \cdot \cos \beta_4 / 2 \cos \alpha'] [\sin^2 \alpha' + \cos^2 \alpha' \cdot \tan^2 \beta_2 / \cos^2 \beta_4 \\ & + 2 \sin \alpha' \cos \alpha' \tan \beta_2 / \cos \beta_4 \\ & + \cos^2 \alpha' \cdot \tan^2 \beta_4 - 1 \\ & - \cos^2 \alpha' / \cos^2 \beta_2 \cdot \cos^2 \beta_4] \quad (A12) \end{aligned}$$

Substituting equations (A2) and (A3) into (A12) yields

$$\begin{aligned} -\sin \beta_3 = & [\cos \beta_2 \cdot \cos \beta_4 / 2 \sin \alpha] [\cos^2 \alpha + \sin^2 \alpha \cdot \tan^2 \beta_2 / \cos^2 \beta_4 \\ & + 2 \sin \alpha \cdot \cos \alpha \cdot \tan \beta_2 / \cos \beta_4 \\ & + \sin^2 \alpha \cdot \tan^2 \beta_4 - 1 \\ & - \sin^2 \alpha / \cos^2 \beta_2 \cdot \cos^2 \beta_4] \quad (A13) \end{aligned}$$

Equation (A13) agrees with the results of a similar derivation presented by Heskestad (8) and Champagne and Sleicher (2).

The angles  $\beta_2$  and  $\beta_4$  are defined by (see the diagram)

$$\sin \beta_2 = q_y [(Q_z + q_z)^2 + q_y^2 + q_x^2]^{-1/2} \quad (A14)$$

$$\cos \beta_2 = [(Q_z + q_z)^2 + q_x^2]^{1/2} \cdot [(Q_z + q_z)^2 + q_y^2 + q_x^2]^{-1/2} \quad (A15)$$

$$\sin \beta_4 = q_x [(Q_z + q_z)^2 + q_x^2]^{-1/2} \quad (A16)$$

$$\cos \beta_4 = [Q_z + q_z] [(Q_z + q_z)^2 + q_x^2]^{-1/2} \quad (A17)$$

Introducing eqns. (A14) to (A17) into eqn. (A13) and rearranging gives

$$-\sin \beta_3 = [(Q_z + q_z)^{-1} \cdot q_y \cdot \cos \alpha - \sin \alpha] [Q_z + q_z] [(Q_z + q_z)^2 + q_x^2 + q_y^2]^{-1/2} \quad (A18)$$

Squaring (A18) and dividing through by  $Q_z^2$ , yields

$$\begin{aligned} \sin^2 \beta_s = & [(1 + q_z/Q_z)^2 + (q_x^2 + q_y^2)/Q_z^2]^{-1} [\sin^2 \alpha (1 + q_z/Q_z)^2 \\ & - 2 \sin \alpha \cos \alpha q_y (1/Q_z + q_z/Q_z) \\ & + \cos^2 \alpha q_y^2/Q_z^2] \end{aligned} \quad (A19)$$

Now, if we expand the denominator of the above equation in binomial series, taking the first four terms, and neglecting all the 4th order terms we get:

$$\begin{aligned} [(1 + q_z/Q_z)^2 + (q_x^2 + q_y^2)/Q_z^2]^{-1} = & 1 - 2q_z/Q_z + 3q_z^2/Q_z^2 \\ & - (q_x^2 + q_y^2)/Q_z^2 \\ & + 4(q_z q_x^2 + q_z q_y^2)/Q_z^3 \\ & + 4q_z^3/Q_z^3 \\ & - 8q_z^3/Q_z^3 \end{aligned} \quad (A20)$$

Substituting (A20) into (A19) and neglecting the 4th order terms gives:

$$\begin{aligned} \sin^2 \beta_s = & \sin^2 \alpha + \sin^2 \alpha [-(q_x^2 + q_y^2)/Q_z^2 + 2(q_z q_x^2 + q_z q_y^2)/Q_z^3] \\ & + \cos^2 \alpha [q_y^2/Q_z^2 - 2(q_z q_y^2)/Q_z^3] \\ & - 2 \sin \alpha \cos \alpha [q_y/Q_z - q_y q_z/Q_z^2 + q_y q_x^2/Q_z^3 - q_y^3/Q_z^3] \end{aligned} \quad (A21)$$

Introducing (A21) into (A5) yields:

$$\cos^2 \beta_s + K^2 \sin^2 \beta_s = \cos^2 \alpha [1 + K^2 \tan^2 \alpha]$$

$$\begin{aligned}
& + (K^2-1)\{1/\cos^2\alpha[-(q_x^2 + q_y^2)/Q_z^2 + 2(q_z q_x^2 + q_z q_y^2)/Q_z^3] \\
& + (q_x^2 + 2q_y^2)/Q_z^2 \\
& - 2(q_z q_x^2 + 2q_z q_y^2)/Q_z^3 \\
& - 2\tan\alpha(q_y/Q_z - q_y q_z/Q_z^2 + q_y q_z^2/Q_z^3 \\
& - q_y q_x^2/Q_z^3 - q_y^3/Q_z^3)\} \quad (A22)
\end{aligned}$$

From Fig. A-2 the instantaneous resultant velocity  $q_i$  is given by

$$q_i^2 = [(Q_z + q_z)^2 + q_x^2 + q_y^2]$$

or

$$q_i^2 = Q_z^2 [1 + 2q_z/Q_z + (q_x^2 + q_y^2 + q_z^2)/Q_z^2] \quad (A23)$$

now substituting eqns. (A22) and (A23) into (A4) we get the following expression of the effective cooling velocity:

$$\begin{aligned}
q_e^2 = & Q_z^2 \cdot \cos^2\alpha [1 + 2q_z/Q_z + (q_x^2 + q_y^2 + q_z^2)/Q_z^2] \\
& \times [1 + K^2 \tan^2\alpha + (K^2-1)\{ \frac{1}{\cos^2\alpha} [ -q_x^2 + q_y^2 ] / Q_z^2 \\
& + 2(q_z q_x^2 + q_z q_y^2)/Q_z^3 \\
& + (q_x^2 + 2q_y^2)/Q_z^2 \\
& - 2(q_z q_x^2 + 2q_z q_y^2)/Q_z^3 \\
& - 2 \tan\alpha (q_y/Q_z - q_y q_z/Q_z^2 + q_y q_z^2/Q_z^3 \\
& - q_y q_x^2/Q_z^3 - q_y^3/Q_z^3) \}] \quad (A24)
\end{aligned}$$

Multiplying through and neglecting terms of order higher than 3, gives

$$q_e^2 = Q_z^2 \cdot \cos^2 \alpha \{ A + B[q_z/Q_z] + C[q_z^2/Q_z^2] + D[q_y/Q_z] + E[q_y^2/Q_z^2] + F[q_x^2/Q_z^2] + G[q_y q_z/Q_z^2] \} \quad (A25)$$

where

$$\begin{aligned} A &= 1 + K^2 \tan^2 \alpha \\ B &= 2(1 + K^2 \tan^2 \alpha) = 2A \\ C &= 1 + K^2 \tan^2 \alpha = A \\ D &= 2 \tan \alpha (1 - K^2) \\ E &= \tan^2 \alpha + K^2 \\ F &= \sec^2 \alpha \\ G &= 2 \tan \alpha (1 - K^2) = D \end{aligned} \quad (A26)$$

are all constants for an inclined wire with a yaw factor of  $K$ . Champagne and Sleicher (2) expand these as Taylor Series; however it is more convenient to evaluate them exactly.

As  $q_e$  is required, an approximation to the square root of equation (A25) must be sought. This can be achieved by expanding into a Taylor series in terms of  $q_z$ :

$$f(q_z) = f(0) + f'(0)q_z + f''(0)q_z^2/2! + f'''(0)q_z^3/3! + \dots \quad (A27)$$

The terms of equation (A26) are as follows:

$$f(0) = [A + D q_y/Q_z + E q_y^2/Q_z^2 + F q_x^2/Q_z^2]^{1/2} \quad (A28)$$

$$\begin{aligned} f'(0)q_z &= q_z/Q_z [A^{-1/2} B/2 - A^{-3/2} B D q_y/4Q_z - A^{-3/2} B E q_y^2/4Q_z^2 \\ &\quad - A^{-3/2} B F q_x^2/4Q_z^2 + 3A^{-5/2} B D^2 q_y^2/16 Q_z^2 \\ &\quad + 3A^{-5/2} B D E q_y^3/8Q_z^3 + 3A^{-5/2} B D F q_y q_x^2/8Q_z^3 \end{aligned}$$

$$\begin{aligned}
& - 15 A^{-7/2} B D^3 q_y^3 / 96 Q_z^3 + A^{-1/2} G q_y / 2 Q_z \\
& - A^{-3/2} D G q_y^2 / 4 Q_z^2 - A^{-3/2} E G q_y^3 / 4 Q_z^3 \\
& - A^{-3/2} F G q_y q_x^2 / 4 Q_z^3 + 3 A^{-3/2} D^2 G q_y^3 / 16 Q_z^3 ] \quad (A29)
\end{aligned}$$

where all the terms of fourth order or greater are dropped.

Similarly,

$$\begin{aligned}
f''(0) q_z^2 / 2! &= q_z^2 / 2 Q_z^2 [ - A^{-3/2} B^2 / 4 + 3 A^{-3/2} B^2 D q_y / 8 Q_z \\
&+ 3 A^{-3/2} B^2 E q_y^2 / 8 Q_z^2 \\
&+ 3 A^{-3/2} B^2 F q_x^2 / 8 Q_z^2 - 15 A^{-7/2} B^2 D^2 q_y^2 / 32 Q_z^2 \\
&- 15 A^{-7/2} B^2 D E q_y^3 / 16 Q_z^3 \\
&- 15 A^{-7/2} B^2 D F q_x^2 q_y / 16 Q_z^3 \\
&+ 35 A^{-9/2} B^2 D^3 q_y^3 / 64 Q_z^3 - A^{-3/2} B G q_y / 2 Q_z \\
&+ 3 A^{-3/2} B G D q_y^2 / 4 Q_z^2 + 3 A^{-3/2} B G E q_y^3 / 4 Q_z^3 \\
&+ 3 A^{-3/2} B G F q_y q_x^2 / 4 Q_z^3 + A^{-1/2} C \\
&- 15 A^{-7/2} B G D^2 q_y^3 / 16 Q_z^3 - A^{-3/2} C D q_y / 2 Q_z \\
&- A^{-3/2} E C q_y^2 / 2 Q_z^2 - A^{-3/2} C F q_x^2 / 2 Q_z^2 \\
&+ 3 A^{-3/2} C D^2 q_y^2 / 8 Q_z^2 + 3 A^{-3/2} C D E q_y^3 / 4 Q_z^3 \\
&+ 3 A^{-3/2} C D F q_y q_x^2 / 4 Q_z^3 \\
&- 15 A^{-7/2} C D^3 q_y^3 / 48 Q_z^3 ] \quad (A30)
\end{aligned}$$

and finally

$$f'''(0) q_z^3 / 3! = q_z^3 / Q_z^3 [ A^{-3/2} B^3 / 16 - A^{-3/2} B C / 4 ] \quad (A31)$$

Substituting equations (A28, A29, A30 and A31) into equation (A27), and collecting terms gives:

$$\begin{aligned}
 q_e = a_1 Q_Z \cos \alpha \{ & 1 + a_2 [q_Z / Q_Z] + a_3 [q_Z^2 / Q_Z^2] \\
 & + a_4 [q_Z^3 / Q_Z^3] + a_5 [q_Y / Q_Z] \\
 & + a_6 [q_Y^2 / Q_Z^2] + a_7 [q_Y^3 / Q_Z^3] \\
 & + a_8 [q_X^2 / Q_Z^2] + a_9 [q_Y q_Z / Q_Z^2] \\
 & + a_{10} [q_Y q_Z^2 / Q_Z^3] + a_{11} [q_Y^2 q_Z / Q_Z^3] \\
 & + a_{12} [q_X^2 q_Z / Q_Z^3] + a_{13} [q_X^2 q_Y / Q_Z^3] \} \quad (A32)
 \end{aligned}$$

where

$$\begin{aligned}
 a_1 &= A^{1/2} \\
 a_2 &= BA^{-1/2} \\
 a_3 &= A^{-1}C/2 - B^2A^{-3/8} \\
 a_4 &= B^3A^{-3/16} - BCA^{-2}/4 \\
 a_5 &= DA^{-1/2} \\
 a_6 &= EA^{-1/2} - D^2A^{-2}/8 \\
 a_7 &= A^{-3}D^3/16 - A^{-2}DE/4 \\
 a_8 &= A^{-1}F/2 \\
 a_9 &= A^{-1}G/2 - A^{-2}BD/4 \\
 a_{10} &= 3A^{-3}B^2D/16 - A^{-2}BG/4 - A^{-2}CD/4 \\
 a_{11} &= 3A^{-3}BD^2/16 - A^{-2}BE/4 - A^{-2}GD/4 \\
 a_{12} &= -A^{-2}BF/4 \\
 a_{13} &= -A^{-2}DF/4
 \end{aligned} \quad (A33)$$

For most applications, in particular low intensity turbulences, the third-order turbulence terms are often negligible, and dropping these terms from equation (A32) yields:

$$q_e = a_1 Q_z \cos \alpha \{ 1 + a_2 [q_z^2 / Q_z^2] + a_3 [q_z^2 / Q_z^2] + a_3 [q_y / Q_z] + a_4 [q_y^2 / Q_z^2] + a_5 [q_x^2 / Q_z^2] + a_6 [q_y q_z / Q_z^2] \} \quad (A34)$$

To get separate expressions for mean and fluctuating components, we can decompose the instantaneous velocities into mean and fluctuating parts:

$$\begin{aligned} q_e &= \bar{q} + q' \\ Q_z &= W_0 \\ q_z &= \bar{w} + w' \\ q_y &= (\bar{u} + u') \cos \theta + (\bar{v} + v') \sin \theta \\ q_x &= (\bar{v} + v') \cos \theta - (\bar{u} + u') \sin \theta \end{aligned} \quad (A35)$$

Substituting (A35) into (A34), taking the mean and separating the fluctuating part, gives:

$$\begin{aligned} \bar{q} &= a_1 \cos \alpha W_0 \{ 1 + a_2 [\bar{w} / W_0] + a_3 [(\bar{w}^2 + \overline{w'^2}) / W_0^2] \\ &\quad + a_4 [(\bar{u} \cos \theta + \bar{v} \sin \theta) / W_0] \\ &\quad + (a_5 / W_0^2) [(\bar{u}^2 + \overline{u'^2}) \cos^2 \theta + (\bar{v}^2 + \overline{v'^2}) \sin^2 \theta + 2 \sin \theta \cos \theta (\bar{u} \bar{v} + \overline{u' v'})] \\ &\quad + (a_6 / W_0^2) [(\bar{v}^2 + \overline{v'^2}) \cos^2 \theta + (\bar{u}^2 + \overline{u'^2}) \sin^2 \theta - 2 \sin \theta \cos \theta (\bar{u} \bar{v} + \overline{u' v'})] \\ &\quad + (a_7 / W_0^2) [(\bar{u} \bar{w} + \overline{u' w'}) \cos \theta + (\bar{v} \bar{w} + \overline{v' w'}) \sin \theta] \} \end{aligned} \quad (A36)$$

and

$$\begin{aligned}
 q' = & a_1 \cos \alpha W_0 \{ a_2 [w'/W_0] + 2a_3 [\bar{w}w'/W_0^2] \\
 & + a_5 [(u' \cos \theta + v' \sin \theta)/W_0] \\
 & + (2a_6/W_0^2) [\bar{u}u' \cos^2 \theta + \bar{v}v' \sin^2 \theta + \sin \theta \cos \theta (\bar{u}v' + u'\bar{v})] \\
 & + (2a_8/W_0^2) [\bar{v}v' \cos^2 \theta + \bar{u}u' \sin^2 \theta - \sin \theta \cos \theta (\bar{u}v' + u'\bar{v})] \\
 & + (a_9/W_0^2) [(u'\bar{w} + \bar{u}w') \cos \theta + (v'\bar{w} + \bar{v}w') \sin \theta] \} \quad (A37)
 \end{aligned}$$

It is to be noted that in the above equation

$$\bar{u}' = \bar{v}' = \bar{w}' = 0$$

$$\bar{\bar{u}} = \bar{u}$$

$$\overline{u'^2}, \overline{v'^2}, \overline{w'^2} \neq 0$$

It is possible to obtain the velocity components  $\bar{w}$ ,  $\bar{v}$ , and  $\bar{u}$  from equation (A36), but it will not yield the coupled velocities: these are obtained from square of eqn. (A37).

$$\begin{aligned}
 \overline{q'^2} = & a_1^2 \cos^2 \alpha W_0^2 \{ a_2^2 [\overline{w'^2}/W_0^2] + 2a_2 a_3 [(\overline{u'w'} \cos \theta + \overline{v'w'} \sin \theta)/W_0^2] \\
 & + a_5^2 [(\overline{u'^2} \cos^2 \theta + \overline{v'^2} \sin^2 \theta + 2\overline{u'v'} \sin \theta \cos \theta)/W_0^2] \\
 & + 4a_3^2 [\overline{w^2 w'^2}/W_0^4] + 4a_2 a_3 [\overline{w w'^2}/W_0^3] \\
 & + 4a_2 a_8 [(\overline{v'w'} \bar{v} \cos^2 \theta + \overline{u'w'} \bar{u} \sin^2 \theta - \overline{v'w'} \bar{u} \sin \theta \cos \theta} \\
 & \quad - \overline{u'w'} \bar{v} \sin \theta \cos \theta)/W_0^3]
 \end{aligned}$$

$$\begin{aligned}
& + 4a_2a_6[(\overline{u'w'u} \cos^2\theta + \overline{v'w'v} \sin^2\theta + \overline{v'w'u} \sin\theta\cos\theta \\
& \quad + \overline{u'w'v} \sin\theta\cos\theta)/W_0^3] \\
& + 4a_3a_6[(\overline{u'v'u} \sin^3\theta + \overline{u'v'v} \cos^3\theta + \sin^2\theta\cos\theta(\overline{u'u'^2} - \overline{uv'^2} - \overline{vu'v'}) \\
& \quad + \sin\theta\cos^2\theta(\overline{vv'^2} - \overline{uu'v'} - \overline{vu'^2}))/W_0^3] \\
& + 4a_3a_5[(\overline{wu'w'}\cos\theta + \overline{wv'w'}\sin\theta)/W_0^3] \\
& + 4a_3a_6[(\overline{v'v} \sin^3\theta + \overline{u'u} \cos^3\theta + \sin\theta\cos^2\theta(\overline{uu'v'} + \overline{uu'v'} + \overline{vu'^2}) \\
& \quad + \sin^2\theta\cos\theta(\overline{vu'v'} + \overline{vu'v'} + \overline{uv'^2}))/W_0^3] \\
& + 2a_2a_5[(\overline{wu'w'} + \overline{uw'^2})\cos\theta + (\overline{wv'w'} + \overline{vw'^2})\sin\theta]/W_0^3] \\
& + 2a_3a_5[(\overline{wu'^2} + \overline{uu'w'})\cos^2\theta + (\overline{wv'^2} + \overline{vw'v'})\sin^2\theta \\
& \quad + \sin\theta\cos\theta(2\overline{wu'v'} + \overline{vu'w'} + \overline{uv'w'})]/W_0^3] \tag{A38}
\end{aligned}$$

where again all the fourth order terms (with the exception of  $\overline{w'w'^2}$ ) have been dropped.

#### EVALUATION OF CALIBRATION CONSTANTS

Before equations (A37) and (A38) can be used, a relationship between the measured voltages  $\overline{e}$  and  $\overline{e'}$  and  $\overline{q}$  and  $\overline{q'}$  must be found.

It was noted in equation (A4) that,

$$q_e^2 = q_i^2[\cos^2\beta_s + K^2\sin^2\beta_s] \tag{A4}$$

or

$$q_e = q_i \cos\beta_s [1 + K^2 \tan^2\beta_s]^{1/2} \tag{A39}$$

expanding in binomial series and taking the first two terms gives

$$q_e = q_i \cos \beta_s [1 + \frac{1}{2} K^2 \tan^2 \beta_s] \quad (A40)$$

but during the calibration, the flow was one dimensional so that

$$\beta_s = \alpha$$

therefore

$$q_e = q_i \cos \alpha [1 + \frac{1}{2} K^2 \tan^2 \alpha] \quad (A41)$$

and according to eqn. (A26)

$$q_e = q_i \cos \alpha (A) \quad (A42)$$

or

$$q_i = q_e / A \cos \alpha \quad (A43)$$

the relationship between the instantaneous linearized output voltage,  $e_i$ , of a constant temperature anemometer, and the instantaneous cooling  $q_i$ , velocity is

$$e_i = m \cdot q_i \quad (A44)$$

where  $m$  is the slope of the calibration curve

or

$$e_i \cdot \frac{q_e}{q_i} = m \cdot q_i \cdot \frac{q_e}{q_i}$$

or

$$A \cdot \cos \alpha \cdot e_i / m = q_e = \bar{q} + q' \quad (A45)$$

Letting  $B_1 = A \cdot \cos \alpha / m$ , and expressing the instantaneous voltage as mean and fluctuating components gives

$$B_1 (\bar{e} + e') = \bar{q} + q' \quad (A46)$$

or

$$\bar{q} = B_1 \bar{e} \quad (A47)$$

and

$$\overline{q'^2} = B_1^2 \overline{e'^2} \quad (A48)$$

which may then be used in equations (A37) and (A38) to find the mean velocity and coupled velocity terms respectively.

#### EVALUATION OF VELOCITY TERMS.

The three velocity components can all be obtained from a single inclined hot wire, each via two readings taken 180° apart. In the case of the present study  $\alpha$  was measured to be 45°, and K was taken to be 0.2, hence the following simplified equations were derived from eqns. (A26, A36 and A47). It is to be noted that in this case the constants  $a_3$ , and  $a_8$  became zero.

$$\bar{u}/W_0 = B_1(\bar{e}_0 - \bar{e}_{180})/(2a_1a_5\cos\alpha W_0) \quad (A49)$$

$$\bar{v}/W_0 = B_1(\bar{e}_{90} - \bar{e}_{270})/(2a_1a_5\cos\alpha W_0) \quad (A50)$$

$$\begin{aligned} \bar{w}/W_0 &= B_1(\bar{e}_0 + \bar{e}_{180})/(2a_1a_2\cos\alpha W_0) \\ &- 1/a_2[1 + a_6(\bar{u}^2 + \bar{u}'^2)/W_0^2 + a_8(\bar{v}^2 + \bar{v}'^2)/W_0^2] \quad (A51) \end{aligned}$$

#### EVALUATION OF TURBULENCE INTENSITIES

The turbulence terms are each found from the sum of two readings from an inclined hot wire (180° apart). Again taking  $\alpha = 45^\circ$ , and  $K = 0.2$ , eqns. (A26), (A37), and (A48) yield:

$$\begin{aligned} \overline{w'^2}/W_0^2 &= \left(1/a_2^2\right)[B_1^2(\bar{e}_0'^2 + \bar{e}_{180}'^2)/(2a_1^2\cos^2\alpha W_0^2) \\ &- a_5^2(\bar{u}'^2/W_0^2) \\ &- 4a_2a_8(\bar{v}/W_0)(\bar{v}'/W_0) \\ &- 4a_2a_6(\bar{u}/W_0)(\bar{u}'/W_0)] \quad (A56) \end{aligned}$$

$$\begin{aligned}
\overline{v'^2}/W_0^2 &= \left(1/a_s^2\right) \left[ B_1^2 (\overline{e_{10}^2} + \overline{e_{270}^2}) / (2a_1^2 \cos^2 \alpha W_0^2) \right. \\
&\quad - a_2^2 (\overline{w'^2}/W_0^2) \\
&\quad - 4a_2 a_s (\overline{u}/W_0) (\overline{u'w'}/W_0^2) \\
&\quad \left. - 4a_2 a_s (\overline{v}/W_0) (\overline{v'w'}/W_0^2) \right] \quad (A57)
\end{aligned}$$

and

$$\begin{aligned}
\overline{u'^2}/W_0^2 &= \left(1/a_s^2\right) \left[ B_1^2 (\overline{e_{45}^2} + \overline{e_{225}^2}) / (a_1^2 \cos^2 \alpha W_0^2) \right. \\
&\quad - 2a_2^2 (\overline{w'^2}/W_0^2) - a_s^2 (\overline{v'^2}/W_0^2) \\
&\quad - 2a_s^2 (\overline{u'v'}/W_0^2) \\
&\quad - (\overline{v'w'}/W_0^2) \{ (\overline{v}/W_0) (4a_2 a_s + 4a_2 a_s) \\
&\quad \quad + (\overline{u}/W_0) (4a_2 a_s - 4a_2 a_s) \} \\
&\quad - (\overline{u'w'}/W_0^2) \{ (\overline{v}/W_0) (4a_2 a_s - 4a_2 a_s) \\
&\quad \quad + (\overline{u}/W_0) (4a_2 a_s + 4a_2 a_s) \} \left. \right] \quad (A58)
\end{aligned}$$

The above are, of course, the normal Reynolds stress components, therefore the corresponding turbulence intensities will be:

$$\begin{aligned}
& \left[ \sqrt{\overline{w'^2}/W_0^2} / (\overline{w}/W_0) \right] \times 100.0 \\
& \left[ \sqrt{\overline{v'^2}/W_0^2} / (\overline{v}/W_0) \right] \times 100.0 \quad (A59)
\end{aligned}$$

and

$$\left[ \sqrt{\overline{u'^2}/W_0^2} / (\overline{u}/W_0) \right] \times 100.0$$

### EVALUATION OF REYNOLDS SHEAR STRESSES

The Reynolds shear stress terms are found by difference between two readings from a single inclined hot wire, 180° apart. The same values are taken again for  $\alpha$  and K.

$$\begin{aligned}\overline{w'v'}/W_0^2 &= \left(1/a_2a_3\right)\left[B_1^2(\overline{e_{90}^2} - \overline{e_{270}^2})/(4a_1^2\cos^2\alpha W_0^2)\right. \\ &\quad - 2a_3a_6(\overline{v}/W_0)(\overline{v'^2}/W_0^2) \\ &\quad \left.- 2a_3a_8(\overline{u}/W_0)(\overline{u'v'}/W_0^2)\right] \quad (A60)\end{aligned}$$

$$\begin{aligned}\overline{w'u'}/W_0^2 &= \left(1/a_2a_3\right)\left[B_1^2(\overline{e_0^2} - \overline{e_{180}^2})/(4a_1^2\cos^2\alpha W_0^2)\right. \\ &\quad - 2a_3a_6(\overline{u}/W_0)(\overline{u'^2}/W_0^2) \\ &\quad \left.- 2a_3a_8(\overline{v}/W_0)(\overline{u'v'}/W_0^2)\right] \quad (A61)\end{aligned}$$

and

$$\begin{aligned}\overline{u'v'}/W_0^2 &= [a_3^2 + 2\sqrt{2}a_3a_6\overline{v}/W_0]^{-1}\left[B_1^2(\overline{e_{45}^2} - \overline{e_{135}^2})/(2a_1^2\cos^2\alpha W_0^2)\right. \\ &\quad - (\overline{u'w'}/W_0^2)(a_2a_3\sqrt{2} - 2a_2a_8\overline{v}/W_0 + 2a_2a_6\overline{v}/W_0) \\ &\quad - (\overline{v'w'}/W_0^2)(2a_2a_6\overline{u}/W_0 - 2a_2a_8\overline{u}/W_0) \\ &\quad - (\overline{v'^2}/W_0^2)(a_3a_6\sqrt{2}\overline{u}/W_0 - a_3a_8\sqrt{2}\overline{u}/W_0) \\ &\quad \left.- (\overline{u'^2}/W_0^2)(a_3a_8\sqrt{2}\overline{u}/W_0 + a_3a_6\sqrt{2}\overline{u}/W_0)\right] \quad (A62)\end{aligned}$$

It is to be mentioned that the above equations are similar to the equations obtained by Phillips (9) who, in his study of turbulent trailing vortices, included the effects of blockage and pitch as well as a correction for yaw. In the present case the dominant flow was taken to be in the tangential direction and only the yaw factor was included, hence, yielding different constant coefficients for the parameters under investigation, than the ones obtained in Ref. (110).

BIBLIOGRAPHY

1. Champagne, F.H., Sleicher, C.A., and Wehrmann, O.H. "Turbulence Measurements with Inclined Hot-Wires," J. Fluid Mech., Vol. 28, part 1, (1967), 153-175.
2. *ibid*, part 2.
3. Davies, P.A.O.L., and Davis, M.R., University of Southampton, I.S.A.V. 155, (1966).
4. Webster, C.A.G. "Note on Sensitivity to Yaw of a Hot-wire Anemometer," J. Fluid Mechs., Vol. 13, (1962), 307-312.
5. Kjellstrom, B., and Larsson, A.E., Aktiebolaget Atomenergi, AE-RTL-958, (1967).
6. Hoole, B., and Calvert, J.R. "The Use of a Hot-Wire Anemometer in Turbulent Flow," J. Royal Aeronaut. Soc., Vol. 71, No. 679, (1967), 511-513.
7. Eyre, D., U.K.A.E.A. Report TRG 1521(W), (1967).
8. Heskestad, Gunnar, "Two Turbulent Shear Flows," Ph.D. Thesis, Department of Mechanics, John Hopkins University, (1963).
9. Phillips, W.R., "Turbulence Prediction and Measurement in a Turbulent Trailing Vortex," M.Eng. Thesis, Dept. of Mech. Eng. Rep. No. 74-5, McGill University, (June 1974).

APPENDIX II

TABULATED EXPERIMENTAL DATA

# NOMENCLATURE

AC1	R.M.S. voltage at			$\theta = 0^\circ$
AC2	"	"	"	$\theta = 45^\circ$
AC3	"	"	"	$\theta = 90^\circ$
AC4	"	"	"	$\theta = 135^\circ$
AC5	"	"	"	$\theta = 180^\circ$
AC6	"	"	"	$\theta = 225^\circ$
AC7	"	"	"	$\theta = 270^\circ$
AC8	"	"	"	$\theta = 315^\circ$

DC1	Mean voltage at			$\theta = 0^\circ$
DC2	"	"	"	$\theta = 45^\circ$
DC3	"	"	"	$\theta = 90^\circ$
DC4	"	"	"	$\theta = 135^\circ$
DC5	"	"	"	$\theta = 180^\circ$
DC6	"	"	"	$\theta = 225^\circ$
DC7	"	"	"	$\theta = 270^\circ$
DC8	"	"	"	$\theta = 315^\circ$

## LIST OF TABLES

<u>Table</u>		<u>Page</u>
I	Experimental R.M.S. and Mean Voltages Obtained for Station 1, at Inlet Velocity of 1.6 m/s (2.83 m <sup>3</sup> /s)	A-24
II	Experimental R.M.S. and Mean Voltages Obtained for Station 2, at Inlet Velocity of 1.6 m/s (2.83 m <sup>3</sup> /s)	A-25
III	Experimental R.M.S. and Mean Voltages Obtained for Station 3, at Inlet Velocity of 1.6 m/s (2.83 m <sup>3</sup> /s)	A-26
IV	Experimental R.M.S. and Mean Voltages Obtained for Station 4, at Inlet Velocity of 1.6 m/s (2.83 m <sup>3</sup> /s)	A-27
V	Experimental R.M.S. and Mean Voltages Obtained for Station 5, at Inlet Velocity of 1.6 m/s (2.83 m <sup>3</sup> /s)	A-28
VI	Experimental R.M.S. and Mean Voltages Obtained for Station 6, at Inlet Velocity of 1.6 m/s (2.83 m <sup>3</sup> /s)	A-29
VII	Experimental R.M.S. and Mean Voltages Obtained for Station 7, at Inlet Velocity of 1.6 m/s (2.83 m <sup>3</sup> /s)	A-30
VIII	Experimental R.M.S. and Mean Voltages Obtained for Station 8, at Inlet Velocity of 1.6 m/s (2.83 m <sup>3</sup> /s)	A-31
IX	Experimental R.M.S. and Mean Voltages Obtained for Station 9, at Inlet Velocity of 1.6 m/s (2.83 m <sup>3</sup> /s)	A-32
X	Experimental R.M.S. and Mean Voltages Obtained for Station 1, at Inlet Velocity of 3.2 m/s (5.66 m <sup>3</sup> /s)	A-33
XI	Experimental R.M.S. and Mean Voltages Obtained for Station 2, at Inlet Velocity of 3.2 m/s (5.66 m <sup>3</sup> /s)	A-34
XII	Experimental R.M.S. and Mean Voltages Obtained for Station 3, at Inlet Velocity of 3.2 m/s (5.66 m <sup>3</sup> /s)	A-35
XIII	Experimental R.M.S. and Mean Voltages Obtained for Station 4, at Inlet Velocity of 3.2 m/s (5.66 m <sup>3</sup> /s)	A-36
XIV	Experimental R.M.S. and Mean Voltages Obtained for Station 5, at Inlet Velocity of 3.2 m/s (5.66 m <sup>3</sup> /s)	A-37
XV	Experimental R.M.S. and Mean Voltages Obtained for Station 6, at Inlet Velocity of 3.2 m/s (5.66 m <sup>3</sup> /s)	A-38

<u>Table</u>	<u>Page</u>
XVI Experimental R.M.S. and Mean Voltages Obtained for Station 7, at Inlet Velocity of 3.2 m/s (5.66 m <sup>3</sup> /s)	A-39
XVII Experimental R.M.S. and Mean Voltages Obtained for Station 8, at Inlet Velocity of 3.2 m/s (5.66 m <sup>3</sup> /s)	A-40
XVIII Experimental R.M.S. and Mean Voltages Obtained for Station 9, at Inlet Velocity of 3.2 m/s (5.66 m <sup>3</sup> /s)	A-41
XIX Experimental R.M.S. and Mean Voltages Obtained for Station 7, at Inlet Velocity of 2.4 m/s (4.25 m <sup>3</sup> /s)	A-42

TABLE - I

STATION NUMBER - 1

FLOW RATE = 2.830 (CU-M/MIN) INLET PRESSURE = 451.3 (N/SU-M.)  
 INLET AIR TEMPERATURE = 20.000 (DEG-C) OUTLET PRESSURE = 102.9 (N/SU-M.)

DISTANCE FROM THE WALL TO THE CENTER (CM)	AC1	AC2	AC3	AC4	AC5	AC6	AC7	AC8
(CM)	(VOLTS)	(VOLTS)	(VOLTS)	(VOLTS)	(VOLTS)	(VOLTS)	(VOLTS)	(VOLTS)
59.09	9.41	9.20	7.15	8.10	9.41	10.91	7.12	9.20
50.70	8.70	8.50	5.00	6.50	8.30	10.12	4.00	8.10
53.98	6.90	6.70	5.00	5.00	6.40	8.50	2.10	6.90
48.90	5.90	5.80	3.30	4.00	3.70	4.00	0.80	3.00
43.82	5.13	5.00	2.90	3.15	3.10	3.60	0.59	3.00
38.74	5.10	5.10	3.00	5.30	3.10	3.30	0.59	3.00
31.12	3.40	3.00	5.10	3.00	3.50	4.10	0.79	4.10
23.50	5.70	6.90	0.50	7.70	5.90	7.50	1.25	7.50

DISTANCE FROM THE WALL TO THE CENTER (CM)	DC1	DC2	DC3	DC4	DC5	DC6	DC7	DC8
(CM)	(VOLTS)	(VOLTS)	(VOLTS)	(VOLTS)	(VOLTS)	(VOLTS)	(VOLTS)	(VOLTS)
59.09	0.105	0.094	0.057	0.069	0.103	0.101	0.022	0.063
50.70	0.094	0.084	0.052	0.072	0.099	0.089	0.017	0.067
53.98	0.092	0.075	0.050	0.072	0.092	0.078	0.014	0.072
48.90	0.095	0.070	0.052	0.080	0.099	0.078	0.015	0.082
43.82	0.108	0.084	0.050	0.080	0.109	0.080	0.013	0.089
38.74	0.114	0.095	0.054	0.094	0.121	0.094	0.014	0.097
31.12	0.143	0.112	0.074	0.110	0.141	0.120	0.015	0.110
23.50	0.101	0.142	0.094	0.143	0.185	0.157	0.015	0.155

TABLE - 11

STATION NUMBER - 2

FLOW RATE = 2.330 (CU-M/MIN) INLET PRESSURE = 443.4 (N/50-M.M.)  
 INLET AIR TEMPERATURE = 19.000 (DEG-C) OUTLET PRESSURE = 102.9 (N/50-M.M.)

DISTANCE FROM THE WALL TO THE CENTER (CM)	AC1	AC2	AC3	AC4	AC5	AC6	AC7	AC8
(CM)	(MILLIVOLTS)	(MILLIVOLTS)	(MILLIVOLTS)	(MILLIVOLTS)	(MILLIVOLTS)	(MILLIVOLTS)	(MILLIVOLTS)	(MILLIVOLTS)
55.26	9.30	9.10	9.20	9.10	9.30	9.30	5.90	11.40
53.34	8.40	7.90	8.00	8.70	8.00	9.90	2.40	9.40
49.20	4.90	5.00	4.30	4.70	4.80	5.40	1.14	4.70
43.13	3.10	3.10	2.70	3.30	3.00	3.60	0.62	3.90
38.10	3.00	3.00	2.70	3.10	3.10	3.30	0.62	3.30
30.48	3.50	4.00	3.50	4.00	3.60	4.40	0.76	4.50
22.80	2.70	7.80	7.70	8.40	6.80	8.10	1.40	7.90
15.88	11.40	13.60	12.70	14.20	10.80	13.00	3.20	13.00

DISTANCE FROM THE WALL TO THE CENTER (CM)	DC1	DC2	DC3	DC4	DC5	DC6	DC7	DC8
(CM)	(VOLTS)	(VOLTS)	(VOLTS)	(VOLTS)	(VOLTS)	(VOLTS)	(VOLTS)	(VOLTS)
55.26	0.113	0.090	0.059	0.060	0.109	0.094	0.020	0.076
53.34	0.104	0.083	0.054	0.079	0.106	0.086	0.016	0.081
48.26	0.100	0.082	0.050	0.066	0.108	0.085	0.015	0.090
43.18	0.117	0.091	0.061	0.072	0.117	0.096	0.014	0.093
38.10	0.127	0.100	0.060	0.097	0.120	0.100	0.015	0.102
30.48	0.131	0.119	0.077	0.115	0.151	0.129	0.015	0.123
22.80	0.190	0.148	0.097	0.140	0.195	0.168	0.016	0.161
15.88	0.260	0.195	0.123	0.188	0.250	0.220	0.016	0.215

TABLE - III

STATION NUMBER - 3

FLOW RATE = 2.830 (CU-M/MIN) INLET PRESSURE = 459.3 (N/50-M<sup>2</sup>)  
 INLET AIR TEMPERATURE = 11.500 (DEG-C) OUTLET PRESSURE = 102.4 (N/50-M<sup>2</sup>)

DISTANCE FROM THE WALL TO THE CENTER (CM)	AC1	AC2	AC3	AC4	AC5	AC6	AC7	AC8
(CM)	(MILLIVOLTS)	(MILLIVOLTS)	(MILLIVOLTS)	(MILLIVOLTS)	(MILLIVOLTS)	(MILLIVOLTS)	(MILLIVOLTS)	(MILLIVOLTS)
50.20	5.30	7.60	5.10	5.90	6.30	7.50	1.60	5.50
53.34	4.40	4.70	4.20	4.50	4.20	5.30	0.80	4.00
43.25	5.10	3.20	4.00	3.00	2.90	3.50	0.30	3.20
43.13	2.50	2.90	2.50	2.90	2.70	3.40	0.30	3.10
33.10	3.20	3.40	3.40	4.00	3.20	4.10	0.57	4.10
30.48	5.40	5.40	6.00	6.90	5.60	6.20	1.27	6.40
22.80	4.50	12.00	11.70	12.00	9.80	12.70	2.20	11.40
15.88	19.00	25.00	25.50	24.70	22.10	26.60	6.50	25.00

DISTANCE FROM THE WALL TO THE CENTER (CM)	DC1	DC2	DC3	DC4	DC5	DC6	DC7	DC8
(CM)	(VOLTS)	(VOLTS)	(VOLTS)	(VOLTS)	(VOLTS)	(VOLTS)	(VOLTS)	(VOLTS)
50.20	0.099	0.080	0.050	0.074	0.099	0.080	0.014	0.077
53.34	0.103	0.079	0.053	0.079	0.103	0.086	0.014	0.082
43.25	0.111	0.080	0.057	0.080	0.111	0.091	0.013	0.091
43.13	0.121	0.095	0.062	0.094	0.122	0.099	0.014	0.098
33.10	0.130	0.107	0.070	0.107	0.137	0.114	0.014	0.113
30.48	0.171	0.131	0.087	0.132	0.172	0.147	0.015	0.146
22.80	0.250	0.179	0.113	0.179	0.238	0.200	0.016	0.202
15.88	0.304	0.275	0.173	0.284	0.370	0.322	0.020	0.322

TABLE - IV

STATION NUMBER - 4

FLOW RATE = 2.830 (CU-M/MIN) INLET PRESSURE = 431.3 (N/SU-M.)  
 INLET AIR TEMPERATURE = 19.000 (DEG-C) OUTLET PRESSURE = 103.5 (N/SU-M.)

DISTANCE FROM THE WALL TO THE CENTER (CM)	AC1	AC2	AC3	AC4 (MILLIVOLTS)	AC5	AC6	AC7	AC8
53.09	6.10	6.50	5.20	5.50	6.10	6.40	1.90	5.80
50.17	4.00	5.00	5.50	4.10	4.10	4.50	1.11	4.20
45.09	2.90	3.00	2.70	2.97	3.00	3.00	0.74	3.50
40.00	3.80	4.00	3.80	4.40	3.60	4.70	0.84	4.00
34.93	5.10	5.80	5.50	6.50	5.00	6.50	1.11	5.70
27.51	8.00	9.70	8.90	9.50	8.20	9.30	1.90	9.20
19.59	15.20	19.00	17.70	18.70	15.20	19.30	4.50	17.70
12.70	37.00	39.50	43.20	45.50	40.30	56.70	23.40	45.50

DISTANCE FROM THE WALL TO THE CENTER (CM)	DC1	DC2	DC3	DC4 (VOLTS)	DC5	DC6	DC7	DC8
53.09	0.112	0.093	0.060	0.080	0.112	0.096	0.017	0.086
50.17	0.117	0.093	0.060	0.088	0.116	0.098	0.015	0.090
45.09	0.124	0.099	0.064	0.095	0.124	0.102	0.014	0.099
40.00	0.137	0.107	0.070	0.105	0.136	0.114	0.015	0.111
34.93	0.157	0.123	0.079	0.120	0.157	0.132	0.015	0.131
27.51	0.205	0.150	0.101	0.155	0.205	0.178	0.015	0.171
19.59	0.502	0.225	0.142	0.231	0.505	0.264	0.019	0.260
12.70	0.615	0.477	0.272	0.451	0.610	0.558	0.046	0.514

TABLE - V

STATION NUMBER - 5

FLUX RATE = 2.000 (CU-M/MIN) INLET PRESSURE = 443.4 (N/S-M-M.)  
 INLET AIR TEMPERATURE = 19.000 (DEG-C) OUTLET PRESSURE = 93.0 (N/S-M-M.)

DISTANCE FROM THE WALL TO THE CENTER (CM)	AC1	AC2	AC3	AC4	AC5	ACC	AC7	AC8
(CM)	(MILLIVOLTS)	(MILLIVOLTS)	(MILLIVOLTS)	(MILLIVOLTS)	(MILLIVOLTS)	(MILLIVOLTS)	(MILLIVOLTS)	(MILLIVOLTS)
42.30	6.00	6.00	4.90	6.00	5.50	6.30	1.70	5.70
39.37	4.50	4.60	4.10	4.20	4.50	5.50	1.20	5.00
34.29	3.60	3.60	3.20	3.70	3.50	4.30	0.74	3.10
29.21	5.00	5.50	5.50	5.90	5.00	6.00	1.10	5.50
24.13	7.10	8.40	8.00	8.90	7.10	8.70	1.40	7.90
19.51	11.40	14.20	13.60	14.50	11.40	14.90	3.70	13.00
8.89	26.90	31.40	29.00	33.00	29.00	28.20	13.90	33.40
1.91	142.30	156.50	118.90	155.00	121.30	136.00	113.80	110.70

DISTANCE FROM THE WALL TO THE CENTER (CM)	UC1	UC2	UC3	UC4	UC5	UC6	UC7	UC8
(CM)	(VOLTS)	(VOLTS)	(VOLTS)	(VOLTS)	(VOLTS)	(VOLTS)	(VOLTS)	(VOLTS)
42.30	0.112	0.090	0.050	0.061	0.112	0.095	0.015	0.085
39.37	0.119	0.094	0.059	0.090	0.118	0.101	0.014	0.095
34.29	0.132	0.105	0.064	0.099	0.131	0.111	0.014	0.108
29.21	0.151	0.116	0.073	0.115	0.151	0.128	0.014	0.127
24.13	0.180	0.134	0.080	0.130	0.181	0.152	0.015	0.158
19.51	0.251	0.187	0.113	0.188	0.252	0.217	0.016	0.222
8.89	0.747	0.351	0.125	0.317	0.445	0.415	0.031	0.397
1.91	0.535	0.645	0.585	0.650	0.660	0.521	0.368	0.370

TABLE - VI

STATION NUMBER = 6

FLOW RATE = 2.830 (CU-M/MIN)  
 INLET AIR TEMPERATURE = 19.000 (DEG-C)

INLET PRESSURE = 435.5 (N/SU-M.)  
 OUTLET PRESSURE = 95.0 (N/SU-M.)

DISTANCE FROM THE WALL (CM)	DISTANCE FROM THE CENTER (CM)	AC1	AC2	AC3	AC4	AC5	AC6	AC7	AC8
(MILLIVOLTS)									
50.26	4.70	7.90	9.10	7.90	8.50	7.80	9.30	2.80	7.70
53.34	7.62	6.90	8.10	7.00	7.10	7.30	7.90	1.58	6.40
48.20	12.70	6.00	7.30	6.80	6.70	5.80	8.50	1.25	6.80
43.18	17.78	8.40	12.70	9.20	10.10	8.50	12.70	3.10	9.50
38.10	22.80	11.70	14.90	13.30	14.20	12.00	16.13	4.00	13.20
30.48	30.48	22.80	25.90	26.90	28.30	24.00	26.90	7.20	29.10
22.80	38.10	230.90	272.00	208.70	256.20	234.60	281.40	186.50	189.70
15.88	45.09	139.10	230.80	148.20	139.10	151.30	199.20	117.00	129.70
DISTANCE FROM THE WALL (CM)	DISTANCE FROM THE CENTER (CM)	DC1	DC2	DC3	DC4	DC5	DC6	DC7	DC8
(VOLTS)									
50.26	4.70	0.137	0.111	0.089	0.102	0.136	0.117	0.017	0.106
53.34	7.62	0.148	0.117	0.074	0.112	0.148	0.129	0.016	0.119
48.20	12.70	0.164	0.127	0.082	0.125	0.164	0.140	0.016	0.140
43.18	17.78	0.204	0.155	0.103	0.159	0.205	0.174	0.017	0.178
38.10	22.80	0.260	0.191	0.127	0.201	0.262	0.220	0.018	0.230
30.48	30.48	0.415	0.314	0.191	0.315	0.417	0.370	0.031	0.363
22.80	38.10	0.875	1.070	1.030	1.100	1.180	0.909	0.595	0.835
15.88	45.09	1.130	0.956	0.457	1.070	1.120	0.780	0.465	0.855

TABLE - VII

STATION NUMBER, - 7

FLOW RATE = 2.830, (CU-M/MIN) INLET PRESSURE = 435.5 (N/50-M.)  
 INLET AIR TEMPERATURE = 19.000 (DEG-C) OUTLET PRESSURE = 102.9 (N/50-M.)

DISTANCE FROM THE WALL TO THE CENTER (CM)	AC1	AC2	AC3	AC4 (MILLIVOLTS)	AC5	AC6	AL7	AC8
27.67	10.40	12.36	10.11	12.02	10.73	12.30	0.00	11.07
24.77	9.80	11.40	9.80	11.07	9.50	11.34	4.00	9.00
22.23	9.30	10.40	9.80	10.75	9.30	12.28	1.93	9.80
19.69	10.12	12.33	11.40	11.40	10.40	12.97	2.53	10.44
17.15	12.98	15.18	14.23	14.55	12.33	12.44	3.50	12.97
14.61	15.50	18.08	17.40	18.03	14.80	20.58	5.80	12.13
12.07	18.02	24.03	21.20	23.10	18.90	26.80	0.90	21.20
9.53	24.67	39.04	29.73	31.30	28.88	30.04	8.30	31.30
5.72	45.38	49.00	33.30	52.30	49.20	48.40	28.80	34.30

DISTANCE FROM THE WALL TO THE CENTER (CM)	UC1	UC2	UC3	UC4 (VOLTS)	UC5	UC6	UC7	UC8
27.67	0.171	0.137	0.086	0.126	0.167	0.147	0.021	0.130
24.77	0.183	0.147	0.092	0.135	0.185	0.161	0.017	0.148
22.23	0.200	0.154	0.101	0.150	0.200	0.173	0.016	0.155
19.69	0.220	0.167	0.108	0.166	0.219	0.188	0.016	0.187
17.15	0.247	0.183	0.120	0.190	0.248	0.209	0.016	0.216
14.61	0.284	0.204	0.140	0.225	0.287	0.240	0.019	0.254
12.07	0.339	0.251	0.165	0.270	0.341	0.288	0.024	0.305
9.53	0.431	0.330	0.200	0.332	0.431	0.384	0.032	0.377
5.72	0.718	0.558	0.330	0.549	0.715	0.635	0.060	0.617

TABLE - VIII

STATION NUMBER - 8

FLOW RATE = 2.830 (CU-M/MIN)  
 INLET AIR TEMPERATURE = 19.500 (DEG-C)

INLET PRESSURE = 451.3 (N/SQ-M.)  
 OUTLET PRESSURE = 102.9 (N/SQ-M.)

DISTANCE FROM THE WALL (CM)	DISTANCE FROM THE CENTER (CM)		AC1	AC2	AC3	AC4	AC5	AC6	AC7	AC8
			( MILLIVOLTS )							
20.07	4.70	1	14.90	17.70	16.40	17.10	15.20	18.00	6.80	16.10
17.15	7.62	1	14.00	18.00	15.80	16.80	15.20	17.40	4.00	15.80
14.61	10.16	1	17.10	20.20	17.70	18.00	17.40	19.60	3.90	17.70
12.07	12.70	1	20.00	26.30	23.30	25.30	22.80	25.90	7.30	26.90
9.53	15.24	1	26.30	35.00	34.50	35.80	29.70	35.20	12.00	33.00
6.99	17.73	1	39.80	45.50	47.50	49.40	42.80	44.50	18.30	48.10
4.45	20.32	1	62.50	62.50	67.90	75.10	53.70	61.30	57.00	67.50
1.91	22.85	1	164.40	126.50	224.50	227.70	170.80	199.20	195.00	205.60
0.01	24.77	1	159.10	243.50	177.10	148.00	155.00	199.20	126.50	158.00

DISTANCE FROM THE WALL (CM)	DISTANCE FROM THE CENTER (CM)		DC1	DC2	DC3	DC4	DC5	DC6	DC7	DC8
			( VOLTS )							
20.07	4.70	1	0.239	0.188	0.118	0.174	0.235	0.212	0.021	0.192
17.15	7.62	1	0.272	0.223	0.135	0.199	0.272	0.244	0.019	0.225
14.61	10.16	1	0.312	0.240	0.154	0.234	0.310	0.274	0.020	0.259
12.07	12.70	1	0.369	0.283	0.162	0.285	0.370	0.328	0.028	0.321
9.53	15.24	1	0.400	0.350	0.219	0.362	0.461	0.401	0.037	0.405
6.99	17.73	1	0.622	0.473	0.290	0.477	0.622	0.550	0.049	0.539
4.45	20.32	1	0.935	0.725	0.538	0.688	0.935	0.852	0.121	0.791
1.91	22.85	1	1.240	0.990	0.810	0.970	0.980	1.280	0.840	1.010
0.01	24.77	1	1.360	1.090	0.575	1.400	1.370	0.879	0.550	1.100

TABLE - IX

STATION NUMBER = 9

FLOW RATE = 2.000 (CU-M/MIN) INLET PRESSURE = 443.4 (N/50-0.0)  
 INLET AIR TEMPERATURE = 19.500 (DEG-C) OUTLET PRESSURE = 102.9 (N/50-0.0)

DISTANCE FROM THE WALL TO THE CENTER (CM)	AC1	AC2	AC3	AC4	ACS	ACC	AC7	ACS
13.08	20.40	25.00	23.70	24.00	20.90	23.70	0.90	25.00
11.43	22.50	24.70	23.30	23.70	22.10	20.20	0.20	23.40
10.16	22.00	25.30	23.70	24.40	22.80	25.30	0.70	22.30
8.89	24.70	27.50	27.30	25.30	20.90	27.80	0.60	20.90
7.02	30.30	34.00	30.90	30.70	32.10	34.30	13.30	33.70
5.35	40.30	49.00	50.70	51.70	53.20	52.70	22.10	44.30
3.08	55.40	62.40	60.20	69.20	57.90	61.40	35.80	50.30
3.81	60.70	74.50	62.30	63.00	72.00	72.50	71.50	70.30
2.34	80.70	94.50	129.70	107.30	91.70	82.20	120.50	92.90
1.27	200.30	272.00	308.00	384.00	304.00	375.00	310.00	347.00

DISTANCE FROM THE WALL TO THE CENTER (CM)	DC1	DC2	DC3	DC4	DC5	DC6	DC7	DC8
13.08	0.342	0.270	0.163	0.251	0.339	0.312	0.025	0.272
11.43	0.385	0.307	0.180	0.232	0.381	0.345	0.025	0.310
10.16	0.407	0.327	0.202	0.310	0.404	0.370	0.022	0.333
8.89	0.437	0.304	0.222	0.340	0.450	0.407	0.034	0.383
7.02	0.529	0.417	0.262	0.400	0.523	0.425	0.030	0.400
5.35	0.627	0.493	0.314	0.480	0.621	0.532	0.049	0.529
3.08	0.770	0.605	0.383	0.620	0.778	0.623	0.074	0.629
3.81	1.000	0.825	0.490	0.824	1.000	0.975	0.154	0.872
2.34	1.430	1.220	0.510	0.900	1.380	1.410	0.319	1.000
1.27	1.440	1.370	1.010	1.100	1.230	1.430	1.100	1.000

TABLE 7A

STATION NUMBER - 1

FLOW RATE = 3.000 (CU-M/MIN) INLET PRESSURE = 1234.7 (N/CM<sup>2</sup>)  
 INLET AIR TEMPERATURE = 21.000 (DEG-C) OUTLET PRESSURE = 253.4 (N/CM<sup>2</sup>)

DISTANCE FROM THE WALL TO THE CENTER (CM)	AC1	AC2	AC3	AC4	AC5	AC6	AC7	AC8
59.69	13.80	13.90	9.60	11.10	12.30	14.90	7.20	13.30
50.90	12.00	12.30	7.90	10.10	11.40	14.90	3.30	12.00
53.98	8.90	9.50	7.10	8.90	9.20	10.80	1.50	9.30
40.90	5.40	5.80	5.10	6.20	5.40	7.50	1.40	7.10
43.82	4.90	5.00	4.30	5.10	5.00	5.90	1.00	5.90
33.74	5.00	5.20	4.80	5.80	5.00	6.00	0.92	5.10
31.12	6.00	6.70	5.70	7.00	6.00	7.20	1.30	6.00
23.50	9.80	11.10	11.10	12.70	10.10	13.30	2.70	11.00

DISTANCE FROM THE WALL TO THE CENTER (CM)	UC1	UC2	UC3	UC4	UC5	UC6	UC7	UC8
59.69	0.160	0.130	0.050	0.100	0.150	0.130	0.020	0.030
50.90	0.140	0.110	0.070	0.100	0.140	0.110	0.010	0.010
53.98	0.137	0.105	0.070	0.100	0.135	0.100	0.014	0.010
40.90	0.148	0.112	0.074	0.120	0.150	0.105	0.015	0.017
43.82	0.160	0.120	0.081	0.134	0.167	0.121	0.015	0.014
33.74	0.185	0.140	0.090	0.140	0.185	0.142	0.015	0.017
31.12	0.217	0.166	0.107	0.171	0.219	0.174	0.010	0.017
23.50	0.270	0.208	0.130	0.216	0.281	0.221	0.019	0.020

TABLE - XI

STATION NUMBER - 2

FLOW RATE = 5.660 (CU-M/MIN)  
 INLET AIR TEMPERATURE = 19.500 (DEG-C)

INLET PRESSURE = 1282.7 (N/SQ-M.)  
 OUTLET PRESSURE = 269.2 (N/SQ-M.)

DISTANCE FROM THE WALL (CM)	DISTANCE FROM THE CENTER (CM)	AC1	AC2	AC3	AC4	AC5	AC6	AC7	AC8
(MILLIVOLTS)									
59.26	4.70	12.30	11.40	9.10	13.30	13.30	14.20	4.70	18.20
53.34	7.62	13.60	12.00	9.30	13.90	13.00	17.10	2.90	15.50
48.26	12.70	7.80	8.60	7.00	8.20	8.30	9.50	1.80	8.40
43.18	17.73	5.50	5.30	4.30	5.60	5.70	6.50	2.80	6.60
38.10	22.86	5.10	5.30	4.50	5.40	5.30	6.50	0.85	5.70
30.48	30.48	6.50	7.90	5.70	8.10	6.90	8.00	1.23	6.90
22.86	38.10	11.10	12.50	12.00	13.90	11.40	14.60	2.30	13.00
15.88	45.09	18.00	20.90	20.20	22.30	18.50	65.00	10.10	55.00

DISTANCE FROM THE WALL (CM)	DISTANCE FROM THE CENTER (CM)	DC1	DC2	DC3	DC4	DC5	DC6	DC7	DC8
(VOLTS)									
59.26	4.70	0.162	0.131	0.077	0.112	0.159	0.137	0.020	0.121
53.34	7.62	0.169	0.129	0.080	0.129	0.169	0.129	0.018	0.138
48.26	12.70	0.182	0.135	0.087	0.144	0.181	0.131	0.018	0.154
43.18	17.73	0.189	0.143	0.090	0.146	0.187	0.141	0.015	0.166
38.10	22.86	0.202	0.156	0.095	0.157	0.202	0.156	0.016	0.167
30.48	30.48	0.236	0.180	0.111	0.179	0.237	0.187	0.016	0.201
22.86	38.10	0.296	0.222	0.140	0.227	0.297	0.238	0.018	0.265
15.88	45.09	0.400	0.295	0.188	0.303	0.400	0.725	0.053	0.940

TABLE - XII

STATION NUMBER - 3

FLUX RATE = 5.000 (CU-M/MIN) INLET PRESSURE = 1282.7 (N/SU-M.)  
 INLET AIR TEMPERATURE = 21.000 (DEG-C) OUTLET PRESSURE = 277.1 (N/SU-M.)

DISTANCE FROM THE WALL TO THE CENTER (CM)	AC1	AC2	AC3	( MILLIVOLTS )			AC6	AC7	AC8
				AC4	AC5	AC6			
50.20	10.10	10.75	9.00	10.00	9.80	11.40		0.02	9.80
53.34	8.00	8.20	8.00	8.20	7.80	8.80		1.30	7.20
48.20	5.20	5.70	4.40	5.40	5.00	5.00		0.02	5.90
43.10	4.50	5.00	4.10	5.40	4.60	5.20		0.90	5.00
35.10	5.70	6.30	5.90	7.00	5.90	6.20		0.95	7.00
30.48	9.00	10.40	10.10	11.70	9.90	11.40		1.99	11.40
22.80	15.20	17.70	17.40	18.70	16.10	19.30		4.10	19.00
15.08	20.50	35.30	30.00	37.40	30.50	38.70		10.80	39.70

DISTANCE FROM THE WALL TO THE CENTER (CM)	DC1	DC2	DC3	( VOLTS )			DC6	DC7	DC8
				DC4	DC5	DC6			
50.20	0.109	0.135	0.079	0.121	0.165	0.136		0.019	0.129
53.34	0.175	0.138	0.079	0.120	0.172	0.141		0.017	0.141
48.20	0.189	0.146	0.085	0.141	0.180	0.150		0.017	0.149
43.10	0.202	0.159	0.097	0.152	0.200	0.164		0.017	0.161
35.10	0.220	0.174	0.100	0.165	0.218	0.182		0.017	0.177
30.48	0.271	0.210	0.132	0.201	0.269	0.226		0.018	0.229
22.80	0.366	0.280	0.175	0.269	0.363	0.309		0.022	0.317
15.08	0.570	0.427	0.259	0.409	0.501	0.484		0.040	0.505

TABLE - XIII

STATION NUMBER - 4

FLOW RATE = 3.660 (CU-M/MIN) INLET PRESSURE = 1251.1 (N/SU-M.)  
 INLET AIR TEMPERATURE = 21.000 (CEU-C) OUTLET PRESSURE = 253.4 (N/SU-M.)

DISTANCE FROM THE WALL (CM)	AC1	AC2	AC3	AC4	AC5	AC6	AC7	AC8
(CM)	( MILLIVOLTS )							
53.09	4.70	8.90	7.50	10.40	8.10	9.50	2.34	9.10
50.17	7.62	6.90	6.00	6.90	6.30	7.20	1.36	6.30
45.09	12.70	4.70	3.80	4.70	4.40	5.00	0.79	5.40
40.00	17.78	6.80	6.10	7.90	6.30	7.10	1.30	7.30
34.93	22.85	9.50	8.70	11.40	8.80	10.40	1.70	10.40
27.31	30.48	13.90	13.60	13.20	12.30	15.50	3.00	15.80
19.69	38.10	28.50	27.20	28.30	24.00	31.00	7.80	28.20
12.70	45.09	56.90	66.80	68.70	58.50	59.50	38.50	85.00

DISTANCE FROM THE WALL (CM)	DC1	DC2	DC3	DC4	DC5	DC6	DC7	DC8
(CM)	( VOLTS )							
53.09	4.70	0.133	0.079	0.116	0.162	0.138	0.017	0.123
50.17	7.62	0.141	0.084	0.128	0.172	0.144	0.016	0.135
45.09	12.70	0.150	0.089	0.139	0.167	0.156	0.015	0.149
40.00	17.78	0.165	0.099	0.155	0.210	0.175	0.016	0.170
34.93	22.85	0.186	0.115	0.176	0.239	0.198	0.016	0.197
27.31	30.48	0.242	0.150	0.230	0.312	0.261	0.019	0.298
19.69	38.10	0.350	0.215	0.341	0.462	0.395	0.031	0.418
12.70	45.09	0.717	0.433	0.847	0.913	0.812	0.069	0.810

TABLE - XIV

STATION NUMBER - 3

FLUX RATE = 5.000 (CU-M/MIN) INLET PRESSURE = 1266.4 (N/50-M.)  
 INLET AIR TEMPERATURE = 21.000 (DEG-C) OUTLET PRESSURE = 253.4 (N/50-M.)

DISTANCE FROM THE WALL TO THE CENTER (CM)	AC1	AC2	AC3	AC4 (MILLIVOLTS)	AC5	AC6	AC7	AC8
42.30	8.40	9.20	8.10	11.40	78.00	9.70	2.80	9.70
39.37	7.10	7.80	6.30	8.20	7.20	8.00	1.74	7.80
34.29	5.90	6.60	5.00	6.20	5.90	6.90	0.95	6.00
29.21	8.30	9.40	5.80	10.30	5.40	10.40	1.36	9.10
24.13	11.40	12.70	12.00	13.10	11.40	14.20	1.90	12.70
19.01	18.30	21.50	19.00	23.10	19.00	25.00	4.30	22.30
8.89	38.40	44.70	48.30	50.70	40.20	42.00	24.40	38.50
1.91	192.90	173.90	186.60	230.90	180.30	199.20	199.20	188.90

DISTANCE FROM THE WALL TO THE CENTER (CM)	UC1	UC2	UC3	UC4 (VOLTS)	UC5	UC6	UC7	UC8
42.30	0.175	0.141	0.061	0.122	0.172	0.149	0.017	0.132
39.37	0.180	0.149	0.085	0.130	0.184	0.158	0.016	0.144
34.29	0.200	0.156	0.093	0.148	0.202	0.171	0.015	0.171
29.21	0.232	0.177	0.105	0.171	0.231	0.192	0.015	0.199
24.13	0.277	0.204	0.124	0.201	0.274	0.224	0.017	0.244
19.01	0.388	0.281	0.184	0.279	0.382	0.321	0.025	0.351
8.89	0.099	0.505	0.251	0.447	0.679	0.620	0.048	0.628
1.91	1.000	1.030	1.010	1.020	1.120	1.130	0.875	0.820

TABLE - XV

STATION NUMBER - 0

FLUX RATE = 3.000 (CU-M/MIN) INLET PRESSURE = 1279.0 (N/30-M.)  
 INLET AIR TEMPERATURE = 19.500 (LEG-C) OUTLET PRESSURE = 253.4 (N/30-M.)

DISTANCE FROM THE WALL TO THE CENTER (CM)	AC1	AC2	AC3	AC4 (MILLIVOLTS)	AC5	AC6	AC7	AC8
59.26	11.10	12.70	10.70	12.97	12.00	13.30	3.70	12.02
53.34	10.12	10.44	9.70	11.38	9.40	12.02	2.59	10.44
48.26	9.40	9.80	9.20	10.70	9.40	12.02	1.93	9.80
43.18	12.90	15.18	14.20	15.01	13.84	18.03	2.91	14.20
38.10	17.71	21.82	20.80	22.77	10.66	25.93	4.80	20.84
30.46	36.30	42.50	35.50	48.20	39.00	44.40	16.10	36.10
22.80	275.12	237.20	303.30	340.00	256.10	255.30	281.40	265.80
15.38	202.40	356.00	259.31	243.30	237.20	303.60	173.90	205.90

DISTANCE FROM THE WALL TO THE CENTER (CM)	LC1	LC2	LC3	LC4 (VOLTS)	LC5	LC6	LC7	LC8
59.26	0.203	0.160	0.091	0.137	0.195	0.167	0.016	0.148
53.34	0.211	0.165	0.096	0.151	0.209	0.176	0.015	0.164
48.26	0.239	0.182	0.110	0.172	0.237	0.199	0.014	0.199
43.18	0.290	0.218	0.135	0.215	0.292	0.239	0.017	0.260
38.10	0.376	0.276	0.171	0.267	0.378	0.307	0.023	0.347
30.46	0.890	0.518	0.303	0.488	0.577	0.605	0.043	0.618
22.80	1.510	1.580	1.440	1.490	1.660	1.740	1.320	1.220
15.38	1.760	1.520	0.580	2.070	2.020	1.310	0.615	1.250

TABLE - XVI

STATION NUMBER - 7

FLOW RATE = 5.000 (CU-M/MIN) INLET PRESSURE = 1251.1 (N/30-M.)  
 INLET AIR TEMPERATURE = 19.000 (DEG-C) OUTLET PRESSURE = 243.0 (N/30-M.)

DISTANCE FROM THE WALL TO THE CENTER (CM)	AC1	AC2	AC3	(MILLIVOLTS)				AC6	AC7	AC8
				AC4	AC5	AC9	AC10			
27.07	15.20	18.00	15.20	19.00	15.00	17.10	17.10	17.70	20.30	
27.77	13.90	17.10	15.20	18.70	13.50	16.10	16.10	14.50	24.40	
22.23	13.30	15.10	14.20	15.00	14.20	15.20	15.20	11.80	21.80	
19.69	14.90	16.50	15.10	18.70	14.90	15.80	15.80	11.10	26.30	
17.15	17.40	20.40	20.00	24.00	19.00	20.00	20.00	12.70	31.30	
14.01	21.20	25.00	25.00	28.00	24.00	25.30	25.30	11.70	38.20	
12.07	25.20	30.40	31.70	35.70	27.20	30.40	30.40	14.90	48.60	
9.53	34.00	40.40	43.40	47.00	39.20	37.00	37.00	30.70	84.70	
5.72	54.50	66.10	74.00	87.50	74.50	62.80	62.80	78.10	145.50	

DISTANCE FROM THE WALL TO THE CENTER (CM)	UC1	UC2	UC3	(VOLTS)				UC6	UC7	UC8
				UC4	UC5	UC9	UC10			
27.07	0.245	0.209	0.120	0.120	0.225	0.225	0.225	0.040	0.136	
24.77	0.205	0.224	0.127	0.162	0.250	0.244	0.244	0.035	0.102	
22.23	0.280	0.236	0.135	0.175	0.271	0.263	0.263	0.029	0.191	
19.69	0.300	0.256	0.144	0.191	0.293	0.283	0.283	0.029	0.211	
17.15	0.353	0.289	0.160	0.225	0.338	0.321	0.321	0.027	0.259	
14.01	0.411	0.329	0.162	0.269	0.392	0.372	0.372	0.027	0.322	
12.07	0.497	0.395	0.217	0.327	0.480	0.453	0.453	0.033	0.435	
9.53	0.641	0.513	0.276	0.392	0.603	0.591	0.591	0.051	0.491	
5.72	1.050	0.841	0.449	0.551	0.993	0.988	0.988	0.191	0.706	

TABLE 7 AVII

STATION NUMBER - 8

FLOW RATE = 5.000 (CU-M/MIN) INLET PRESSURE = 1235.2 (N/SQ-M.)  
 INLET AIR TEMPERATURE = 19.500 (DEG-C) OUTLET PRESSURE = 237.5 (N/SQ-M.)

DISTANCE FROM THE WALL TO THE CENTER (CM)	AC1	AC2	AC3	( MILLIVOLTS )			AC6	AC7	AC8
				AC4	AC5	AC6			
20.07	21.20	24.00	23.40	25.00	21.50	23.10	25.30		39.90
17.15	19.60	23.10	22.50	21.80	21.20	22.10	21.50		35.80
14.01	22.10	24.40	24.00	25.30	23.70	24.00	18.00		42.00
12.07	28.80	33.80	34.50	38.40	31.70	33.20	20.20		57.50
9.53	30.30	42.80	40.00	50.90	41.70	41.70	31.30		80.90
8.99	51.50	58.20	04.00	60.20	57.50	53.50	53.80		117.00
4.45	78.50	79.90	89.50	110.70	94.60	77.50	95.40		170.80
1.91	192.90	145.50	240.70	337.00	205.00	185.70	196.10		215.00
0.01	221.40	358.00	334.00	300.00	262.50	334.00	237.20		253.00

DISTANCE FROM THE WALL TO THE CENTER (CM)	LC1	DC2	DC3	( VOLTS )			DC6	DC7	DC8
				DC4	DC5	DC6			
20.07	0.337	0.287	0.100	0.200	0.311	0.312	0.052		0.191
17.15	0.374	0.314	0.170	0.220	0.340	0.345	0.044		0.240
14.01	0.415	0.351	0.201	0.202	0.357	0.389	0.041		0.278
12.07	0.504	0.414	0.231	0.322	0.470	0.465	0.041		0.367
9.53	0.041	0.510	0.200	0.422	0.009	0.578	0.051		0.485
8.99	0.801	0.701	0.380	0.340	0.812	0.782	0.085		0.541
4.45	1.290	1.040	0.557	0.801	1.210	1.210	0.281		0.936
1.91	2.010	1.600	0.760	0.000	1.590	2.070	1.430		1.170
0.01	1.910	1.750	0.735	2.100	2.210	1.560	0.685		1.300

TABLE - XVIII

STATION NUMBER - 9

FLOW RATE = 5.660 (CU-M/MIN)  
 INLET AIR TEMPERATURE = 19.200 (DEG-C)

INLET PRESSURE = 1235.2 (N/SQ-M.)  
 OUTLET PRESSURE = 237.5 (N/SQ-M.)

DISTANCE FROM THE WALL (CM)	DISTANCE FROM THE CENTER (CM)	AC1	AC2	AC3	AC4	AC5	AC6	AC7	AC8
(MILLIVOLTS)									
13.08	4.70	27.50	32.10	32.80	31.50	28.80	34.90	9.60	35.70
11.43	6.35	28.50	33.60	32.90	32.90	28.70	36.10	9.50	33.20
10.16	7.62	29.40	33.50	33.50	34.10	28.80	38.30	11.10	34.50
8.89	8.89	34.50	37.80	38.50	41.30	34.50	40.20	12.70	39.90
7.62	10.16	45.20	52.30	57.30	56.20	47.50	59.80	20.60	55.40
6.35	11.43	59.30	69.80	81.00	81.70	61.00	80.80	38.20	75.60
5.08	12.70	75.60	85.80	104.40	104.40	80.50	91.00	66.30	94.90
3.81	13.97	85.20	88.70	113.80	113.80	91.30	87.80	104.40	97.60
2.54	15.24	107.50	107.50	180.30	189.70	117.00	104.40	155.00	136.00
1.27	16.51	339.00	350.00	401.00	505.00	505.00	416.00	348.00	338.00

DISTANCE FROM THE WALL (CM)	DISTANCE FROM THE CENTER (CM)	DC1	DC2	DC3	DC4	DC5	DC6	DC7	DC8
(VOLTS)									
13.08	4.70	0.470	0.371	0.221	0.336	0.464	0.416	0.030	0.401
11.43	6.35	0.537	0.415	0.254	0.382	0.525	0.459	0.034	0.458
10.16	7.62	0.591	0.448	0.281	0.425	0.588	0.516	0.039	0.523
8.89	8.89	0.683	0.516	0.325	0.498	0.664	0.571	0.040	0.587
7.62	10.16	0.788	0.584	0.371	0.571	0.771	0.657	0.046	0.692
6.35	11.43	0.931	0.686	0.447	0.691	0.925	0.761	0.074	0.841
5.08	12.70	1.140	0.844	0.558	0.870	1.150	0.948	0.144	1.060
3.81	13.97	1.450	1.100	0.603	1.020	1.430	1.260	0.291	1.320
2.54	15.24	1.970	1.520	0.603	1.090	1.830	1.830	0.764	1.440
1.27	16.51	1.770	1.870	1.540	1.620	1.690	1.620	1.250	1.370

TABLE - XIX

STATION NUMBER - 7

FLOW RATE = 4.250 (CU-M/MIN)  
 INLET AIR TEMPERATURE = 20.000 (DEG-C)

INLET PRESSURE = 728.5 (N/SQ-M.)  
 OUTLET PRESSURE = 158.4 (N/SQ-M.)

DISTANCE FROM THE WALL (CM)	THE CENTER (CM)	AC1	AC2	AC3	AC4	AC5	AC6	AC7	AC8
( MILLIVOLTS )									
27.67	4.70	14.23	16.13	14.23	15.30	15.55	16.13	15.90	13.90
24.77	7.62	13.29	15.50	14.23	15.30	13.60	15.80	4.00	13.30
22.23	10.16	12.33	15.20	12.97	13.60	12.97	16.44	3.00	12.65
19.69	12.70	13.90	16.76	15.50	15.30	14.23	16.44	3.20	14.55
17.15	15.24	17.08	20.00	18.97	20.37	17.08	22.14	4.70	18.66
14.61	17.78	21.19	25.30	23.40	24.98	20.55	28.78	7.00	22.77
12.07	20.32	25.60	31.00	29.73	31.04	26.60	36.10	9.50	27.80
9.53	22.86	35.40	40.40	40.10	41.30	35.20	40.40	17.70	41.00
5.72	25.67	60.40	54.70	75.40	80.10	67.70	62.40	47.10	70.20

DISTANCE FROM THE WALL (CM)	THE CENTER (CM)	DC1	DC2	DC3	DC4	DC5	DC6	DC7	DC8
( VOLTS )									
27.67	4.70	0.228	0.181	0.111	0.165	0.221	0.202	0.020	0.177
24.77	7.62	0.249	0.197	0.123	0.186	0.246	0.219	0.019	0.204
22.23	10.16	0.268	0.209	0.135	0.202	0.268	0.237	0.018	0.228
19.69	12.70	0.297	0.230	0.147	0.227	0.298	0.262	0.019	0.254
17.15	15.24	0.335	0.257	0.167	0.260	0.339	0.293	0.022	0.291
14.61	17.78	0.392	0.290	0.191	0.311	0.392	0.334	0.029	0.348
12.07	20.32	0.464	0.342	0.225	0.320	0.470	0.403	0.039	0.425
9.53	22.86	0.595	0.457	0.271	0.448	0.595	0.531	0.049	0.522
5.72	25.67	0.965	0.761	0.440	0.742	0.971	0.876	0.096	0.841